

Aus der Institut für Pharmakologie der Universität Heidelberg

(Geschäftsführender Direktor: Prof. Dr. med. Marc Freichel)

Abteilung für Molekulare Pharmakologie

(Direktorin: Prof. Dr. Rohini Kuner)

**Spinal cord circuits underlying dynamic and punctate
allodynia in inflammatory pain & Cellular basis for
prefrontal modulation of inflammatory pain by fear**

Inauguraldissertation

zur Erlangung des Doctor scientiarum humanarum (Dr. sc. hum.)

an der

Medizinischen Fakultät Heidelberg

der

Ruprecht-Karls-Universität

vorgelegt von

Sheng Liu 刘圣

aus Zunyi, Guizhou, China

2021

Dekan: Herr Prof. Dr. med. Hans-Georg Kräusslich

Doktormutter: Frau Prof. Dr. Rohini Kuner

Table of Contents

1 Introduction.....	1
1.1 Acute and Chronic inflammatory pain.....	1
1.2 Peripheral sensory neuron related to nociception.....	2
1.3 Spinal cord circuit related to nociception.....	4
1.3.1 Gate control.....	5
1.3.2 Spinal GABA inhibition.....	7
1.3.3 Pre- and postsynaptic GABA inhibition.....	7
1.3.4 Pathological changes of presynaptic spinal GABA inhibition.....	9
1.4 Allodynia circuits in inflammatory pain.....	21
1.5 Brain areas related to nociception.....	14
1.6 Role of the prefrontal cortex in pain processing.....	15
1.7 Role of the prefrontal cortex in fear.....	17
1.8 Cellular basis of pain and fear in the prefrontal cortex.....	19
1.9 IEG-dependent molecular tools to functionally label and manipulate activated neural ensembles.....	20
1.9.1 Dual-epoch mapping technique to discriminate different pain modality circuits.....	21
1.9.2 Tetracycline-off based “dual-tiered” tool to dissection emotion and pain.....	22
1.10 Aims of Study.....	23
2 Materials and Methods.....	25
2.1 Animal.....	25
2.1.1 Transgenic mice.....	25
2.1.2 Genotype verification.....	26
2.2 Basal sensation.....	25
2.2.1 Light touch sensation assay.....	29
2.2.2 Noxious thermal and cold sensation assay.....	29
2.2.3 Sensory-motor function assay.....	30
2.3 Induction of inflammatory pain.....	31
2.4 Testing mechanical and thermal sensitivity.....	32
2.5 Induction of expression of Fos protein and <i>c-fos</i> mRNA.....	34
2.6 Mouse spinal cord tissue preparation.....	35
2.7 Dual staining of tyramide amplified fluorescent in situ hybridization with Immunofluorescent.....	35
2.7.1 Plasmid transformation.....	36
2.7.2 DNA preparation.....	37

2.7.3 RNA probe preparation.....	38
2.7.4 Tyramine synthesis.....	40
2.7.5 Tyramide-amplified in situ hybridization.....	40
2.8 Imaging.....	42
2.9 Cell counting and data analysis.....	42
2.10 Marker signal image transformation.....	43
2.11 Data analysis and statistics.....	46
2.12 Animal.....	47
2.13 Virus combination preparation.....	47
2.14 Virus injection and optogenetic dual-implants.....	48
2.15 Fear condition and recall behavior.....	50
2.16 <i>In vivo</i> optical stimulation.....	51
2.17 Fear recall testing.....	51
2.18 Heat hypersensitivity Hargreaves test.....	52
2.19 Aversive related white noise test.....	52
2.19.1 Open field test.....	53
2.19.2 Elevated plus maze test.....	53
2.20 Heat stimulus and Fos induction.....	54
2.21 Capsaicin-induced acute nocifensive behavior.....	54
2.22 Fos immunohistology.....	55
2.23 Image acquisition and quantification.....	55
2.24 Data analysis and statistics.....	56
3 Results.....	57
3.1 Conditioned knock-out of GABAA β 3 does not impact motor function.....	57
3.2 Impact of conditional GABAA β 3 knock out on somatosensation.....	62
3.2.1 Innocuous touch sensation.....	62
3.2.2 Innocuous punctate and dynamic mechanical sensation.....	62
3.2.3 Thermal sensation.....	63
3.3 Impact of GABAA β 3 knock-out on the development of punctate allodynia in CFA model.....	66
3.4 Discrimination of punctate and dynamic mechanical allodynia circuits using dual-epoch mapping in spinal cord.....	71
3.5 Intermingled pattern of spinal cord c-fos labelling following punctate and dynamic mechanical stimuli post CFA injury.....	77
3.6 Conditional deletion of GABAA β 3 in nociceptors reduced activation of CR neurons for punctate but not dynamic mechanical allodynia.....	87
3.7 Conditional deletion of GABAA β 3 in nociceptors reduced activation of PV	

neurons for punctate mechanical allodynia.....	91
3.8 Analysis of relation between fear-associated and pain-associated neurons under baseline and inflammatory condition.....	94
3.9 Suppression of PL fear engram coding neuron decreases heat post-inflammatory hypersensitivity.....	101
3.10 Suppression of random neurons in the prelimbic cortex does not impact on post inflammatory heat hypersensitivity.....	108
3.11 Activation of PL fear engram coding neuron deteriorating acute pain behavior post capsaicin injection.....	111
4 Discussion.....	115
4.1 Motor function of GABAA β 3 knock out functions of PSI in mechanosensation and behavior.....	115
4.2 Pain-related sensation change of GABAA β 3 knock out.....	116
4.3 GABAA β 3 deletion from nociceptors impacts on punctate, but not dynamic, inflammatory allodynia.....	117
4.4 An intermingled pattern of punctate and dynamic allodynia post-inflammation.....	119
4.5 Calretinin neurons participate in the punctate allodynia formation in the spinal cord.....	121
4.6 PV neurons participate in the punctate allodynia formation in the spinal cord.....	123
4.7 Dual-epoch mapping method to discriminate punctate and dynamic allodynia circuits in spinal cord.....	124
4.8 Partial colocalization of the fear engram with neuronal ensemble activated in heat pain in the murine prelimbic cortex.....	125
4.9 PL fear engram coding neuron activation increase the acute pain perception.....	126
4.10 PL fear engram suppression decrease the heat hypersensitivity in chronic inflammatory pain.....	127
4.11 Conclusion.....	129
5 Summary.....	131
6 Reference.....	136
7 Publications.....	158
Acknowledgments.....	159
Curriculum Vitae.....	160
EIDESSTATTLICHE VERSICHERUNG.....	161

List of Tables

Table 1. PCR primers.....	27
Table 2. DNA extract reagent mixture.....	27
Table 3. PCR reaction reagent mixture.....	27
Table 4. PCR reaction protocol.....	28
Table 5. Parameters description of CatWalk XT [®] software.....	31
Table 6. Plasmid DNA Restriction digest reagent mixture.....	39
Table 7. DIG labelling probe synthesis reagent mixture.....	39
Table 8. <i>c-fos</i> probe hydrolysis reagent mixture.....	39
Table 9. TAI-FISH and dual-TAI-FISH primary antibodies.....	42
Table 10. TAI-FISH and dual-TAI-FISH secondary antibodies.....	42

List of Figures

Figure 1. Illustration graph of gate control theory.....	6
Figure 2. Scheme of presynaptic GABA inhibition on nociceptors in different conditions.....	12
Figure 3. Agarose gel electrophoresis of PCR products. Genotyping of transgenic mice using DNA extracted from ear punch tissue.....	28
Figure 4. <i>c-fos</i> in situ probe plasmid Snapgene map and <i>c-Fos</i> in situ probe sequence.....	37
Figure 5. Schematic of Marker signal image transformation method.....	45
Figure 6. Voluntary motor behavior and passive locomotor behavior of GABAA β 3 knock out mice.....	59
Figure 7. Home cage behavior of GABAA β 3 knockout mice. Different Home cage behavior parameters of grouped mice.....	60
Figure 8. Changes in static weight parameters of GABAA β 3 knockout mice using the CatWalk system (Noldus). Different static weight parameters of grouped mice.....	61
Figure 9. The basal touch and mechanical sensitivity of SNS-GABAA β 3 ^{-/-} and Advillin-GABAA β 3 ^{-/-} mice.....	64
Figure 10. The basal thermal sensitivity of SNS-GABAA β 3 ^{-/-} and Advillin-GABAA β 3 ^{-/-} mice.	65
Figure 11. Mechanical pain behavior in nociceptor GABAA β 3 knock-out (KO) or DRG sensory neuron GABAA β 3 KO mice.....	68
Figure 12. Nociceptive mechanical pain behavior in nociceptor GABAA β 3 knock-out (KO) mice or DRG sensory neuron GABAA β 3 KO mice.	69
Figure 13. Thermal pain behavior in nociceptor-specific GABAA β 3 knock-out (KO) mice or DRG sensory neuron GABAA β 3 KO mice.....	70
Figure 14. <i>c-Fos</i> expression sample image of noxious mechanical stimuli in the spinal cord.....	74
Figure 15. Time interval test for the dual-epoch mapping method.....	75
Figure 16. Activation test for dual-epoch mapping method. A, schematic showing animal groups sacrificed after nociceptive pinprick stimulus at different time points, or both of time points.....	76
Figure 17. Spinal neural activate representations of punctate and dynamic mechanical stimulation under physiological conditions.....	80
Figure 18. Spinal neurons activated by punctate and dynamic mechanical stimulation under physiological conditions.....	81
Figure 19. Spinal neuronal activation representations of punctate and dynamic	

mechanical stimulation under inflammation.....	82
Figure 20. Spinal neurons activated by punctate and dynamic mechanical stimulation following hindpaw inflammation.....	83
Figure 21. Laminar distribution of spinal neurons activated by punctate and dynamic mechanical stimulation following hindpaw inflammation.....	84
Figure 22. Plotting distribution of spinal neurons activated by punctate and dynamic mechanical stimulation following hindpaw inflammation.....	85
Figure 23. Regionally specific of the dynamic and punctate mechanical nociception under inflammation.....	86
Figure 24. Spinal CR neuron activate representations of punctate and dynamic mechanical stimulation under inflammation.....	89
Figure 25. Spinal CR neuron counting of of punctate and dynamic mechanical stimulation under inflammation of nociceptor GABAA β 3 KO mice.....	90
Figure 26. Spinal PV neuron activate representations of punctate mechanical stimulation under inflammation.....	92
Figure 27. Spinal PV neuron activate representations and distribution of punctate mechanical stimulation under inflammation.....	93
Figure 28. Prelimbic c-Fos expression upon hindpaw heat stimulation.....	97
Figure 29. Prelimbic fear labeling and heat c-Fos expression post-CFA.....	98
Figure 30. Prelimbic ArchT-Venus and c-Fos expression upon fear recall labeling and heat stimulus.....	99
Figure 31. Labeling of the prelimbic fear engram and heat engram under inflammatory pain conditions.....	100
Figure 33. Analysis of fear and pain behavior upon optogenetic suppression of the PL fear engram.....	105
Figure 34.....	106
Figure 35. Analysis of fear cue stimulus-activated c-Fos expression upon optogenetic suppression of PL fear engram.....	107
Figure 36. Optogenetic (ArchT) suppression of random prelimbic population and associated behavioral tests.....	109
Figure 37. Analysis of fear cue stimulus-activated c-Fos expression upon optogenetic suppression of PL random neurons.....	110
Figure 38. Impact of optogenetic activation of PL fear engram on capsaicin-mediated tonic pain.....	113
Figure 39. Analysis of c-Fos expression after optogenetic activation of PL fear engram or capsaicin injection.....	114

INTRODUCTION

1 Introduction

1.1 Acute and Chronic inflammatory pain

Pain is an unpleasant vital sensation that signals danger, prevents us from harming ourselves, and alerts us to injury. However, not all kinds of pain are coordinated; for instance, in some circumstances, acute pain becomes chronic and even the strongest analgesics are unable to control this agonizing sensation or emotional experience. In 1979, the International Association for the Study of Pain defined pain as “An unpleasant sensory and emotional experience associated with actual or potential tissue damage or described in terms of such damage”; however, after 40 years of recognition and research, the definition was recently revised as “An unpleasant sensory and emotional experience associated with, or resembling that associated with, actual or potential tissue damage” (Raja et al. 2020). Pain can be classified into acute or chronic. In healthy conditions, acute pain is produced by the application of a noxious stimulus to the receptive field of the nerve center. In pathological conditions, chronic pain may be more intense and enduring when a noxious stimulus is applied (hyperalgesia), while harmless stimuli (allodynia) or even no stimulus at all (spontaneous pain) may also cause pain. Globally, chronic pain is a significant contributor to disability. One-fifth of the European population experiences chronic pain, and it also annually impacts the United States economy by 635 billion US dollars, which is higher than that impacted by heart disease, cancer, and diabetes combined (Phillips 2009). Despite this burden, the treatment of chronic pain is currently inadequate.

Unlike acute pain as a normal biological warning system, chronic pain is a result of a complicated interplay between the brain and dysfunctional neural pathways. Chronic pain lasts more than 3 months after normal tissue healing time has elapsed. It is originating in the peripheral nervous system (PNS), and

INTRODUCTION

can be divided into two subgroups depending on the etiology, namely, neuropathic and inflammatory. Neuropathic pain is caused by a lesion or pathology change of the somatic sensory nervous system (Colloca et al. 2017). In contrast, chronic inflammatory pain is owing to injury to non-neural tissues and the subsequent release of inflammatory factors (Ji et al. 2016). Most known inflammatory mediators cause pain by binding to receptors of nociceptive primary sensory neurons (nociceptor) in the peripheral nervous system that innervate the injured tissues (Basbaum et al. 2009; Gold and Gebhart 2010). Acute inflammation is a protective response of tissues that eliminates the initial cause of cellular injury and initiates tissue repair. Chronic inflammation, in contrast to acute inflammation, is generally harmful and usually accompanied by diseases like periodontitis, atherosclerosis, rheumatoid arthritis, and cancer. (Gold and Gebhart 2010). It is unclear whether acute and chronic inflammation drive acute and chronic pain, respectively. Pain research recently has demonstrated that neuronal plasticity is the key mechanism in development or maintenance of chronic pain (Basbaum et al. 2009; Coull et al. 2005). Peripheral sensitization of injury receptors is critical for chronic pain development and transition from acute pain to chronic pain (Reichling and Levine 2009). Central sensitization (enhancing the response of pain circuits in the spinal cord and brain) modulates the chronicity progress of pain, leads to pain spreading beyond the injury site, and impacts the affective and emotional of pain patients (Kuner and Flor 2016; Reichling and Levine 2009).

1.2 Peripheral sensory neuron related to nociception

Pain signal from external to the spinal cord is produced through the activation of nociceptive primary sensory neurons located in dorsal root ganglion (DRG) for the body or the trigeminal ganglion (TG) for the face, namely, the nociceptors, which could be classified depending on axon caliber, degree of

INTRODUCTION

myelination, and conductance. Nociceptors could be divided in two major classes, named as A or C afferent, according to their myelination properties (Meyer 2008). Medium-diameter myelinated A fibers, rather than large-diameter myelinated A fibers, mediate acute, localized fast conductance signals (light touch). In contrast, unmyelinated C fibers from small-diameter neurons convey poorly localized slow conductance pain signals. These subpopulations of peripheral nerve fibers detecting intense physical or chemical stimuli by modality-specific sensory transduction molecules on the axon terminal innervate the skin, tissues, and internal organs (Julius and Carlson 2015). Sodium ion channel subtype Nav1.8 is specifically expressed in nociceptors. Because the gene SCN10A encodes Nav1.8, it was named sensory neuron-specific (SNS). It plays a crucial role in nociception and chronic pain, since it is located in free nerve terminals, responds to external stimuli, and initiated action potentials. (Hameed 2019). Loss of Nav1.8 function could attenuates pain behavior in animal models. Nav1.8-null mice manifest attenuated response to cold, heat and mechanical stimuli in intraplantar carrageenan injection model. (Bennett et al. 2019). Nav1.8 null mice also exhibit decreased pain behaviors from capsaicin or mustard oil injection inflammatory models (Laird et al. 2002). Selectively pharmacological blockade of Nav1.8 could effectively attenuated mechanical or thermal nociceptive sensitization in animal (Jarvis et al. 2007). In recent years, some sensory transduction molecules like transient receptor potential cation channel V1 (TRPV1) or transient receptor potential cation channel subfamily M8 (TRPM8) have been observed, which are specific to sense high noxious heat and cold sensitivity respectively (Knowlton et al. 2013); however, the molecules that transduce mechanical pain sensation remain stubborn and elusive (Caterina et al. 2000). Deletion of major candidate molecules like Piezo2 for nociceptive mechanical stimuli results in little change in sensitivity to harmful mechanical pain (Murthy et al. 2018). This may be owing to most somatosensation modalities being conveyed through the activation of more

INTRODUCTION

than one sensor molecules (Roudaut et al. 2012; Sharif-Naeini 2015). However, recent investigations of selected population ablation in mice have revealed sensory output of neurons based on their chemical and biophysical characteristics. Ablation of Mas-related G protein-coupled receptor subtype D positive nociceptors in DRG markedly reduce acute and persistent mechanical pain; however, does not impact thermal sensitivity of animal (Cavanaugh et al. 2009). Alternatively, ablation of the calcitonin gene-related peptide (CGRP) expression neurons from DRG cause profound loss of noxious heat sensation but not innocuous or noxious mechanical sensation (McCoy et al. 2013). These anatomical bases result in a diversity of coding patterns in the manner in which the organisms perceive the external stimuli. However, this progress also poses many challenges in interpreting their organization and transmission patterns.

1.3 Spinal cord circuit related to nociception

The spinal cord not only relays, but also integrates, the peripheral sensory information that projects to the higher pain processing center. Primary sensory neurons through the presynaptic terminal innervate the 6 Rexed layers (Lamina I-VI) of the dorsal horn (DH) of spinal cord, which are the main components of integrating peripheral sensory input and descending regulation. Nociceptive afferents from C and A δ nociceptor mostly form the synaptic contacts in superficial lamina I and II terminals of DH, relaying and processing nociceptive information. These superficial lamina I and II could be delaminated by afferent specific marker CGRP and IB4, respectively (Todd 2017). Alternatively, the non-nociceptive information from low-threshold A δ or A β afferents, like touch, generally project synaptic contact to deeper lamina (III to V) of DH. Extensive research regarding the spinal cord has shown that superficial lamina neurons mainly respond to noxious stimuli, whereas the interneurons in deeper lamina are more relay to innocuous touch information

INTRODUCTION

(Solorzano et al. 2015; Todd 2010b) . These anatomical data suggest that in the pain caused by touch, neurons from different laminae form a complex crosstalk circuit (Benarroch 2016).

1.3.1 Gate control

Many potential mechanisms for understanding the crosstalk between touch and pain have been discovered in previous studies. Overall, the question leading to allodynia was most noticeable. As per one scenario, peripheral sensitization following tissue inflammation enables high-threshold nociceptors to respond to the innocuous stimuli. However, most other scenarios prefer to be based on the “gate control theory” which first proposed by Melzack and Wall in 1965 (Melzack and Wall 1965). This theory argues that nociceptive transmission neurons in the spinal cord superficial lamina also receive inputs from low-threshold mechanoreceptors. Here, the inhibitory neurons located at the dorsal horn deep lamina inhibit pain information transduction from nociceptive neurons through feedforward activation, thereby controlling the transmission of pain information project to the brain, such innocuous mechanical information could generally suppress the nociceptive information flow. Alternatively, the nociceptive information can also be regulated by descending inputs from various brain regions. In contrast, under pathological conditions, strong nociceptive inputs induced by inflammation attenuate the inhibitory inputs from inhibitory neurons or sensitize transmission neurons; therefore, this loss of inhibition of inhibitory neurons or descending pathway may both underlie the mechanical allodynia that usually manifests as chronic pain symptoms (Duan et al. 2014; Gradwell et al. 2020).

INTRODUCTION

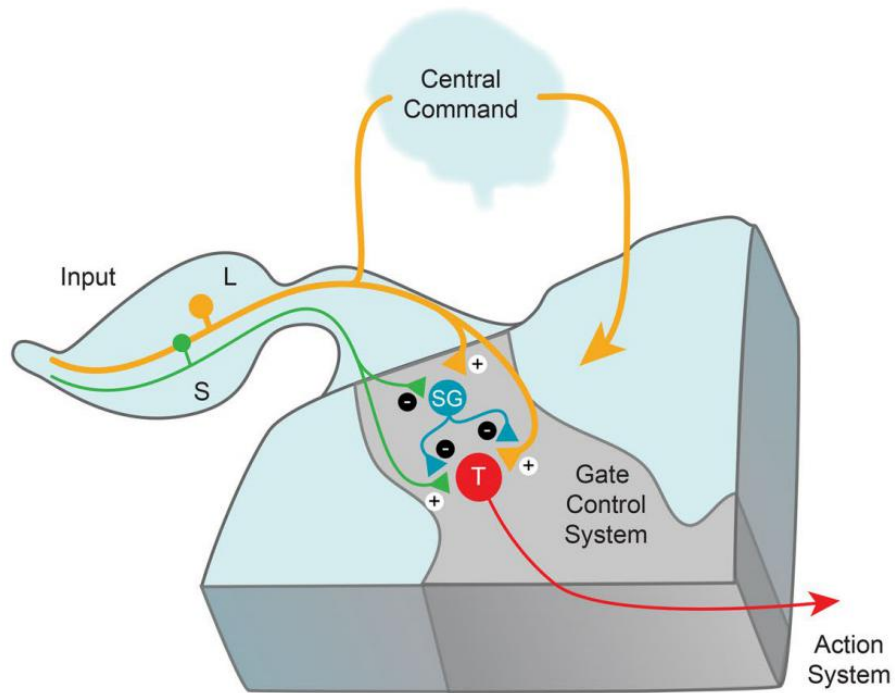


Figure 1. Illustration graph of gate control theory (Gradwell et al. 2020). Melzack and Wall (1965) proposed a gate control circuit that was superimposed over the dorsal horn of the spinal cord. Inhibitory interneurons as mediators of a spinal gate for sensory processing (marked SG, Melzack and Wall's terminology for substantial gelatinosa cells/neurons). Inhibitory interneurons reduce dorsal horn output signals conveyed by projection neurons (labeled T — transmission neurons) when the SG inhibitory neurons are activated by low-threshold afferent inputs (L). In the Action System, nociceptive afferent inputs (S) suppress inhibitory interneurons while activating projection neurons and generating pain. Descending central command signals were also included in this.

INTRODUCTION

1.3.2 Spinal GABA inhibition

It is widely believed that the loss of inhibition of the spinal cord dorsal horn is a key mechanism to promote and maintain chronic pain (Guo and Hu 2014). This inhibition is mainly delivered by inhibitory neurotransmitters. Among these inhibitory neurotransmitters, γ -aminobutyric acid (GABA) is a major inhibitory neurotransmitter in the brain and spinal cord, which is released from GABAergic neurons and binds to both GABAA receptors and GABAB receptors. In lamina I, lamina II, and lamina III of the rodent spinal cord dorsal horn, GABAergic neurons are occupied 25%, 30%, and 40%, respectively. (Polgár et al. 2003). Mammalian GABAA receptors are ligand-gated chloride channels comprising a family of 19 subunits (Olsen and Sieghart 2009). Despite the large diversity of isoforms, the $\beta 3$ subunit (GABAA $\beta 3$) localized in DRG and spinal cord dorsal horn plays a synapse-specific role in GABAergic inhibitory synaptic transmission, while knockout of $\beta 3$ could impair inhibitory synaptic transmission (Nguyen and Nicoll 2018; Orefice et al. 2016). These evidence indicates that the GABAA $\beta 3$ subunit plays a key role in the inhibitory transmission and plays a synapse-specific role in GABAergic synaptic transmission.

1.3.3 Pre- and postsynaptic GABA inhibition

Spinal GABA-mediated inhibition can be divided into two different types, depending on the locus, namely postsynaptic or presynaptic inhibition (Gradwell et al. 2020). Postsynaptic inhibition occurs post-synaptically at the connection between an inhibitory interneuron and a neighboring dorsal horn neuron. In contrast, presynaptic inhibition is attributed to the locus of a connection between inhibitory interneurons and primary afferents, and refers to inhibition of the spinal terminal of the primary afferent (Guo and Hu 2014).

INTRODUCTION

Postsynaptic inhibition in the dorsal horn can be mediated by the neurotransmitters GABA or glycine. The effect of GABAA receptor activation critically depends upon intracellular chloride concentration within and outside of the target neuron. Activation of the GABAA or glycine receptors induces chloride influx and hyperpolarization of the membrane (Rivera et al. 1999). Prescott et al. demonstrated the value of this interaction for inhibition integrity, while chloride concentration $[Cl^-]$ reversal potential shifting can compromise inhibitory control and results in hyperexcitability of the spinal cord dorsal horn lamina I neurons (Prescott et al. 2006). If the intracellular $[Cl^-]$ is strong enough to induce the reversal potential of chloride (E_{Cl}) positive to membrane potential (V_m), the chloride permeable pore in the GABAA receptor opens, resulting in chloride efflux, which depolarizes the neuron. But if the $[Cl^-]$ is too low and the E_{Cl} is negative to the V_m , the activation of the GABAA receptor can cause chloride ion influx then induces neuron hyperpolarization. The Na-K-2Cl co-transporter (NKCC1) is primarily responsible for chloride accumulation in mammalian neurons, while K-Cl co-transporter 2 is primarily responsible for chloride extrusion (KCC2). NKCC1 expression is high in the CNS during development; however, KCC2 expression is poor (Kahle et al. 2008). However, in adult animals, accompanied with down regulation of NKCC1 in the mature process, an increase in KCC2 reduces $[Cl^-]$. Therefore, the E_{Cl} is hyperpolarized, which is markedly low to trigger chloride influx, while the GABAA receptor is activated, thereby inhibiting the postsynaptic neuron (Guo and Hu 2014).

Frank and Fuortes first proposed presynaptic inhibition in 1957 (Frank & Fuortes., 1957). Unlike postsynaptic inhibition, presynaptic inhibition is only mediated by the neurotransmitter GABA. Eccles et al. studied presynaptic inhibition and demonstrated that the afferent excitatory postsynaptic potential (EPSP) decrease was caused by primary afferent depolarization (PAD) (Eccles., 1963; Willis., 2006). In contrast to CNS neurons, peripheral DRG

INTRODUCTION

neurons maintain a high concentration of NKCC1 expression level, while KCC2 is expressed at a low level or even absent (Alvarez-Leefmans et al. 2001; Kanaka et al. 2001). Consequently, adult RG neurons preserve a high intracellular $[Cl^-]$, causing the chloride reversal potential (E_{Cl}) higher than the resting membrane potential (Mao et al. 2012; Price et al. 2006). Therefore, the opening of Cl^- channels, and specifically GABAA receptors, allows the efflux of Cl^- and PAD. Several theories have been proposed to clarify how PAD causes presynaptic inhibition (Rocha-González et al. 2008). For example, PAD can result in the inactivation of voltage-dependent Na^+ or Ca^{2+} channels, as well as 'shunting' effects that disrupt propagating action potentials (APs) along the afferent fiber (Graham and Redman 1994; Segev 1990). Both pre-and postsynaptic inhibition have effective pathways to control and gate sensory signaling in the spinal cord, despite opposite effects on the membrane potential (Figure 2a).

1.3.4 Pathological changes of presynaptic spinal GABA inhibition

Pain perception is a result of a redundant and dynamic mechanism, not just a simple signal relay in the spinal cord triggered by noxious stimuli. Noxious stimuli are transmitted internally (from the brain) and external (from non-noxious and/or noxious stimuli) feedback controls the generated signals through multiple pathways involving different cell types. The malfunctioning component can disrupt the system's equilibrium and prevent somatosensory sensations from being coded, resulting in pathological pain such as hyperalgesia and allodynia. Recently, many studies have resolved the pathological changes after injury at the cellular circuitry level and some key components have been identified (Peirs et al. 2015a; Bourane et al. 2015; Duan et al. 2014; Cheng et al. 2017; Peirs et al. 2021) . However, these findings do not adequately account for different modes of inhibition (pre versus post)

INTRODUCTION

in various pain modalities, mainly owing to challenges in selectively manipulating pre- or postsynaptic inhibition.

Our previous study on a neuropathic pain model suggested that, owing to the upregulation of intracellular $[Cl^-]$ in DRG neurons, there is a transient depolarizing shift in EGABA and a reduction in the conductance of presynaptic GABAA receptor in DRG neurons immediately after nerve injury (Chen et al. 2014). Simultaneously, calcium signal two-photon imaging evidence in primary afferent terminals in the spinal cord dorsal horn also confirmed the reduction of GABA-mediated presynaptic inhibition effect (Chen et al. 2014). These changes collectively lead to a reduction of presynaptic inhibition causing a hypersensitivity post-injury. Alternatively, presynaptic GABA loses its ability to close the pain gate, and nociceptive stimuli generates stronger pain (Figure 2b). To specifically determine the outcome of these changes on pain behavior, mice deficient of GABAA receptor in primary nociceptors were used to investigate the role of presynaptic inhibition in pain behavior. Unlike wild-type littermates control, hypersensitivity in these mice did not further develop after nerve lesions (Chen et al. 2014). These results suggest that presynaptic GABA inhibition is essential for the intensity of pain behavior under physiological condition, and that presynaptic disinhibition is critical for neuropathic pain initiation.

However, such a mechanism may not apply to inflammatory pain conditions. Although inflammation also elevates nociceptor $[Cl^-]$ in peripheral, the conductance of the presynaptic GABAA receptor is not diminished (Guo and Hu 2014). This characteristic rises the depolarization caused by GABAA receptors, in which a low signal is sufficiently intense to induce action potentials in nociceptor central terminals. These action potentials could activate projection neurons in lamina I and facilitate nociceptive processing. Thus opened the “gate”, then the low-threshold stimuli could also generate a

INTRODUCTION

pain sensation, which is termed allodynia (Figure 2c). Moreover, Our colleagues Da Guo et al. investigated the presynaptic GABA β 3 receptor function with spinal cord slices from complete Freund's adjuvant (CFA) injected animals using two-photon calcium imaging. They generated SNS-Ai38 mice harbouring nociceptor-specific expression of the calcium indicator GCaMP3. Two days after induction of hindpaw inflammation with injection of Complete Freund's Adjuvant (CFA), GABA alone could generate calcium influx in more presynaptic terminals in the spinal cord, which implies that GABA not only loses inhibitory effect but also lead terminal switch to excitation in inflammatory pain conditions (Guo 2017) .

INTRODUCTION

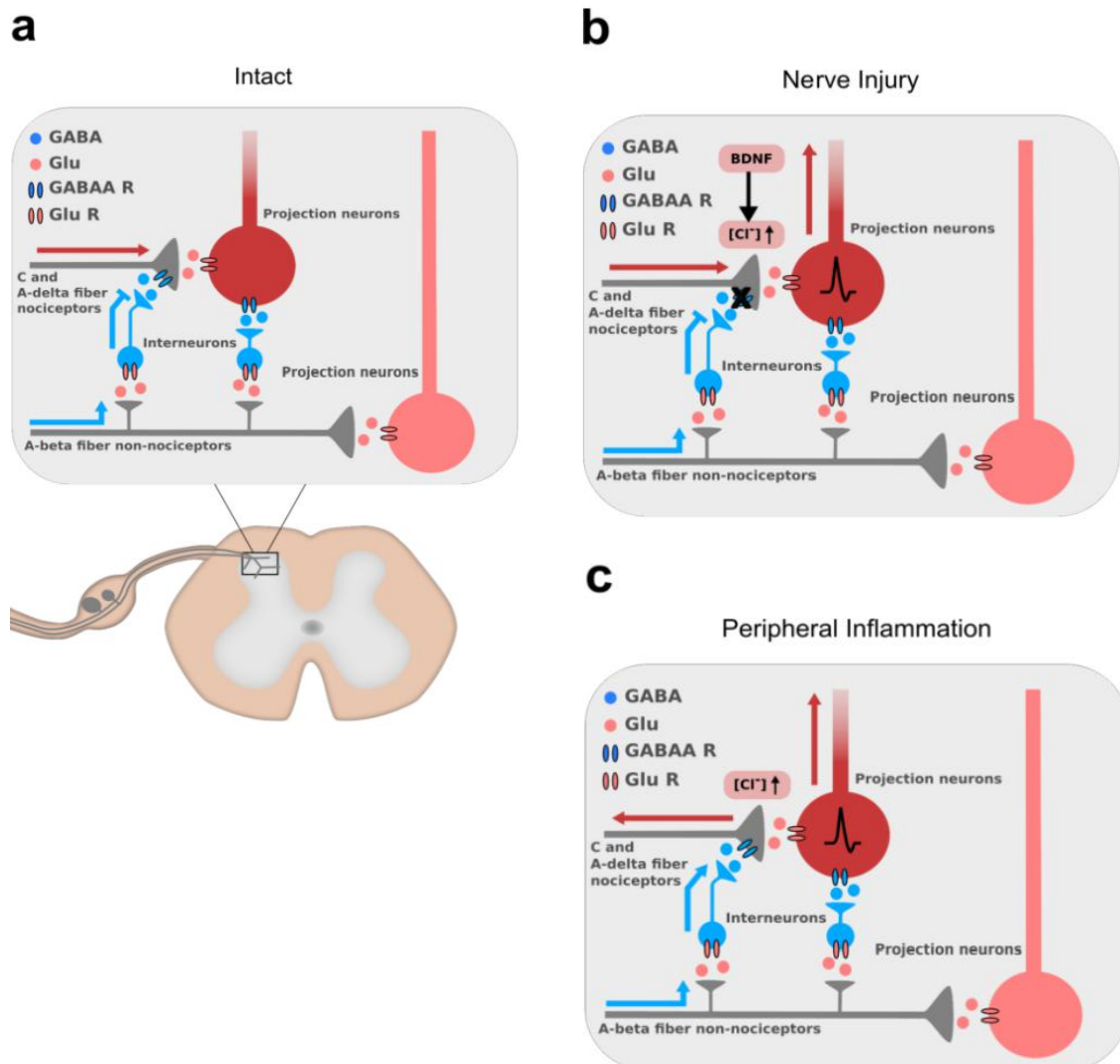


Figure 2. Scheme of presynaptic GABA inhibition on nociceptors in different conditions (Da Guo, 2017). Both, presynaptic central terminals of nociceptors and postsynaptic projection neurons are regulated by GABAergic inhibitory interneurons receiving input from A-beta fiber non-nociceptive inputs. Presynaptic inhibition occurs when synapses form connections with the primary afferent terminal; otherwise, postsynaptic inhibition occurs when synapses make connections with the inhibitory interneuron.. GABA inhibition can vary across different conditions: **a**, projection neuron regulated by both pre-and postsynaptic inhibition; **b**, presynaptic disinhibition after nerve injury; **c**, presynaptic inhibition switches to excitation.

INTRODUCTION

1.4 Allodynia circuits in inflammatory pain

A common symptom of patients with chronic pain is allodynia, which represents pain in response to a normally innocuous stimulus, such as a tactile stimulus (mechanical allodynia) or a mild change in temperature (heat/cold allodynia) (Kuner 2010; Kuner and Flor 2016). In contrast to hyperalgesia (an abnormally increased sensitivity to noxious stimuli), allodynia is triggered by ordinary touch, stroking, or sensations that are generally pleasant to the senses. Since the mechanical sensation comprises many aspects, mechanical allodynia also exists in multiple forms, including static, punctate, and dynamic. Static allodynia is evoked by pressure in a larger surface, which is generated by a large probe (> 1 cm) in human studies, commonly measured using Randall-Selitto assay for animal studies. Alternatively, punctate allodynia is evoked by a small diameter filament, more akin to a needle prick-like sensation using von Frey filament measurement in animal studies. Dynamic allodynia is one of the most distressing and prevalent forms of chronic pain, which is evoked by gentle touching from clothes, running water, or the wind blowing on the skin. A fluffy cotton swab or soft brush hairs have been used for measurements in animal studies (Cheng et al. 2017).

The spinal circuits of dynamic mechanical nociceptive sensitization and their mechanisms have been well studied. Qiufu Ma's laboratory demonstrated that spinal cord Vgult3 neurons in lamina III form a morphine-resistant microcircuit that is needed for brush-evoked dynamic mechanical allodynia transmission (Cheng et al. 2017). Cedric Peirs and Rebecca P. Seal have also performed significant work on this aspect. They reported mechanical pain requiring the temporary expression of Vgult3 by a separate population of neurons in the deep dorsal horn, and that stimulation of the cells in adults results in mechanical hypersensitivity (Peirs et al. 2015a). Next, they identified additional calretinin (CR) expressing excitatory neurons that

INTRODUCTION

participate in the dorsal horn circuit for chronic mechanical hypersensitivity. According to their latest study, these CR neurons in lamina II inner, convey mechanical allodynia induced by inflammatory injury information from the Vgult3/CCK neuron in deep lamina III-IV, which convey primarily dynamic allodynia (Peirs et al. 2021). These result suggest that the deep dorsal horn neurons also provide critical input to inflammatory mechanical allodynia.

Although the above studies provide a clear account of postsynaptic inhibition for the circuitry of dynamic allodynia, another aspect of spinal cord inhibition, namely the presynaptic type, has not been reported. As one of the links of gate control theory, only postsynaptic inhibition evidence does not provide a complete view of the mechanical allodynia circuit. The effect of presynaptic inhibition on mechanical allodynia should be investigated using appropriate technical means to comprehend the mechanisms of allodynia macroscopically.

1.5 Brain areas related to nociception

Sensory inputs signal from periphery to the spinal cord dorsal horn, where integration and processing occurs (Todd 2010b). Thereafter, the output signal from the spinal cord circuit network is sent to several distinct brain centers via ascending pathways (Finnerup et al. 2021). Pain is a complex sensory and emotional experience, and the perception of pain appears to be co-coded by brain centers related to emotion as well as sensory processing (Bushnell et al. 2013). Based on a myriad of imaging studies, there is widespread consensus that the origin of the pain is not restricted to a single brain area, but rather results from integrated function across brain networks. For example, a human functional magnetic resonance imaging study by Wager et al. used a regression model of pain perception based on machine learning, which the result shows heat-induced acute pain neurological feature includes somatic-specific brain areas such as the ventrolateral thalamus, secondary somatosensory cortex, and dorsal posterior insula, as well as the brain regions

INTRODUCTION

related to affect and moods, such as the anterior insula, dorsal anterior cingulate cortex, and medial thalamus (Wager et al. 2013). Although specific brain regions have been implicated to play an important role in the processing of pain, such as the cingulate cortex or the anterior insula, it has been suggested that this process is not only performed by a single brain structure. There is broad consensus that limbic circuits play a key function in the emotional regulation of pain and are important in the transition to several forms of chronic pain. According to a meta-analysis of research using experimental pain stimuli, the main and secondary somatosensory cortices, insular cortex, anterior cingulate cortex (ACC), prefrontal cortex (PFC), and thalamus are all positively correlated with pain (Apkarian et al. 2005). Pain intensity discrimination activates a ventrally guided pathway that extends bilaterally from the insular cortex to the PFC, while pain spatial discrimination activates a dorsally directed pathway that extends from the posterior parietal cortex to the PFC (Oshiro et al. 2009).

1.6 Role of the prefrontal cortex in pain processing

The PFC is the cerebral cortex area that encompasses the frontal lobe's anterior part, and is especially well-developed in humans. (Ongür and Price 2000). The medial prefrontal cortex (mPFC) is composed of granular cortical areas and agranular regions which encompass the ACC, infralimbic (IL) cortex, and the prelimbic (PL) cortex. The PFC is a crucial region in executive activities including planning, problem-solving, and social control. It has the ability to represent information that is not immediately available in the environment, and this representational information is utilized to regulate actions and emotions, including the suppression of inappropriate actions, and feelings (Goldman-Rakic 1996). The PFC, on the other hand, is critical for pain perception. The PFC link to other areas such as periaqueductal gray matter (PAG), thalamus, amygdala, and basal nucleus, which makes it

INTRODUCTION

relevant to pain. (Ong et al. 2019).

The PAG serves as the primary control center for pain reduction modulation and pain relief, specifically this input is derived from the mPFC and extends to the ACC and frontal insular cortex (An et al. 1998). Using tracer approaches, which microinjection of the neuronal tracer horseradish peroxidase into the monkey PAG provided retrograde evidence that the dorsal mPFC are the major origins of cortical PAG projections, according to one research. (Hardy and Leichnetz 1981). Another research of PFC-amygdala connections found that inhibiting the paraventricular thalamic nucleus by pharmacogenetic inhibition reduces visceral pain. The paraventricular nucleus projects to the mPFC cortical layer, where it inhibits synapse formation with GABAergic neurons (Jurik et al. 2015). The analgesic effects of the GABA analog Gabapentin may be linked to the decrease in thalamocortical input. In animal research, the latter was discovered to be analgesic by reversing the increase in connectivity between the thalamus and cortex in response to nerve injury (Lin et al. 2014). All of this evidence points to a strong synergy between PFC and PAG, working together in the management of pain.

Another important brain area amygdala is involved in fear or phobia regulation also interconnected with the PFC (Mai JK 2011). On re-exposure to a context previously conditioned aversive stimulus, the PFC-amygdala-dorsal PAG pathway may also mediate fear-conditioned analgesia (Butler et al. 2011). Studies have shown that selective metabotropic glutamate receptor antagonists could reverse the pain-related reduction and evoke the activity of mPFC neurons in the arthritic pain model (Ji and Neugebauer 2011). In another study of rat models with arthritic pain, direct excitatory transmission in the amygdala was not altered; however, the inhibitory transmission was increased in the mPFC (Ji et al. 2010). This could occur through endogenous activation of GABA_A receptors, which leads to abnormally increased

INTRODUCTION

inhibition of main cells in the mPFC, resulting in decreased output from the mPFC to the PAG as well as decreased injury resistance. Moreover, it also reduces the inhibitory effect of the amygdala itself, which may lead to an uncontrolled amygdala pain mechanism (Neugebauer 2015). mPFC also causes significant synaptic inhibition of neurons in the central nucleus of the amygdala, which is reduced in arthritic pain models. (Kiritoshi and Neugebauer 2018). The evidences presented above demonstrates the importance of PAG-amygdala-PFC communication in pain and emotion regulation.

During acute and chronic pain, the PFC changes neurotransmitters and gene expression, leading to alterations in its structure, activity, and connectivity. The mPFC can play a dual, opposing role in pain. 1) Owing to its connections to other cortical areas, it can mediate antinociceptive effects and serve as a major source of cortical afferent PAG to modulate pain. This is a “cycle” in which sensory stimuli on one side are converted into perceptual signals through high brain processing activity, which is then used to control the flow of afferent sensory stimuli to the CNS at its entrance (dorsal horn). 2) It can induce chronicity of pain through its cortico-cortical brain projections, potentially depending on the level of dopamine receptor activity in the ventral tegmental area-avuncular nucleus reward pathway (Ong et al. 2019).

1.7 Role of the prefrontal cortex in fear

In addition to the roles aforementioned, the PL and IL subdivisions of the mPFC have been suggested to control the expression and suppression of fear in rodents, respectively (Giustino and Maren 2015). A fearful memory may last a lifetime once it has been developed. Extinguishing acquired fear is possible, but extinction memories are unstable. Fear memories' resistance to extinction may play a role in the persistence of anxiety and fear disorders.

INTRODUCTION

Pavlovian fear conditioning is a form of learning used to investigate the neurobiological underpinnings of anxiety and fear disorders. A harmless conditioned stimulus (CS; an auditory tone) is combined with an aversive unconditioned stimulus in a traditional rodent experiment (US; an electric footshock). After more training, once only presenting the CS could induce a conditioned fear response, such as freezing behavior (Iwamura et al. 2002; LeDoux 2000; Maren 2001). Most of the existing fear-related research is based on such a paradigm.

Recently, PL appears to be implicated in the expression of fear, according to pharmacological studies. (Laurent and Westbrook 2009; Sierra-Mercado et al. 2006; Morawska and Fendt 2012; Sangha et al. 2014). During behavioral experiments, some pharmacological approaches were employed to temporarily inactivate the mPFC neurons, allowing for manipulation of the fear circuit at different time points. For example, PL injection of the Na⁺ channel blocker tetrodotoxin, does not prevent the development of conditioned fear, but it does specifically diminish fear behavior to CS. (Corcoran and Quirk 2007). Inactivation of PL with the GABA-A receptor agonist might also decrease fear expression, which is consistent with PL activity is required for fear expression. (Laurent and Westbrook 2009; Sierra-Mercado et al. 2011). Immediate early genes (IEGs) *c-fos*, *Arc*, and *Zif268* are activated in response to stimuli and have been associated with learning and memory (Davis et al. 2003; Plath et al. 2006). During fear renewal, PL exhibited a significant increase in *c-fos* expression (Knapska and Maren 2009). Although suggests that PL plays a function in fear, it lacks a clear cellular specificity, showing that the acquisition of fear memories is dependent on complex neural circuits from distinct neuronal populations. Optogenetic approaches have recently been used to investigate these questions. Carvalho et al. have shown that fear

INTRODUCTION

conditioning causes disruption of PL inhibitory-excitatory balance. In this study, the PL to BLA pathway is crucial for encoding fear memories and may be engaged in CS stimulation to promote fear state (Arruda-Carvalho and Clem 2014). Using a similar method, Hübner et al. further confirmed that mPFC sends monosynaptic excitatory projections to the amygdala. With optogenetic activating of inputs resulted in inhibition of mPFC neurons and promoting disinhibition of amygdala neurons (Hübner et al. 2014). From another study, optogenetic inhibition of PV interneurons in the mPFC caused freezing behavior in intact animals and also regulate fear in fear conditioned animals (Courtin et al. 2014). These evidence suggests that PL activation is critical for the formation as well as facilitation of fear memory and that this same region plays an important role in pain modulation, as described above.

1.8 Cellular basis of pain and fear in the prefrontal cortex

Pain elicits anxiety and fear memory, which this complex biological interaction is conserved across species (Rusu et al. 2014; Labrenz et al. 2016; Vlaeyen and Linton 2000; Wiech and Tracey 2013). The cellular and molecular basis of acute and long-term remote fear memory triggered by strong aversive stimuli, such as pain, has been foreshadowed the association between these two distinct but inter-related behavioral states (Rashid et al. 2016; Kitamura et al. 2017; Grewe et al. 2017; Do-Monte et al. 2015; Frankland and Bontempi 2005; Silva et al. 2009). Discrete corticolimbic regions are typically triggered through anxiety and pain in human macroscopic imaging experiments (Labrenz et al. 2016; Wiech and Tracey 2013), and synaptic long-term potentiation and plasticity-related molecules, such as the calcium/calmodulin-dependent protein kinase IV and cyclic AMP response element-binding protein, have been identified to play a role in chronic pain states as well as fear memory modulation (Labrenz et al., 2016; Wiech and Tracey, 2013). While psychosocial behavioral levels of correlations

INTRODUCTION

between fear and pain have been identified (Labrenz et al. 2016), the mechanistic interpretation has remained elusive. In particular, there is a lack of cellular-level evidence to support macroscopic imaging and molecular-level findings.

Previously our laboratory has identified cellular assemblies in PL selectively recruited during tonic pain via IEG gene-based activity-tagging tools, compared them with memory engrams of remote stage fear recall, and addressed their functional impact and interactions via optogenetic manipulations and behavioral analyses. With adeno-associated virus particles expressing a binary, tetracycline-controlled transactivator (tTA) system in the mouse prelimbic cortex, we observed about 15% of the neuronal assemblies activated by capsaicin-induced tonic pain, overlapped with the remote fear memory engram. Using a virus expressing ArchRhodopsin in the TRE-Tight system, silencing activity of remote fear assemblies via illumination with yellow light (Mattis et al. 2011)(Mattis et al., 2012) led to a striking reduction in behavior associated with tonic pain perception. This work furnishes the cellular basis of fear-pain interaction, revealing a powerful synergism between the prefrontal circuitries for retrieval of learned fear and pain. Despite this, our understanding of the mechanisms involved in the effects of fear on long-term chronic pain, and different pain modality is lacking. It will be interesting to address whether activating prefrontal fears memory engrams at chronic time points after fear conditioning can facilitate pain perception in different modality settings of pain.

1.9 IEG-dependent molecular tools to functionally label and manipulate activated neural ensembles

One of the challenges in pain neuroscience analyses is to understand how the CNS responds to different stimulus (Anderson and Adolphs 2014). These

INTRODUCTION

stimuli are thought to be represented or coded by particular neuronal assemblies or ensembles at the cellular level. Elucidating circuits and underlying neural mechanisms will help to understand human behavior and pathological deviations in behavior. IEGs like *c-fos*, *Arc*, and *Zif268* are rapidly activated in stimulated neurons, and IEG activation has widely been utilized to identify stimuli-activated neuronal ensembles using immunohistochemistry (IHC) or in situ hybridization (ISH) (Hope et al. 1992; Moratalla et al. 1992; Morgan et al. 1987; Bartel et al. 1989; Cole et al. 1989). Additionally, co-staining for markers of specific neuronal types could identify the activated neural ensembles, providing support for tracing the circuits engaged by stimuli using the IHC or ISH (Luo et al. 2018). Various approaches have been developed in recent years to expand the usage of IEGs in CNS activation pattern mapping (Qiye He et al. 2019). Here in this study, we focused on two IEG-dependent tools to study neuronal activation in response to external stimuli.

1.9.1 Dual-epoch mapping technique to discriminate different pain modality circuits

It is often desirable to map the neuronal representations of two different stimuli at single-cell resolution across the brain. (Kim et al. 2016; Namburi et al. 2015; Beyeler et al. 2016; Ye et al. 2016; Lammel et al. 2012; Johnson et al. 2010). Experimentally, a single ISH or IHC against does not provide us with information from both stimuli in one animal. It was also unable to distinguish between various stimuli by comparing activity patterns between two different animals due to the heterogeneity in the spatial distribution of neurons between animals. Chaudhuri et al. were the first to create a strategy for detecting *Zif268* signals combining normal IHC and fluorescent ISH (I-FISH) to identify neurons engaged by two distinct sensory stimuli (Chaudhuri et al. 1997; Zangenehpour and Chaudhuri 2001). Xiu et al. were

INTRODUCTION

inspired by this approach and created another tyramide-amplified I - FISH (TAI-FISH) to investigate brain activations triggered by two distinct stimuli. (Xiu et al. 2014; Zhang et al. 2018). Particularly, tyramide signal amplification was employed in TAI-FISH to increase the signal-to-noise ratio of IHC signals and more reliably distinguish the protein and mRNA signal levels generated by two distinct stimuli (Xiu et al. 2014).

1.9.2 Tetracycline-off based “dual-tiered” tool to dissection emotion and pain

One of the most challenging tasks for IEG-dependent molecular tools is to reduce IEG activity in the absence of stimulus. To resolve this problem, “dual-tiered” IEG-dependent tools have been developed in recent years. In these tools, an IEG promoter drives the expression of a primary effector gene (the first tier) when being stimulated by the intended stimulus (e.g foot shock). When triggered by the proper stimuli, an IEG promoter induces the expression of IEG gene (terms the first tier). But this primary induced IEG does not labeling the activated neurons. Instead, it activates a secondary reporter or effector gene (terms the second tier) for the actual labeling or manipulation. An additional layer of temporal control is added into this two-tiered tool to limit the activity of the primary gene in the absence of stimulus, and The temporal control mechanism is only eliminated when the desired stimulus is to be provided, allowing the expression of the second-tier genes (Kitamura et al. 2017; Reijmers et al. 2007; Matsuo et al. 2008; Ramirez et al. 2013; Liu et al. 2012; Ramirez et al. 2015; Redondo et al. 2014). The TetTag transgenic mouse line is such a dual-tiered system (Gossen and Bujard 1992; Reijmers et al. 2007). In the TetTag mouse, the primary effector is tTA, an artificial transcription activator. The primary effector in the TetTag mouse is the tetracycline transactivator (tTA), a transcription activator. Thus, the secondary effect gene includes a synthetic promoter with tetracycline

INTRODUCTION

response elements (TREs) that must be coupled by tTA for expression. TetTag mice are supplied a diet containing doxycycline (Dox), which binds to the cellular tTA and inhibits it from binding TREs, inhibiting expression of the reporter or effector gene. A few days before stimulation, the TetTag mouse is designed to transfer to a diet without Dox. This creates a time window for the effect gene stimulation, thus the stimulus-induced tTA binds to TREs and activates the secondary reporter or effector expression. After this, the TetTag mouse is switched back to a Dox-containing diet. As a result, the expression of the second-tier reporter and effector gene is rigidly confined to the time window during which the stimulus is presented. In this way, we can then use the IEG gene again to label the second stimulus (Qiye He et al. 2019).

1.10 Aims of Study

Presynaptic inhibition has been proposed to play a role in mechanical allodynia in previous studies. To test this hypothesis, it is necessary to know the allodynia circuitry alterations in the spinal cord before and after an inflammatory injury. Further, the perceptual patterns triggered by different mechanical stimuli after inflammation differ, and the role of presynaptic inhibition in the different patterns needs to be established. Here in this study, we attempted to use the dual-epoch mapping technique to discriminate circuits in different modalities of mechanical allodynia. We used nociceptor-specific GABAA receptor knock-out mice to study the effect of presynaptic inhibition on punctate and dynamic mechanical allodynia.

Furthermore, the neuronal basis of the interrelationship between pain and fear in PL is similarly fascinating. Fear has a distinct function in acute pain, according to previous research; however, its role in chronic inflammatory pain remains unknown. Additionally, previous research on the impact of the prefrontal fear ensemble activation on acute pain perception was incomplete.

INTRODUCTION

Using the Tetracycline-off-based “dual-tiered” system as well as optogenetic tools, we explored this uncharted territory.

MATERIALS AND METHODS

2 Materials and Methods

Project 1: Spinal cord circuits underlying dynamic and punctate allodynia in inflammatory pain

2.1 Animal

The animal experiments are performed in accordance to EU and national regulations for animal experimentation and all animal work was approved by the local ethics committee Regierungspräsidium Karlsruhe, Germany (Reffrance number: 35-9185.81/G-128/17). Mice were housed in groups of maximal 4 animals per cage in temperature and humidity- controlled rooms with a 12 h light/dark cycle with access to rodent chow, water and libitum.

2.1.1 Transgenic mice

Cre-Loxp recombination (Cre-loxP) technology were used for conditionally knocking out the GABAA β 3 gene expression specifically in nociceptors or generally in most somatosensory neurons of the peripheral nervous system. Two Cre recombinase-expressing mouse lines were used in this study. Cre recombinase was expressed under the regulatory elements of mouse *Scn10a* gene and mouse *Advillin* gene, respectively in SNS-Cre and Advillin-Cre mouse lines. The murine *Scn10a* gene encodes the tetrodotoxin-resistant Nav1.8 sodium channel and accordingly, the SNS-Cre mice that were generated by our group (Agarwal et al. 2004) previously show a nociceptor-specific expression of Cre recombinase. The Advillin-Cre mouse line was kindly provided by Dr. Paul Heppenstall (Zurborg et al. 2011). The *Advillin* gene encodes the homonymous actin regulatory/binding protein restrictedly expressed in DRG neurons and superior cervical ganglia neurons

MATERIALS AND METHODS

(Zurborg et al. 2011). Gabrb3-loxP mice (B6;129-Gabrb3^{tm2.1Geh1Geh}/J, #008310) were obtained from Jackson Laboratory. Gabrb3-loxP mice possess loxP sites on either side of exon 3 of gene encoding GABAA receptor $\beta 3$ subunit (GABAA $\beta 3$) and mating with Cre-expressing mice enables deletion of exon 3 in Cre-expressing cells of the offspring (Ferguson et al. 2007). We mated Gabrb3-loxP mice independently with SNS-Cre mice and Advillin-Cre mice to generate SNS-GABAA $\beta 3$ and Advillin-GABAA $\beta 3$ mice, respectively.

2.1.2 Genotype verification

The genotype of all mouse used in the following experiments was determine via Polymerase chain reaction (PCR) prior phenotypic analyses and also verified again at the end of the experiments using primers that are shown in Table 1.

All DNA samples was extracted from ear punch tissue of mice using DNA extraction mix reagent (Table 2). Samples were heated on vortex heater (55 °C / 1000 rpm) for 5-6 hours (h) or overnight and the temperature was subsequently increased to 85 °C for 45 minutes (min) to deactivate the reaction. For PCR, we used MyTaqTM HS Red Mix (Bioline, BIO-25048) to improve efficiency and accuracy using reaction components as shown in Table 3 and protocols involving different annealing temperatures and reaction cycles as shown in Table 4. We compared the size of DNA fragments by agarose gel electrophoresis to determine the PCR products. After completion of the electrophoresis, the position of the bands relative to the DNA ladder was read out and the genotype of each mouse was assessed according to the expected band sizes (Figure 3).

MATERIALS AND METHODS

Table 1. PCR primers

Primer	Sequences 5'-3'
SNS-cre Forward	ACA GAC ATA CTC ATAATA TTT CTG TGA TT
SNS-cre Reverse	GCT GAG TGC AGA CAT TCT TAC CC
SNS-cre E Reverse	GCG CGC CTG AAG ATA TAG AAG A
Advillin-cre Forward	GCA CTG ATT TCG ACC AGG TT
Advillin-cre Reverse	GAG TCA TCC TTA GCG CCG TA
Gabr β 3-loxP Forward	ATT CGC CTG AGA CCC GAC T
Gabr β 3-loxP Reverse	GTT CAT CCC CAC GCA GAC

Table 2. DNA extract reagent mixture

Reagent	Volume(μl)
DirectPCR Lysis Reagent (ear)	97.5
10mg/ml Proteinase K	2.5
Ear Tissue (mm ²)	Approx. 2
Total	100

Table 3. PCR reaction reagent mixture

Reagent	Volume(μl)
ddH ₂ O	4.75
MyTaq TM Redmix	6.25
Primer	0.5
DNA	1
Total	12.5

MATERIALS AND METHODS

Table 4. PCR reaction protocol

Reaction step	Gene	Temperature (°C)	Time(s)	Cycles
Heat Lid		110	15	
Initial Denaturation		95	60	
Denaturation		95	15	
Annealing	SNS-cre	58	15	39
	Advillin-cre	61		32
	GABAA β 3-loxP	60		40
Extension		72	10	
Final extension		72	300	
Pause		8	∞	

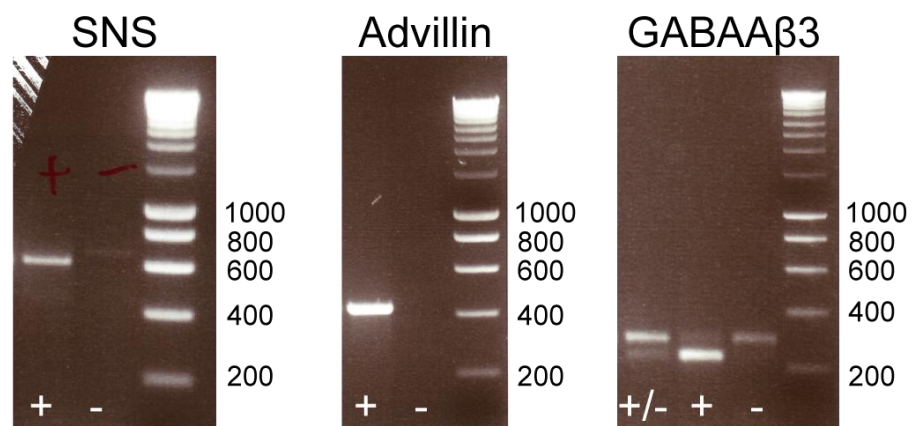


Figure 3. Agarose gel electrophoresis of PCR products. Genotyping of transgenic mice using DNA extracted from ear punch tissue. + represents positive, - represents negative, and +/- represents heterozygote.

MATERIALS AND METHODS

2.2 Basal sensation

To test the effects of the two Gabab₃ gene knockouts on the tactile sensory system, we performed a series of sensory motor tests over a one-week period followed by three days touch (fur clip and sticky tape tests), thermal (hot / cold plate tests, acetone test, Hargreaves test), and mechanical (von Frey and pin prick) sensitivity testing to determine the basal phenotype before injury.

2.2.1 Light touch sensation assay

For fur clip and sticky tape tests, animals were placed in a 20 × 20 cm acrylic transparent chamber and allowed to acclimatize for 20 minutes. For the clip test we then clipped a 3 mm wide alligator clip to the hair on the animal's back just above the tail. The latency until the animal turned towards the clip or tried to remove it was recorded within a 180 second period. Three applications were performed per animal with a 5 minute-interval between applications, and the average response latency determined for each animal.

The sticky tape test was performed on a separate day. We pasted a 1 × 3 cm sticky tape (3M, MM1530) along the spine to the back fur skin, and measured the latency and the number of times the animal turned backwards in an attempt to remove the sticky tape by biting or licking within a 5 minute-period.

2.2.2 Noxious thermal and cold sensation assay

The hot plate (Dynamic Cold/Hot Plate, Bioseb) was set at 54 °C, and the cold plate at -5 °C. Animals were placed onto the heated / cooled plate with surrounding clear acrylic walls and observed closely. The latency of hind paw reflexes such as flinching, jumping and licking were measured. All animals were tested once. A cut-off time of 30 seconds was set for the 54 °C and -5 °C

MATERIALS AND METHODS

tests to avoid tissue injury.

2.2.3 Sensory-motor function assay

This series of experiments was performed on a subgroup of experimental animals as part of baseline phenotype assays using equipment in the Interdisciplinary Neurobehavioral Core (INBC) of the Medical Faculty of Heidelberg University.

Briefly, for the Rotarod performance test, the animal was placed on the roller (Ugo Basile, Italy), and the latency to the animal falling off the roller recorded. A 300 second cut off period was used.

For the voluntary wheel running test the mouse was placed for 24 hours in the cage where the animal can freely access the wheel, food, and water. The wheel running activity was monitored and recorded via a computer.

The automate home cage monitoring system (LABORAS, Metris) was used to measure habitual behavior patterns from the mouse accurately. We tracked the total travelling distance, average or maximal speed and other behavioral parameters that LABORAS software can record, including rearing, locomotion, climbing, grooming, and immobility behavior. Animals were individually placed in the cage under standard housing conditions with free access to food and water. The test started at 8 am and lasted 24 hours.

To assess gait and locomotion a dynamic weight-bearing behavior system (CatWalk XT, Noldus) was used.. The animal was placed in the access of tunnel, from where the mouse voluntarily traversed a glass plate towards a goal box, while the footprints were captured by a camera. The system visualizes and calculates statistics related to print dimensions as well as the

MATERIALS AND METHODS

time and distance relationships between foot strides. Three trails were performed on each animal. The parameter details are summarized in Table 5.

Table 5. Parameters description of CatWalk XT® software

Parameter	Description
Max Variation	The maximum variation in walking speed in the recorded run.
Average Speed	The average value of dividing the distance that the animal's body travelled from one initial contact of the hind paw to the next by the time to travel that distance.
Run Duration	Duration of walking speed in the recorded run.
Max Intensity	Maximum intensity of the complete paw.
Stride Length	The length of animal's hind paw stride.
Stand Duration	The duration during animal's hind paw standing.
Swing Phase	The phase of the animal's hind paws during a swing.

2.3 Induction of inflammatory pain

Inflammatory pain in mice was induced by intradermal injection of Complete Freund's Adjuvant (F5881, Sigma), which consists of inactive Mycobacterium tuberculosis in mineral oil. Animals were anaesthetized with 3% isoflurane anaesthesia, and 20 µl CFA was injected slowly into the metatarsal region of one hind paw, using a 25-gauge needle,. The needle was held still for 10 seconds to maintain pressure before withdrawing (Fehrenbacher et al. 2015). Animal were placed back to the cage after injection and allowed to recover for at least 24 h before any further testing.

MATERIALS AND METHODS

2.4 Testing mechanical and thermal sensitivity

Animals were habituated on behavior test setups for at least 30 min per day for two days prior to the baseline tests performed before CFA injection. The animals were tested again following the CFA injection under identical conditions. All tests were performed at baseline and on day 1 - 7 after CFA injection, as well as day 14, 21 and 28 to monitor for potential chronic pain sensitivity effects.

Mechanical sensitivity was measured with a set of von Frey hairs (in g; 0.008, 0.02, 0.04, 0.07, 0.16, 0.4, 0.6, 1, and 1.4 g). Animal were placed in transparent plastic box sitting on a metal mesh (Ugo Basile, Italy). The elevated setup allows the experimenter to observe animal behavior while applying mechanical stimulation with von Frey hair. The hair was lifted perpendicular to the mid-plantar surface of hind paw until slightly bent, and held for about 3-6 seconds. A quick withdrawal of the stimulated hind paw or immediate flinching upon removal of the hair were considered as a positive response. Other cases, such as a slow withdrawal, or the animal walking away, required a repeat test. Five trials were applied with each hair with an interval of at least 5 s (Chaplan et al. 1994).

Dynamic mechanical sensation was assessed as described previously (Garrison et al. 2012). For dynamic mechanical testing, animals were placed on the von Frey test setup, and tested after acclimation for 30 minutes. The cotton swab for the cotton test was prepared with sharp forceps by teasing the head of a standard cotton swab and puffing it up to approximately three times of its normal size. For the brush test, small (size 0) paintbrushes were used as reported (Duan et al. 2014) . For each of these tests, the cotton swab / small

MATERIALS AND METHODS

brush was moved from heel to the toe of the hind paw to provide a gentle touch on the paw surface. If the animal reacted by lifting, shaking, or licking the paw, a positive response was recorded. A negative response was recorded if the animal did not show any such behavior. The application was repeated 10 times with a 5 minute interval between trials. The following scoring system was used to assess dynamic allodynia: 0, (none-painful response) brief lifting of the paw; 1, extended lifting of the paw or a single flinch; 2, lateral leg lift and raise to the body level or a fast jump; 3, multiple flinching or licking of the paw.

Pinprick stimulation was used to assess noxious mechanical sensation. The top third of a small insect pin (tip diameter approximately 0.03 mm) was glued to a 1 gram von Frey filament. For the test, the pin was applied to the plantar surface of the left hind paw as for the von Frey test. Care was taken not to injure the plantar skin. If the animal showed nocifensive or aversive behavior (lifting, shaking, licking of the paw), a positive response was recorded. A negative response was recorded if the animal showed no such reaction within 2 seconds of application. The application was repeated 10 times with a 5 minute interval between applications.

The acetone evaporation test was used to assess sensitivity to the cooling effect (Knowlton et al. 2013). Briefly, before the test, the mice were habituated for 30 minutes in an elevated chamber with a mesh floor, and a drop of acetone applied to the plantar skin of the hind paw using a 2 mm diameter tube attached to a syringe. Both paws were assessed, alternating the tested paw between stimulations. The application was repeated 3 times for each paw with a 10 minutes interval between applications. The mouse behavior was observed within the sensitive period for 1 minute following acetone application. We used a cooling score to assess the sensitivity of mice to cooling: 0, no response; 1, brief lift, sniff, flick, or scare; 2, jumping, paw shaking; 3,

MATERIALS AND METHODS

multiple lifts, paw lick; 4, prolonged paw lifting, licking, shaking, or jumping; 5, paw guarding.

Plantar test with Hargreaves apparatus (Ugo Basile, Italy) was employed to examine the sensitivity of animals to thermal stimulation. Mice were placed in the same type of plastic box used for the von Frey test, but on a transparent perspex pane instead of metal mesh. A movable infrared light generator with an intensity of 190 ± 10 mW/cm² under the glass pane was placed under a hind paw and the infrared heat stimulus applied until the paw was withdrawn. The withdrawal latency was recorded automatically by the Hargreaves apparatus. Three or four measurements were taken for each animal with a minimal interval of 5 min to avoid adaptation.

2.5 Induction of expression of Fos protein and *c-fos* mRNA

Animals were divided into two per cage 4 day before stimulation, ensure they can be processed and sacrificed simultaneously, to avoid cross-influence on cagemates. In between of these 4 days, animals were habituated in transparent plastic box sitting on a metal mesh as von Frey behavior test setups for at least 30 min per day. Inflammatory pain was induced by intradermal injection of CFA as same as previously discribed. For the sham control, saline was instead of CFA. Inflammatory pain phenotype was confirmed by a brief von Frey test on day 1 after injection. Apply the first stimulus to the mice, which is the innocuous dynamic mechanical stimulated *c-fos* protein induction, we used a cotton swab to gently swept from heel to the toe of the hind paw planta surface, 300 times with a frequency of 0.5 Hz. 2 hours later apply the second stimulus to mice, which is the innocuous punctate mechanical stimulated Fos mRNA induction, we used a 0.07 gram von Frey filament lifted to the random position from heel to the toe of hind

MATERIALS AND METHODS

paw until it slightly bent, also 300 times with a frequency of 0.5 Hz. Animals were sacrificed 30 minutes after second stimulate.

For nociceptive *c-fos* / Fos induction interval test in spinal cord, we used the pinprick pin described previously to stab the mid-plantar of the hind paw for 20 times as 0.01 Hz frequency, but without any injury or CFA injection. The time point of the stimulate was 15 mins, 30 mins, 3 hours, 4 hours(Figure). Animals were sacrificed immediately after fourth stimulate. For TAI-FISH induction test, we use the pinprick pin as well, and give the first and second stimulate with pinprick pin, in the same way describe before, at time point 30mins and 2.5 hours. Animals were sacrificed 30 minutes after second stimulate.

2.6 Mouse spinal cord tissue preparation

Mice were killed with CO₂ at a planned time point after stimulation. The animals were perfused with prechilled diethyl pyrocarbonate (DEPC) treated PBS, followed by a prechilled 4 % PFA fixative solution. To minimize mRNA degradation and variation between samples, the mice should be sacrificed within 10 seconds, and perfusion should be completed within 10 minutes. The lumbar 3-5 spinal cord were dissect and immediately kept in prechilled 4 % PFA fixative solution for 2 h and then transfer to 30% sucrose-PBS solution at 4 °C for 18 hours. 20 µm coronal sections were collected on adhesion slides (Thermo Fisher, SuperFrost Plus) with a cryotome (Leica, CM1950) and save in -80°C. All equipments in the tissue processing are cleaned with RNaseZAP decontamination solution (Sigma, RNaseZAP), and all reagents are based on DEPC-treated PBS to avoid RNase contamination.

2.7 Dual staining of tyramide amplified fluorescent in situ hybridization with Immunofluorescent

MATERIALS AND METHODS

2.7.1 Plasmid transformation

The plasmid DNA for the *c-fos* in situ probe was obtained from Prof. Dr. Jan Siemens's lab as a gift, and the *c-fos* plasmid DNA sequence map is shown as following (Figure 4). We transformed the plasmid into E.coli with a normal protocol of heat shock method (Froger and Hall 2007). After a short incubation on ice, a 50µl mixture of chemically competent E.coli and DNA was placed at 42°C for 30 seconds (heat shock) and then placed back in ice. We added in 950µl of lysogeny broth (LB) medium then incubated E.coli at 37 °C for 1 hour and shake by 250-300 rpm. After a centrifuge, we removed most supernatants, then resuspend the cell pellet with the LB medium. 50-100 µl suspension cell was placed on each LB agar plate containing ampicillin. After incubated the plates overnight at 37°, we placed one colony to 1-2 ml LB medium, tipped 3 µl 1:1000 ampicillin in LB, 37°C culture for 6 hours to amplification the culture. Lastly, the bacterial solution was been secondarily amplified in 300 mL LB, 37°C culture overnight. The product was used for plasmid DNA extraction.

MATERIALS AND METHODS

applied the supernatant to the QIAGEN-tip and allow it to enter the resin by gravity flow, and washed the QIAGEN-tip with 30 ml Wash Buffer. We eluted DNA with 15 ml elution buffer and precipitated DNA by adding isopropanol to the eluted DNA. Mixed and centrifuged the DNA and carefully decanted the supernatant. Finally, we washed the DNA pellet with 70% ethanol and centrifuged it at $\geq 15,000 \times g$ for 10 min, and air-dried the pellet for 10 min, and redissolved the DNA in 10 mM Tris-HCL (pH 8.5) as 1 $\mu\text{g} / \mu\text{L}$ concentration.

2.7.3 RNA probe preparation

Plasmid DNA from DNA extraction was linearized with a typical restriction digest with different enzymes depending on the proposed cutting site of different hybridization probes as in the following table (Table 6), 37 °C for 1 hour, and stop the reaction in 65 °C for 20 minutes. To synthesis Digoxigenin (DIG) labeling hybridization probes from linearized DNA templates, here we used DIG Labeling Mix kit (Roche, 11277065910) and T7 RNA polymerase (NEB, M2051) or SP6 RNA polymerase (NEB, M0207) according to the *c-fos* sense or anti-sense sequence as the following table (Table 7), 37 °C for 2 hours. For the *c-fos* probe which is longer than 1.5 kb, to improving the hybridization signal and reduce the noise, here we hydrolyzed the probe to a smaller size about 0.5 kb as the following table (Table 8), 60 °C for 12 minutes. Then for all probes, we purified the probe with 7.5M $\text{NH}_4\text{CH}_3\text{CO}_2$, and wash with 100% EtOH. With a secondary wash with 70% EtOH, we resuspended the pellet in 50 μL RNase free water and 50 μL deionized formamide and stored the probe at - 20 °C. For identifying the non-specific binding, we set the sense probe as the control of the anti-sense probe. All the probes were confirmed by agarose gel electrophoresis to determine the products.

MATERIALS AND METHODS

Table 6. Plasmid DNA Restriction digest reagent mixture

Probe	Reagent	Volume(μ L)
	10 x NEB Buffer (Cutsmart Buffer)	3
	Plasmid DNA	12 (30 μ g)
	RNase free H ₂ O	12
<i>c-fos</i> anti-sense	EcoRV-HF	3
<i>c-fos</i> sense	Xho I	
	Total	30

Table 7. DIG labelling probe synthesis reagent mixture

Probe	Reagent	Volume(μ L)
	DTT 0.1M	2
	Transcription buffer, 10x	2
	DIG RNA labeling mix 10x	2
	Linearized DNA template	1
	RNase free H ₂ O	12
<i>c-fos</i> anti-sense	T7 polymerase	1
<i>c-fos</i> sense	SP6 polymerase	
	Total	20

Table 8. *c-fos* probe hydrolysis reagent mixture

Reagent	Volume(μ L)
<i>c-fos</i> probe	20
RNase free H ₂ O	21
0.4 M NaHCO ₃	5
0.6 M Na ₂ CO ₃	5
Total	51

MATERIALS AND METHODS

2.7.4 Tyramine synthesis

For signal amplification of in situ hybridization, a tyramide solution was synthesized. Tyramide synthesis has been performed according to the method of Anton et al (Hopman et al. 1998). We first prepared the N-hydroxysuccinimide solution (NHS), which dissolved Rhodamine-NHS ester in Dimethylformamide (DMF) as 10 mg/mL; Next for the DMF-triethylamine (DMF-TEA) solution, we dissolved Tyramine-HCl in DMF as 10mg/mL, and mixtures with 10 μ L TEA. For the final Rhodamine tyramide synthesis, we incubated 100 μ L NHS solution and 30 μ L DMF-TEA solution together for 2 hours in room temperature, then diluted it with 370 μ L 100% EtOH as a final concentration (2 μ g / μ L) and stored it at 4°C under dark light.

2.7.5 Tyramide-amplified in situ hybridization

All the reagents prepared for tyramide-amplified in situ hybridization base on DEPC-treated water or DEPC-treated PBS. All equipment that had been used was processed with RNaseZap RNase decontamination solution.

For tyramide-amplified in situ hybridization, we first dried out slides at room temperature for 5 minutes, then washed the slides with ice-cold PBS for 3 minutes, repeat three times. Then for acetylation, we treated slides with acetylation buffer (50mL water, 670 μ L Triethanolamine, 72 μ L 37% HCl, 125 μ L acetic anhydride, prepare immediately) for 10 minutes at room temperature. The slides were rinsed once with cold PBS, then permeabilized with 0.3% TX100-PBS, 20 minutes at 4°C. For hybridization, slide was placed into the humid chamber and apply hybridization buffer (approx. 500 μ l) and incubated for 1h. Diluted probe (1:75 in hybridization buffer, heat 5 minutes at 80 °C) was applied to the slides (150 μ l) and covered with a coverslip, hybridized overnight at 65°C. Control slides applied sense probe to instead anti-sense probe.

MATERIALS AND METHODS

For the post-hybridization wash, we washed the slide twice with 2 x SSC / 0.1% N-Lauroylsarcosine / 50% formamide at 60°C. The slide was rinsed in RNase buffer (10 mM Tris, pH 8.0, 500mM NaCl, 1mM EDTA), then digested with 20 µg/ml RNaseA in RNase buffer, 15 minutes, 37°C. After we washed slides twice with 2 x SSC / 0.1% N-lauroylsarcosine and 0.2 x SSC / 0.1% N-lauroylsarcosine for 20 minutes at 37°C, slides were rinsed once again with MABT (maleic acid buffer with 1% of Tween 20) and placed into the humid chamber. Blocking buffer (MABT with 10% heat-inactivated goat serum and 1% Blocking reagent (Roche, 11096176001)) was applied on the slides, incubated for 1 hour at room temperature. Then the slides were incubated with anti-DIG-POD (Roche, 11207733910) antibody solution (1:1000 in Blocking reagent) in humid chamber at 4°C, overnight.

For signal amplification, we first washed with MABT 30 minutes at least 6 times. Then we equilibrated slides 5 minutes at room temperature in TSA buffer (10 mM imidazole in PBS) and incubated them with TSA staining solution (Dilute Rhodamine tyramide 1:50 in TSA buffer, add 0.01% H₂O₂ before use) for 30 minutes at room temperature in the dark. After reaction, the slides were washed with PBST (PBS with 1% of Tween 20) for 10 minutes and repeated 5 times at room temperature in the dark.

For immunofluorescent-Tyramide-amplified in situ hybridization co-staining, here we incubated the tissue with primary antibodies in PBST at 4°C as a fixed dilution (Table 9), overnight. At the following day, these slides were washed 4 times for 5 min in 0.2% PBST and then incubated with species-specific fluorescent secondary antibodies (Table 10) in PBST for 1 hour at room temperature. Finally, we washed it with PBST for 10 minutes, 3 times, then rinsed with 10mM Tris-HCl for 10 minutes and mounted the slides in Mowiol mounting medium.

MATERIALS AND METHODS

Table 9. TAI-FISH and dual-TAI-FISH primary antibodies

Antibody	Isotype	Company	Dilution
Anti-Fos	Rabbit	Abcam	1:1000
Anti-PKC- γ	Guinea Pig	Frontier Institute	1:500
Anti-Calretinin	Mouse	Swant	1:1000
Anti-IB-4	Biotin conjugate	Sigma	1:500
Anti-PV	Guinea Pig	Swant	1:2000

Table 10. TAI-FISH and dual-TAI-FISH secondary antibodies

Antibody	Company	Dilution
Donkey anti Rabbit Alexa 488	Invitrogen	1:700
Donkey anti Guinea Pig Alexa 647	Invitrogen	1:700
Donkey anti Mouse Alexa 647	Invitrogen	1:700
Donkey anti Mouse Alexa 594	Invitrogen	1:700
Donkey anti Mouse Alexa 405	Invitrogen	1:700

2.8 Imaging

We imaged the slides using a confocal microscope (Leica, SP8) with a 20 \times objective lens. Rhodamin (reporting *c-fos* mRNA) and Alexa 488 (reporting c-Fos protein) fluorescent signals can be visualized by using 552-nm and 488-nm laser wavelengths, respectively. In addition, Alexa 405 and Alexa 647 fluorescent can be visualized by using 405-nm and 638-nm laser wavelengths, respectively. Single-layer images were taken with a 2048 \times 2048 pixel size for data analysis.

2.9 Cell counting and data analysis

We processed the images and analyzed the data blindly in a random manner.

MATERIALS AND METHODS

We processed the control and experimental groups in parallel. With the image processing software Image J, we adjusted the brightness and contrast of the images and processed them with the same amplification magnitude for manual signal counting. The c-Fos protein signals should be 6–10 μm in diameter, present in the nucleus, and be solidly circular or oval-shaped. Typical *c-fos* mRNA signals occur in the cytoplasm as 8–14 μm diameter particle clusters. The mean gray value of an unlabeled spinal region inside the microscopic field is used to calculate the background signal. The signal intensities of mRNA and protein are typically at least 80 times higher than the background value. The c-Fos protein and *c-fos* mRNA signals are tallied separately, and co-labelling is decided by overlap in the merged channel. Determine the relative position of c-fos protein or *c-fos* mRNA in the spinal cord lamina I-V using the image J point tool and the reference co-staining markers IB-4. We counted the number of Fos protein and *c-fos* mRNA positive neurons in the double-labelled slices to calculate the overlap ratio in the spinal cord regions with convergent and mixed patterns. For the overlap ratio, overlapping cell counts was divided by Fos protein or *c-fos* mRNA positive cell counts, represent overlap ratio in Fos protein or *c-fos* mRNA, respectively.

2.10 Marker signal image transformation

For the standard spinal cord lamina distribution, a CGRP, IB-4, PKC- γ fluorescent immunohistology co-staining was been taken on naive littermate control mice spinal cord lumbar 4 tissue slides (Figure 5A). According to the sample image, we approximately located the lamina I - V distribution as an atlas map, given out the 6 reference point dividing line information according to anatomical features of this image.

For image alignment, we gave 6 control points position information according

MATERIALS AND METHODS

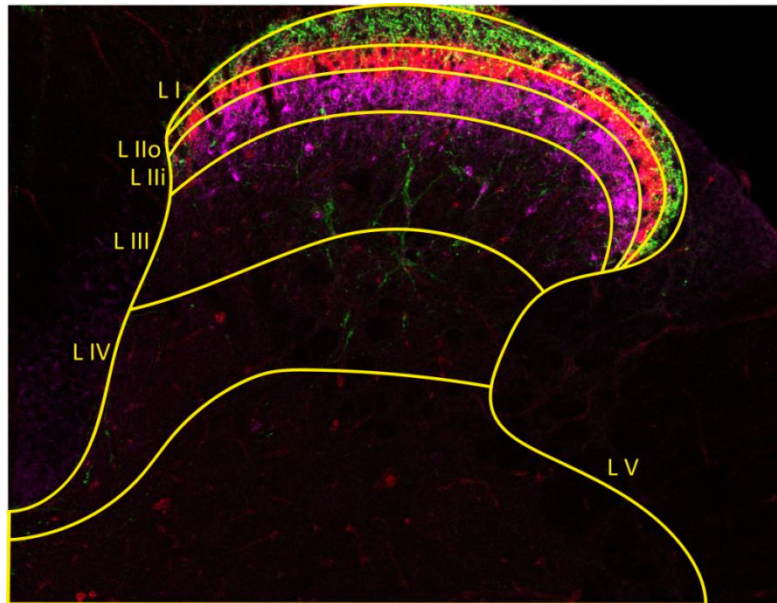
to the spinal cord anatomy that was manually annotated on the dividing line between white matter and gray matter of the image. All images are aligned according to manually annotated control points, which allows direct analysis of the signal accumulation on the 2D flat. The work of image alignment and distribution analysis was performed by our partners from the Biomedical Computer Vision Group at Heidelberg University.

Cartesian coordinates for each neuron were determined in the transverse spinal cord plane with respect to the midpoint of the central canal, defined as the central position. All the position information of different signal channels and co-labeling are given out to this standard atlas map, according to the positional relationship with respect to the reference point. Finally, the transformation of the position data on the standard atlas map was accumulated from different mouse samples and slices of lumbar 3, 4, or 5, respectively (Figure 5B).

The signal distribution was represented by an accumulation plots graph made comprised of plots from different mice in the same group. We then calculated the value of the relative frequency of occurrence of each signal plot using the continuous distribution of discrete distribution points based on the graph's location information (Figure 5B). Estimate values were shown graphically as heat maps with equal probability density.

MATERIALS AND METHODS

A



B

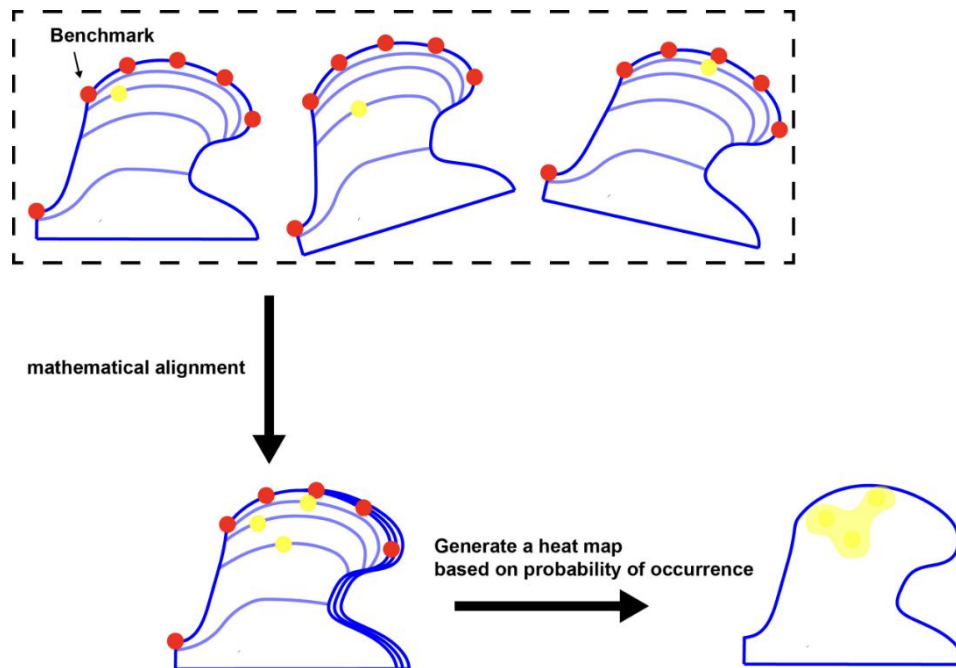


Figure 5. Schematic of Marker signal image transformation method. A, Standard spinal cord immunohistology co-staining of CGRP, IB-4, and PKC- γ shows the lamina anatomy distribution; **B**, schematic of image transformation and spatial analysis.

MATERIALS AND METHODS

2.11 Data analysis and statistics

Here we used mean \pm SEM to express all the data in figures and text. Graphpad Prism software was used for statistical analyses. Paired or unpaired Student's t-test were performed as appropriate for a single comparison. A one-way ANOVA test was employed to compare more than two groups, followed by Tukey's post-hoc test or Dunnett's post-hoc test that alone multiple comparisons. Two-way ANOVA was employed for the comparison between groups, followed by a Bonferroni post-hoc test. For all the tests, a *p*-value $<$ or equal to 0.05 was considered significant.

MATERIALS AND METHODS

Project 2: Cellular basis for prefrontal modulation of inflammatory pain by fear

2.12 Animal

The animal experiments are performed in accordance to EU and national regulations for animal experimentation and all animal work was approved by the local ethics committee Regierungspräsidium Karlsruhe, Germany (Refrance number: 35-9185.81/G-205/18). C57BL/6J wild type mice (25-30 g; 8-15 weeks old) were obtained from Charles River, Sulzfeld, Germany. Mice were housed one animal per cage, with free access to rodent chow and water, in temperature- and humidity-controlled rooms with a 12 h light/dark cycle.

2.13 Virus combination preparation (performed by Oscar Andrés Retana Romero)

The cloning method for the pAAV-cFos-tTA construct has been published and publicly available (Zhang et al. 2015) . The rAAV-hSyn-ArchT2A-Venus AAV1/2 virions were a kind gift from Rolf Sprengel (Tan et al. 2017). For generating the AAV-TREtight-ArchT2A-Venus, the ~1.7 kB ArchT2A-Venus cassette was PCR amplified (forward primer with an AscI site: 5'-ATGCTATTTGGCGCGCCCGAGGCTGTGAGC-3'; reverse primer: 5'-CGGACCTAGTTCGAGTGCGGCCGCTTTACT-3') and subcloned with AscI and BsrGI into parent vector pAAV-ITR-PTREtight-hM3Dq-mCHERRY-WPRE-pA-ITR (Addgene Ref. 66795) to create the final pAAV-ITR-PTREtight-ArchT2A-Venus-WPRE-pA-ITR and pAAV-ITR-PTREtight-ChR2-eYFP-WPRE-pA-ITR plasmids. Recombinant AAV1/2 virions were generated by calcium phosphate co-transfection of HEK293 cells (Stratagene) with each of the above-mentioned plasmids, and

MATERIALS AND METHODS

plasmids pDP1rs and pDP2rs (Plasmid Factory, Bielefeld, Germany; Refs. 401 and 402). These constructs provided adenoviral helper functions as well as the AAV-1 rep, AAV-2 rep and AAV-2 cap genes. Cells were lysed by freeze-thaw cycles and subjected to benzonase nuclease (Merck) digestion to retrieve the crude lysate. The rAAV1/2 particles were then purified via heparin-agarose (Merck) affinity chromatography and concentrated with Amicon filter tubes (Merck Millipore). The AAV1/2-TREtight-hChR2(H134R)-EYFP2 virus was a kind gift from Martin Fuhrman's lab. The pAAV-TREtight-ArchT2A-Venus described above was generated by Oscar Andrés Retana Romero and Chris Njoo and all the virus preparations were performed by Karin Meyer in our laboratory.

2.14 Virus injection and optogenetic dual-implants

Mice were generally anesthetized with intraperitoneal doses of Fentanyl (Janssen-Cilag, Neuss, Germany; 0.01 mg / kg); Medetomidine (Alvetra, Neumünster, Germany; 0.3 mg / kg) and Midazolam (hameln pharma plus, Hameln, Germany; 4 mg / kg). Pedal reflex caused by a firm toe pinch was monitored regularly to ensure continued surgical plane of anesthesia. The animals were affixed in flat-skull position with a stereotaxic alignment system (David Kopf Instruments) and Dexpanthenol ophthalmic ointment (Bayer) was applied to both eyes. Normal body temperature was maintained with a thermal pad (Supertech Instruments, London, UK) throughout the procedure. Median skin incision over the skull and preparation of the pericranium were performed under local anesthesia with 1% lidocaine spray (AstraZeneca). Bregma was identified as the midpoint of the curve of best fit along the coronal suture (Golmohammadi et al. 2008), assisted by a stereo microscope (Leica).

MATERIALS AND METHODS

For the virus injection, with the origin set to bregma, small craniotomies were performed bilaterally with a micromotor (Osada, model OS 40) fitted with a surgical drill tip (Gebr. Brasseler, Lemgo, Germany) over the prelimbic cortex (± 0.25 mm lateral; + 1.9 mm anterior; - 1.35 mm depth from the pia, or ± 0.9 mm lateral; + 1.94 mm anterior; - 1.6 mm depth with 15° sagittal tilt from the midline when implanting chronic optical fibers) (Golmohammadi et al. 2008). Purified virus preparations were suctioned into a glass micropipette (Merck, BR708707) with a fine tip (P-87 micropipette puller, Sutter Instruments) and injected at the points of interest with a flow rate of 25 nL / min and a total injection volume of 300 - 400 nL per side.

Optical fiber implants consisted of a ceramic ferrule (Thorlabs, CFLC230-10) fitted with an optical fiber ($\text{\O} = 200 \mu\text{m}$; NA = 0.39; Thorlabs, FT200UMT) extending 1.9 mm from the ferrule base, and were implanted immediately after the viral injections. The tip of the optical fiber was positioned 50 μm above the injection site and the ceramic ferrule fixed to the skull with Paladur dental cement (Heraeus).

After the surgical procedure, the wound was closed with a 5/0 USP polyglycolic acid suture (Catgut, Markneukirchen, Germany). The stitches were strengthened with Histoacryl tissue adhesive (Braun, Melsungen, Germany) and disinfected with Iodopovidone (Braun). General anesthesia was antagonized with intraperitoneal doses of Naloxone (Inresa Arzneimittel, Freiburg, Germany; 0.4 mg / kg), Flumazenil (Fresenius, Bad Homburg, Germany; 0.5 mg / kg) and Atipamezole (Prodivet pharmaceuticals, Belgium; 2.5 mg / kg). Additionally, the mice received analgesic treatment with Carprofen (Norbrook Laboratories, Northern Ireland; 5 mg / kg). The cages were placed on a warming plate and continuously monitored until the mice recovered upright posture and normal gait.

MATERIALS AND METHODS

2.15 Fear condition and recall behavior

Animals were placed on 200 mg/kg doxycycline (Dox) chow (ssniff Spezialdiäten GmbH, Germany) before virus injection and optical fiber implants. After a 10-day recovery period from virus injection and optical fiber implantation, animals were acclimatized 30 minutes in the morning and afternoon for 2 days in the fear condition chamber and context. Baseline freezing behavior was assessed over 7 minutes following a 90-second habituation period in the fear condition chamber one day before fear conditioning. Animal behavior was recorded by a camera placed underneath the fear conditioning setup and spontaneous freezing or immobility detected by ANYmaze software (Stoelting). Fear conditioning (FC) took place in a different context by placing a blue plastic container around the fear conditioning chamber (Ugo Basile). After 90 s habituation, 5 tones (5 kHz, 75 dB, 30 s) were played in a 7 minutes period with semi-random intervals and paired to a mild electric foot shock (0.6 mA, 1 s) applied during the last second of each tone. The fear conditioning session was repeated after an interval of 3 h to obtain a robust fear memory. Fear engram labeling was carried out 21 days after fear conditioning by placing animals back in the fear recall (FR) context in the DoxOFF state. To take animals off Dox, they were first placed for 48 hours on a 40 mg/kg doxycycline diet followed by 72 hours on normal chow without doxycycline. Animals were subjected to the FR labeling session in the DoxOFF state by placing them back in the same context and again playing the tone (7 min period with semi-random intervals, 5 times 30-sec tone) without foot shock, but also after a 90 s habituation in the same chamber. Freezing behavior and immobility during fear condition and fear recall labeling sessions were also recorded and measured by ANYmaze software. Animals were placed on a 1000 mg/kg doxycycline diet (ON Dox) 1.5 hours after the FR session and return to 200 mg/kg doxycycline diet after 2 days.

MATERIALS AND METHODS

2.16 *In vivo* optical stimulation

For the optical suppression in ArchT-expressing mice we used a yellow diode laser ($\lambda = 589$ nm, Shanghai Laser & Optics Century Co. Ltd., China). The laser power output setting was measured with a calibrated power meter (Thorlabs, PM100D) and adjusted individually to obtain 1.5 mW at the tip of each optic fiber before the implant. Yellow laser illumination was constant over the length of the behavioral testing period. For optical stimulation of mPFC of ChR2-expressing mice, we used a blue diode laser ($\lambda = 473$ nm, Shanghai Laser & Optics Century Co. Ltd.). Light transmission was also measured with the power meter at the tip of the optical fiber before implanting. Light power was then measured daily before experiments at the tip of the optical patch cord. A pulse generator (Meilhaus Electronic GmbH, Germany) was used to generate 20 Hz laser pulses with a pulse length of 10 ms at an intensity of 8 mW at the tip of the patch cord before connecting to the implanted ferrule. Two optical patch cables were connected to the ferrule base of dual-implants of the animal by using forceps before the test. Yellow/blue light filtered protective glasses were used by the experimenter for blinding during behavioral testing to avoid subjective judgment.

2.17 Fear recall testing

Two days after fear recall labeling, animals were connected to optical patch cables (Doric, $\text{\O} = 200$ μm ; NA = 0.5) and exposed to two further fear recall sessions (5 times 30 s tone in the conditioned fear context as for the fear recall labeling session) in successive days with the laser either on or off for the entire 7 min assessment period. Freezing and immobility periods were detected by the ANYmaze software. The same tone and fear context session with or without optical stimulation was performed 1.5 hours before sacrificing animals at the end of the experiment to assess Fos induction.

MATERIALS AND METHODS

2.18 Heat hypersensitivity Hargreaves test

The animals were habituated at least 4 days before the CFA injection. After connected optical patch cables and turning the laser on or off, animals were placed in the transparent plastic box and on the glass pane of the apparatus. With a 15 minutes accommodation, the movable infrared generator with the intensity of 270 ± 10 mW/cm² under the glass pane was applied and measured hind paw withdraw latency automatically. 3 or 4 measurements were taken for each animal with an interval of 5 min to avoid repeated heat stimulation generated.

2.19 Aversive related white noise test

To test for real-time place aversion of white noise (Mollenauer et al. 1992), the setup consisted of two chambers (15 cm x 15 cm each) with a neutral middle chamber (8 cm x 8 cm) separated by removable clapboards. Each of the chambers contained different distinct visual (horizontal or vertical stripes) and olfactory (milk or berry) odor cues. Two audio speakers were placed on each side of the setup. Mice were connected to the optical patch cables and initially placed in the middle chamber with the laser turned on or off. After the removal of the clapboards, mice were allowed to freely move in the whole apparatus for 20 minutes. Animal movement patterns were recorded by a video camera placed above the setup and tracked with ANYmaze software (Stoelting).

For the baseline session, the animal was freely moving in the apparatus with the laser turned off in the absence of white noise. Meanwhile, the chamber in which the animal spent more time during the baseline period (the preference chamber) was paired with white noise played over both speakers in two subsequent real-time place aversion sessions on days 5 and 6 following fear

MATERIALS AND METHODS

engram labeling with laser turned on or off. The sequence of the laser being turned on or off was random, but balanced, to avoid potentially confounding effects over time from FR engram labeling. Animals again had free access to all chambers but white noise (90 dB) was played automatically whenever the animal entered the preferred chamber. Movement patterns were recorded by the camera and ANYmaze software throughout each 20 minute assessment period.

2.19.1 Open field test

The open field (OF) test was performed on day 7 following fear engram labeling. The animal was attached to the fiberoptic patch cords, placed in the centre of the OF chamber and allowed to move freely within the OF chamber for a 10 min assessment period. The laser was turned off or on either during the first or second 5-min period in a balanced fashion. Movement patterns were recorded via a video camera placed above the OF chamber and measured via ANYmaze software. To assess anxiety-like behavior the OF arena was divided into three zones, consisting of centre, intermediate and an outer area.

2.19.2 Elevated plus maze test

The test uses an elevated, plus-shaped apparatus with two open and two enclosed arms. The elevated plus maze (EPM) test was performed on day 8 following fear engram labeling. The animal was placed in the centre of EPM apparatus and allowed to move freely along the tracks for a 10 min assessment period. The laser was turned off or on either during the first or second 5-min period in a balanced fashion. A video camera above the setup was used to track the animal movement pattern via ANYmaze software. To assess anxiety-like behavior the EPM arena was divided into three zones, the centre, the open arms, and the closed arms.

MATERIALS AND METHODS

2.20 Heat stimulus and Fos induction

Inflammatory pain was induced by intradermal injection of Complete Freud's Adjuvant (CFA) on left hind paw 3 days after fear recall labeling. Sham control animals were injected with 0.9 % saline instead. Two days after injection, animals were placed in the plastic box on the transparent perspex pane of the apparatus used for the Hargreaves test. After 20 minutes of acclimation, heat stimuli were applied to the affected hind paw via the infrared generator using an intensity of 270 ± 10 mW/cm² and measuring the withdrawal latency automatically via the Hargreaves apparatus. Ten stimuli were applied using a minimal interval of 1 minute. Animals were placed back in the home cage for 90 minutes and then sacrificed, perfused transcardially by PBS and 4 % PFA. Brains were dissected immediately, post-fixed in 4 % PFA at 4 °C overnight, and 50 µm coronal sections collected with a vibratome (Leica, VT100S). Brain sections were kept in anti-freeze solution at -20 °C until immunohistological staining.

2.21 Capsaicin-induced acute nocifensive behavior

A capsaicin (Sigma) injection solution was prepared from a stock solution of 1 % (weight/vol) in 10 % DMSO by diluting with PBS to 0.02 % before use. Two optical patch cables were connected to the ferrule base of dual-implants of the animal by using forceps before the test. Animals were briefly anesthetized with 2 % isoflurane (Baxter, Unterschleißheim, Germany) and 20 µL of the capsaicin solution was injected with a 30G needle subcutaneously into the plantar surface of the hind paw. Animals were then placed in a transparent box (20 x 20 cm) on an acrylic glass plate, with a optical activation with blue light (). The total time the animal displayed nocifensive behavior (paw lifting, licking, flinching, writhing) was assessed over a period of 5 min by an experimenter blinded to the treatment condition. In addition, the nocifensive behavior was recorded with a firewire camera (UniBrain,

MATERIALS AND METHODS

Greece; Fire-i, BBW 1.3) through the acrylic glass floor over the 5 min monitoring period.

2.22 Fos immunohistology

Sacrifice the animal with CO₂, then the animals were perfused with PBS, followed by 10 % formalin (Merck) fixative solution. The extracted brains were kept in 10 % formalin fixative for 24 h at 4 °C and 50 µm coronal sections collected with a vibratome (Leica, VT100S) and save in anti-freeze solution in -20°C. Tissue sections were washed at room temperature with 50 mM Glycine (AppliChem) for 10 min and treated with 10 % normal donkey serum (Abcam) and 0.2 % Triton X-100 (Carl Roth) blocking solution for 60 min. Fos (Synaptic Systems, 226003; 1:5,000 dilution, host: rabbit) Primary antibodies were diluted in blocking solution (1:1000) and incubated with the brain sections at 4 °C overnight. The sections were then washed twice with 10% horse serum in PBS for 10 min at room temperature, incubated with Donkey anti-rabbit Alexa 647 (Invitrogen, A-31571) secondary antibody (1:700) and DAPI (1:10,000) in 10% horse serum in PBS for 1 h, washed twice with PBST. Lastly, the sections were washed for 10 min in 10 mM TRIS/HCl (Carl Roth) before mounting on glass slides with Mowiol (Carl Roth).

2.23 Image acquisition and quantification

Coronal sections from 1.8 mm to 2.4 mm anterior to bregma were used for analysis. Immunofluorescence in the dorsomedial region of the mPFC was visualized with a LCS SP8 confocal microscope (Leica, Germany). Confocal image stacks (scanned at 2 µm-thick planes) were acquired with a 20x objective using identical illumination exposure parameters for sections used for counting. Stacked images taken were maximally projected and subsequently overlaid with the corresponding atlas section to anatomically define the region of interest for quantification (Golmohammadi et al. 2008).

MATERIALS AND METHODS

All sites of injection were inspected for the correct location of transgene expression at the end of all experiments, and animals with off-target expression sites were excluded from the analysis. ImageJ software was used to visualize and count all Fos+, ArchT-Venus+ and ChR2-EYFP+ cells within the boundaries of the defined regions. A cell was considered positive only if it displayed an intensity value above the intensity threshold of the background. Experimenters were blinded to the identity of the sections they were analyzing.

2.24 Data analysis and statistics

Here we used mean \pm SEM to express all the data in figures and text. Graphpad Prism 8.0 software was used for statistical analysis. Paired or unpaired Student's t-test was performed with each for a single comparison. A one-way ANOVA test was employed to compare more than two groups, followed by Tukey's post-hoc test allowing multiple comparisons. Two-way ANOVA was employed for the comparison between groups, followed by a Bonferroni post-hoc test. For all the tests, a *p*-value $<$ or equal to 0.05 was considered significant.

RESULTS

3 Results

3.1 Conditioned knock-out of GABAA β 3 does not impact motor function

GABAergic presynaptic inhibition is linked to sensory-motor regulation and is involved in lateral inhibition, which contributes to spatial and temporal acuity in other sensory systems (Raccuglia et al. 2016; Göttsche et al. 2016; Buldyrev and Taylor 2013). Recently, a variety of non-evoked measures have been introduced to investigate changes in animal well-being as potential readouts for spontaneous pain or fine movement. Among these measures are voluntary wheel running, home-cage monitoring, and gait analysis (Tappe-Theodor and Kuner 2014). To verify the effect of the conditional knock-out of the GABAA β 3 subunit on motor function in mice, we tested voluntary motor behavior of SNS-GABAA β 3 and Advillin-GABAA β 3 mice using the voluntary wheel running test. There were no significant differences between the knockout mice and the control group, either in the activity profile over 24-hours (Figure 6A) or in the total distance of locomotion during 24 hours (Figure 6B). We also tested the passive locomotor behavior of SNS-GABAA β 3 and Advillin-GABAA β 3 mice using the Rotarod test. The time on the rotarod was not different between knock-out and control mice (Figure 6C). This demonstrates that conditional knock-out of the GABAA β 3 receptor subunit in most DRG neurons (Advillin) as well as nociceptors (SNS) does not affect locomotor function.

To explore further innate behavior in SNS-GABAA β 3 and Advillin-GABAA β 3 conditional knockout mice, home cage activity was monitored using the automated Laboras system. Amongst the measured activity parameters collected over a 24-hour period, no differences were apparent between SNS-GABAA β 3 and littermate control mice. However, Advillin-GABAA β 3 mice were more active than control mice, showing higher total distance

RESULTS

traveled (Figure 7A) at higher average speed (Figure 7B) and over a longer duration (Figure 7D) but less grooming behavior (Figure 7G). This suggests that deletion of the GABAA β 3 subunit in DRG neurons affects voluntary movement patterns. A recent study also reported that, Advillin-GABAA β 3 knock-out mice increased their exploratory behavior, spending more time in the center chamber of the open field test and displaying less aversion to the open arms of the elevated plus-maze test (Zimmerman et al. 2019).

Additionally, we monitored changes in weight distribution and various gait parameters using the CatWalk system (Noldus). While none of the gait parameters for Advillin-GABAA β 3^{-/-} mice differed from littermate controls, SNS-GABAA β 3^{-/-} mice spent more time in a standing position than control mice from the same litter (Figure 8D) and spent more time running (Figure 8A) albeit at lower average speed (Figure 8C) and during running showed a prolonged swing phase (Figure 8G).

RESULTS

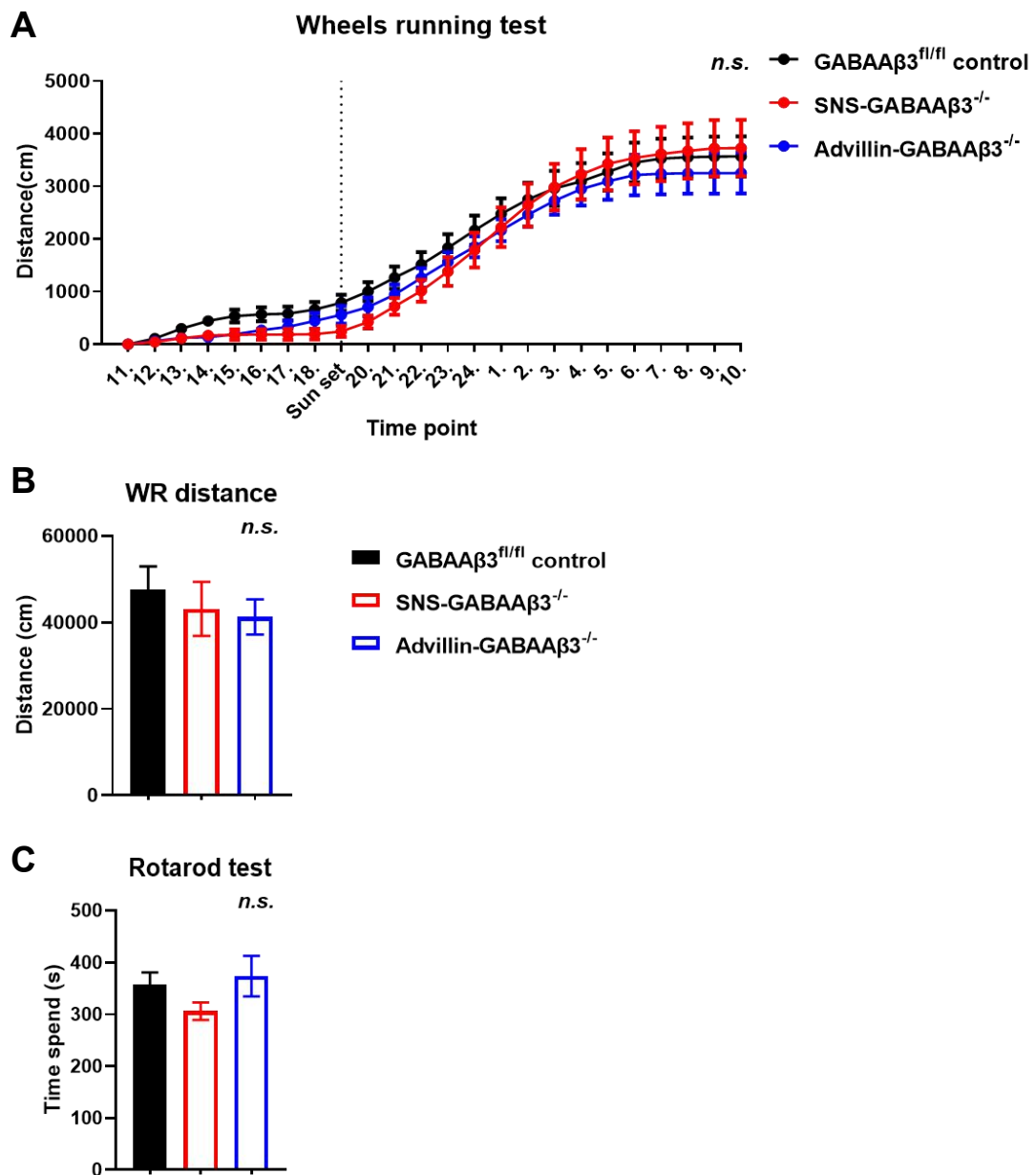


Figure 6. Voluntary motor behavior and passive locomotor behavior of GABAA β 3 knock out mice. **A**, Voluntary wheel running distance profile of grouped mice at day. **B**, Voluntary wheel running distance of grouped mice. **C**, Time spent on the rotarod of grouped mice. Running distance (cm) of untrained of grouped mice which were housed individually and only measured once before injury. 12 mice per group, one-way repeated-measures ANOVA with post-hoc Tukey test. All data points represent mean \pm SEM.

RESULTS

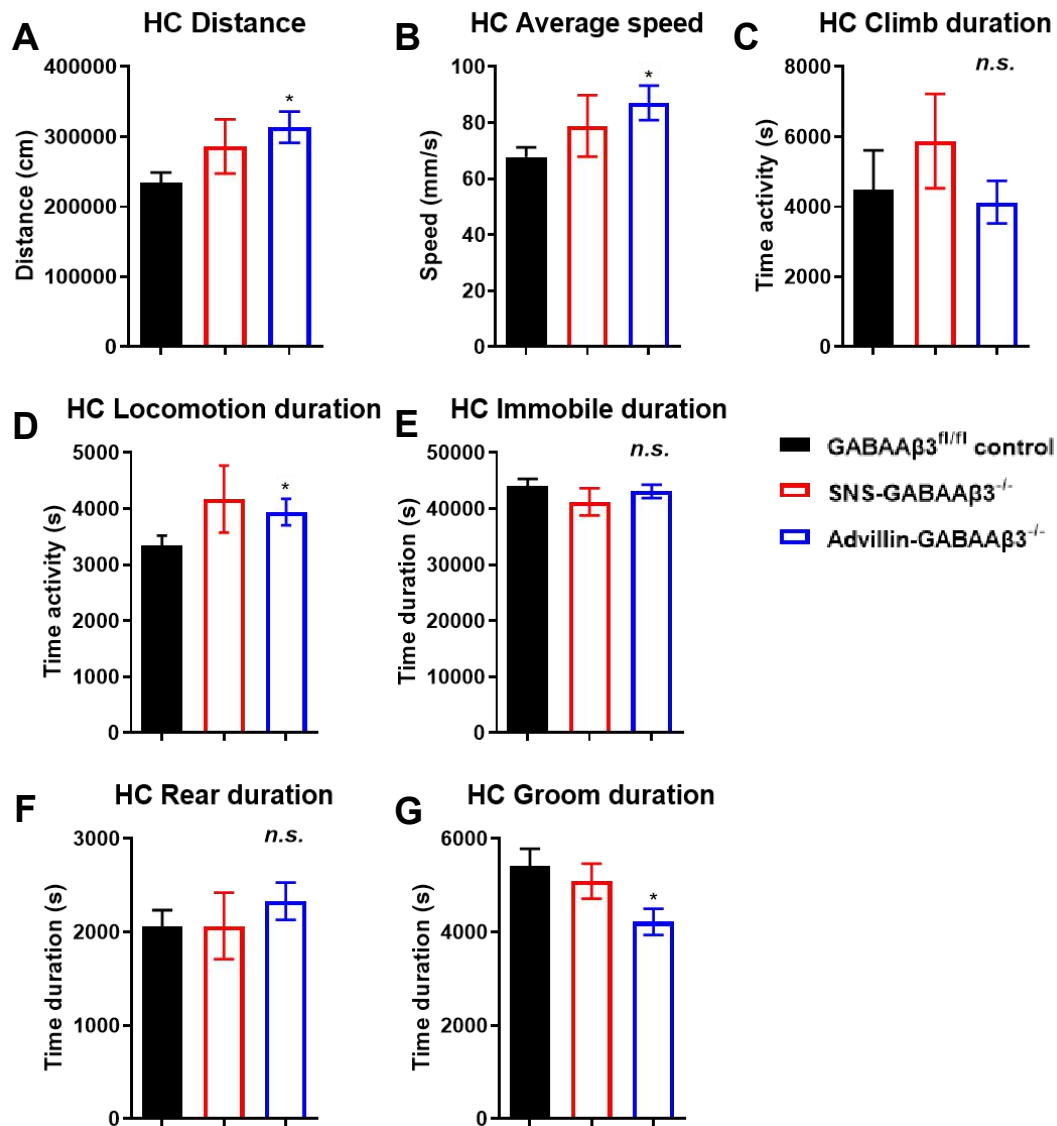


Figure 7. Home cage behavior of GABAA β 3 knockout mice. Different Home cage behavior parameters of grouped mice. **A**, distance of grouped mice moved in home cage in 24 hours. **B**, average moving speed of grouped mice in home cage in 24 hours. **C**, Time spend on climb behavior of grouped mice. **D**, Time spent on locomotion behavior of grouped mice. **E**, Time of immobilization of grouped mice. **F**, Time spent on rearing behavior of grouped mice. **G**, Time spent on grooming behavior of grouped mice. Mice were analyzed for their 24 h voluntary behavior in home cage at basal level before injury. $p < 0.05$ indicated by *, as compared to control group. 12 mice per group, one-way repeated-measures ANOVA with post-hoc Tukey test. All data points represent mean \pm SEM.

RESULTS

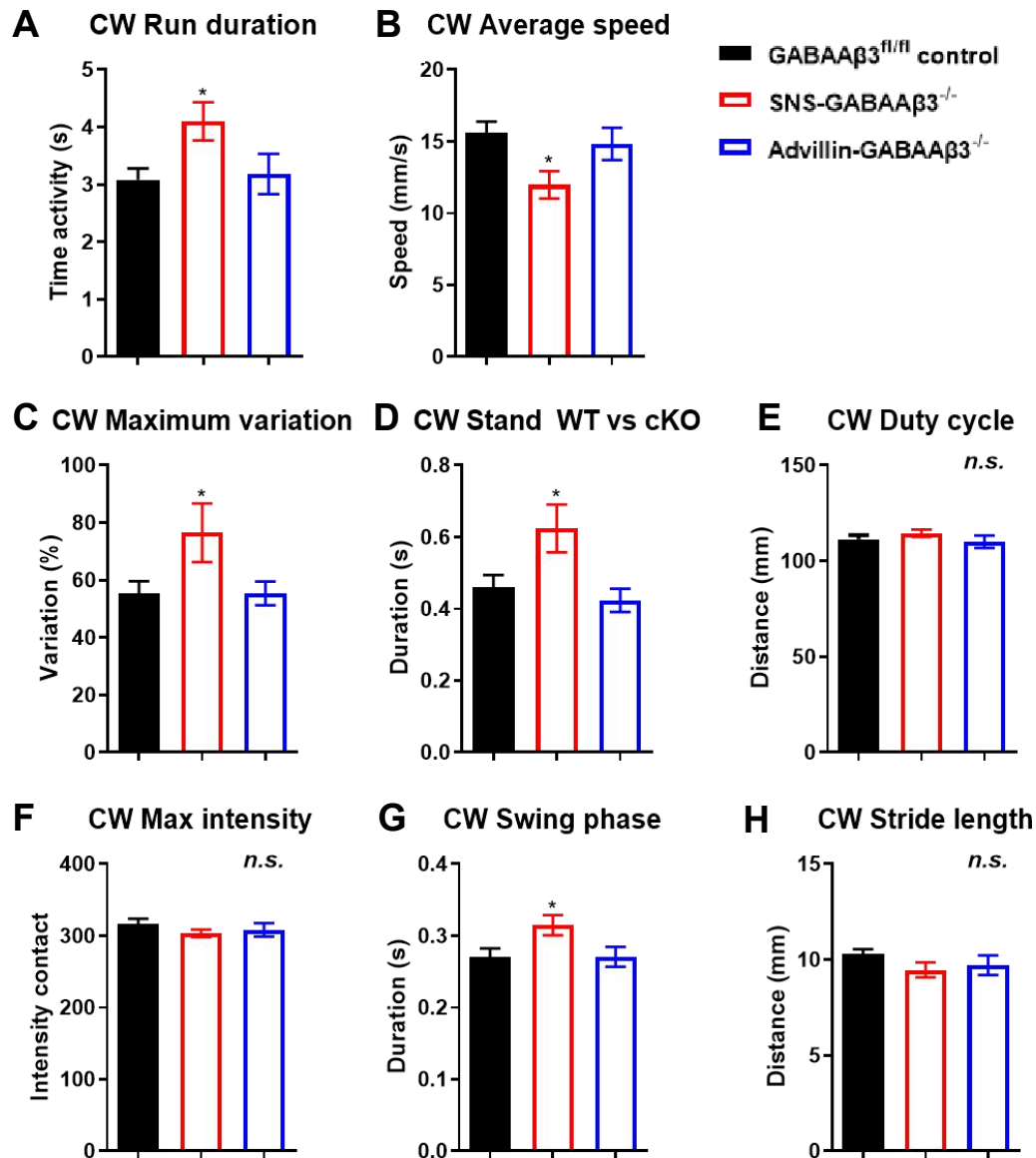


Figure 8. Changes in static weight parameters of GABAA β 3 knockout mice using the CatWalk system (Noldus). Different static weight parameters of grouped mice. **A**, duration of the grouped mice moving through the CatWalk system. **B**, average moving speed of the grouped mice. **C**, the maximum variation in walking speed. **D**, the time spend on stand behavior. **E**, the distance of the entire step cycle. **F**, Maximum intensity contact area of the complete paw. **G**, the duration of the hind paws of the grouped mice. **H**, the length of the grouped mice hind paw stride. Mice were analyzed for their 24 h voluntary behavior in home cage at basal level before injury. $p < 0.05$ indicated by *, as compared to control group. 12 mice per group, one-way repeated-measures ANOVA with post-hoc Tukey test. All data points represent mean \pm SEM.

RESULTS

3.2 Impact of conditional GABAA β 3 knock out on somatosensation

Responses to several behavioral tests of basal somatosensation were used to determine the effect of GABAA β 3 knockout in nociceptive and non-nociceptive DRG neurons.

3.2.1 Innocuous touch sensation

Innocuous touch was assessed using an adhesive tape removal test and a fur clip test (Peirs et al. 2015b). The latency (time) to removal of adhesive tape was not different between knock-out and control mice, either for Advillin-GABAA β 3^{-/-} or SNS-GABAA β 3^{-/-} mice (Figure 9A). Similarly, the response latency for the fur clip test did not differ between Advillin-GABAA β 3^{-/-} mice, SNS-GABAA β 3^{-/-} mice and littermate controls (Figure 9B). This suggested that GABAA β 3 knockout mice have no deficit in D-hair related innocuous touch sensation or sensorimotor function.

3.2.2 Innocuous punctate and dynamic mechanical sensation

According to recent studies, mice exhibit differential behavioral sensitivity to punctate and dynamic (i.e. caused by deflection) mechanical stimuli (Cheng et al. 2017). Accordingly, two independent behavioral tests were used to examine mechanical sensitivity. The von Frey test was used to assess punctate mechanical sensitivity by determining the von Frey filaments threshold required to evoke hindlimb withdrawal when applied to the plantar surface of the hind paw. Dynamic mechanical sensitivity was assessed with a paint brush or cotton swab also applied to the plantar surface of the hindpaw. We found no significant changes in either punctate or dynamic mechanical sensitivity in SNS-GABAA β 3^{-/-} mice as compared to their littermate controls (Figure 9C, D,

RESULTS

E). However, Advillin-GABAA β 3^{-/-} mice showed prominent hypersensitivity to von Frey stimuli (Figure 9C). This is consistent with a previous study that Advillin^{CreER}-GABAA β 3^{-/-} mice also exhibited glabrous skin hypersensitivity, as assessed using von Frey filament stimulation of hind paw glabrous skin (Zimmerman et al. 2019). In contrast responses dynamic brush or cotton were not affected (Figure 9D & E).

3.2.3 Thermal sensation

In a previous study, we found that mice lacking GABAA β 3 in primary nociceptors displayed an increased sensitivity to thermal stimuli in classical plantar Hargreaves test (Chen et al. 2014). In the current study, noxious heat sensitivity was determined using a hot plate test (50°C) and heat sensitivity was assessed using the plantar Hargreaves test. Sensitivity to cold and cooling sensation were determined respectively using a cold plate test (-5°C), and an acetone evaporation test. For the hot / cold plate tests, the latency to hind paw withdrawal reflexes such as flinching, jumping, and licking were measured while for the acetone evaporation test a score was given based upon the response, specifically: 0, no response; 1, brief lift, sniff, flick, or scare; 2, jumping, paw shaking; 3, multiple lifts, paw lick; 4, prolonged paw lifting, licking, shaking, or jumping; 5, paw guarding. SNS-GABAA β 3^{-/-} mice were hypersensitive both the Hargreaves plantar heating test and noxious heat hot plate test as foreshadowed in our previous study (Figure 10A, C). However, Advillin-GABAA β 3^{-/-} mice showed no significant change to either heating or cooling tests compared to their littermate controls (Figure 10B, D).

RESULTS

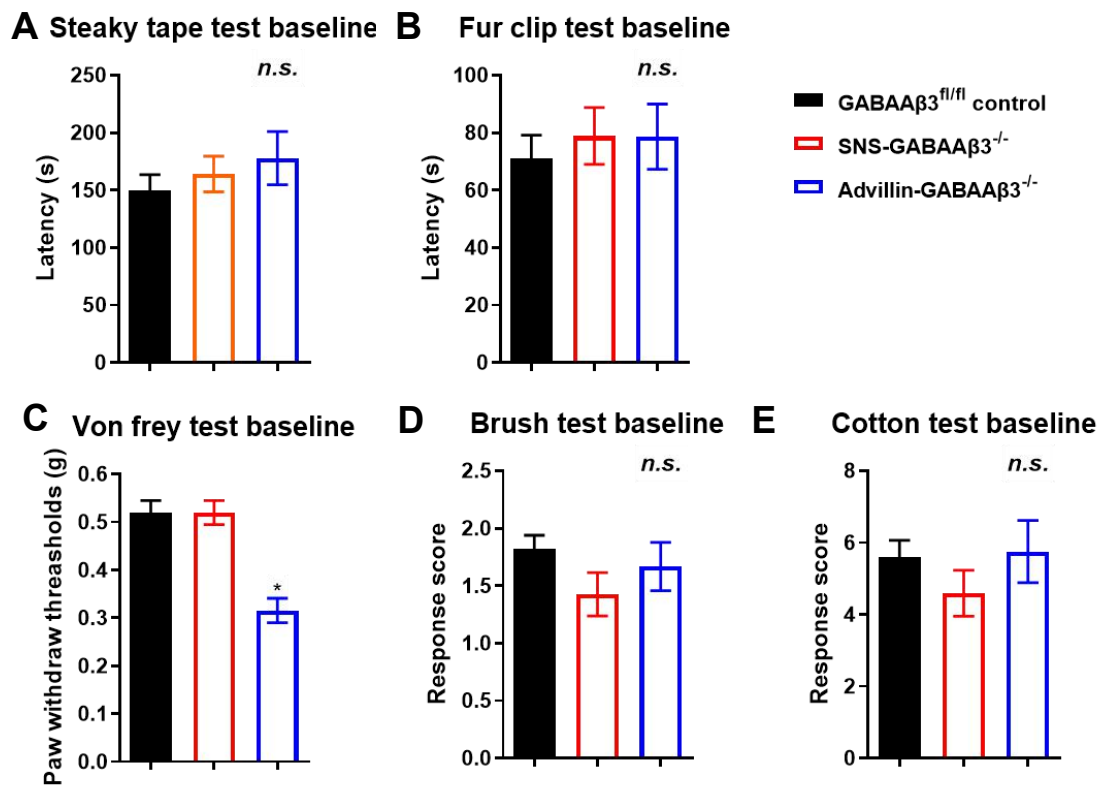


Figure 9. The basal touch and mechanical sensitivity of SNS-GABAA β 3^{-/-} and Advillin-GABAA β 3^{-/-} mice. **A**, Sensorimotor behavior relative tape test. **B**, gentle touch sensory related fur clip test. **C**, punctate mechanical sensation related von Frey test. **D**, dynamic mechanical sensation related brush test. **E**, dynamic mechanical sensation related cotton test. $p < 0.05$ indicated by *, as compared to control group. 12 mice per group, one-way repeated-measures ANOVA with post-hoc Tukey test. All data points represent mean \pm SEM.

RESULTS

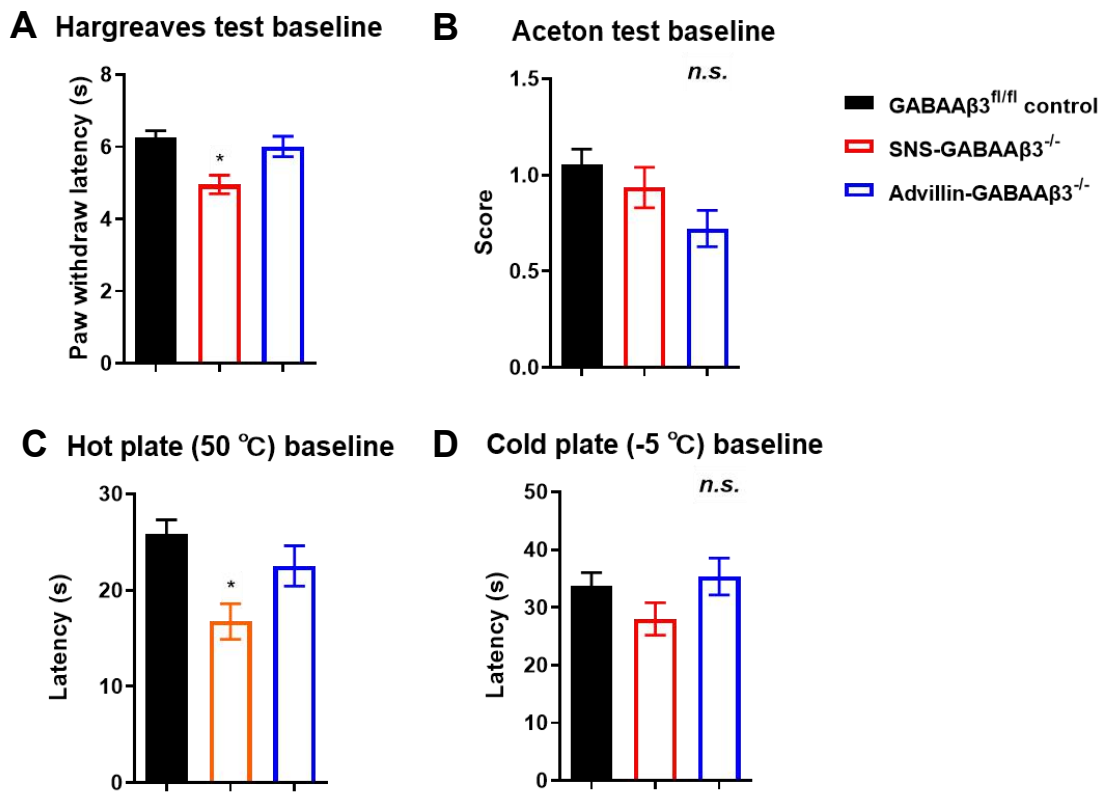


Figure 10. The basal thermal sensitivity of SNS-GABAA β 3^{-/-} and Advillin-GABAA β 3^{-/-} mice. **A**, thermal sensation related Hargreaves test, and **B**, cool perception related acetone test **C**, nociceptive thermal sensation related hot plate test. **D**, nociceptive cold sensation related cold plate test. $p < 0.001$ indicated by ***, as compared to control group. 12 mice per group, one-way repeated-measures ANOVA with post hoc Tukey test. All data points represent mean \pm SEM.

RESULTS

3.3 Impact of GABAA β 3 knock-out on the development of punctate allodynia in CFA model

Inflammatory pain was induced with injection of Complete Freund's Adjuvant (CFA) into the hind paw. Following CFA injection, control mice (GABAA^{fl/fl}) developed a profound, long-lasting (recorded up to 30 days) hypersensitivity to mechanical and thermal stimuli applied to the ipsilateral hind paw after CFA injection (Figure 11, 12). Conditional Advillin-GABAA β 3^{-/-} knock out mice, also became hypersensitive following CFA injection. Withdrawal thresholds to punctate mechanical stimuli fell under 0.02 gram in the first post-injury week and then recovered slowly to nearly 0.04 gram (Figure 11). For SNS-GABAA β 3^{-/-} conditional null mice decreased paw withdrawal thresholds to all stimuli, except one, developed as they did in littermate controls, within the first two days and were maintained for 28 days post-CFA injection. The exception for SNS-GABAA β 3 was the degree of hypersensitivity observed in response to punctate mechanical stimulation with von Frey filaments. While punctate mechanical allodynia was observed in SNS-GABAA β 3^{-/-} mice following CFA injection, -the sensitivity only fell to 0.07 gram, rather than to values below 0.02g in littermate controls (Figure 11A). These experiments thus revealed two important results. First, loss of GABAA β 3 in nociceptors led to an attenuation of inflammatory mechanical allodynia, but not mechanical hyperalgesia; Second, loss of GABAA β 3 in all DRG sensory neurons does not impact the development of hypersensitivity following CFA injury.

The development of mechanical dynamic allodynia to brush/cotton swab stimuli was observed in control mice and Advillin-GABAA β 3^{-/-} and SNS-GABAA β 3^{-/-} mice alike (Figure 11B, C). Similarly, there were no differences between control and conditional knock-out mouse lines with regard to their mechanical nociceptive sensation in response to the pinprick test after CFA injection (Figure 12). To the best of our knowledge, the

RESULTS

reduction in punctate allodynia observed in the SNS-GABAA β 3^{-/-} mouse line is the first report of a specific loss of punctate sensitivity with retained dynamic allodynia post CFA injury. This constellation is the opposite of that observed for VT3^{Lbx1} mice found in Qiufu ma's lab that showed ablation of the vesicular glutamate transporter 3 (VGLUT3) in the spinal cord resulted in specific loss of dynamic allodynia in response to brush stimuli despite persistence of punctate allodynia in response to von Frey stimuli post CFA or nerve injury (Cheng et al. 2017). For thermal pain sensation post-CFA, both Advillin-GABAA β 3^{-/-} and SNS-GABAA β 3^{-/-} mice developed heat hyperalgesia assessed using the plantar test and cold allodynia in response to the acetone test, in a manner similar to their littermate controls (Figure 13).

Taken together, deletion of GABAA β 3 in DRG sensory neurons did not affect the development of mechanical or thermal hypersensitivity in the inflammatory CFA model. However, conditional deletion of GABAA β 3 in nociceptors impacted the development of punctate mechanical allodynia, but not dynamic mechanical allodynia or thermal hypersensitivities. This naturally raises the question, as to whether the punctate and dynamic mechanical allodynia circuits individually comprise labeled line connectivity that are subject to equivalent pre-and postsynaptic tuning in the spinal cord.

RESULTS

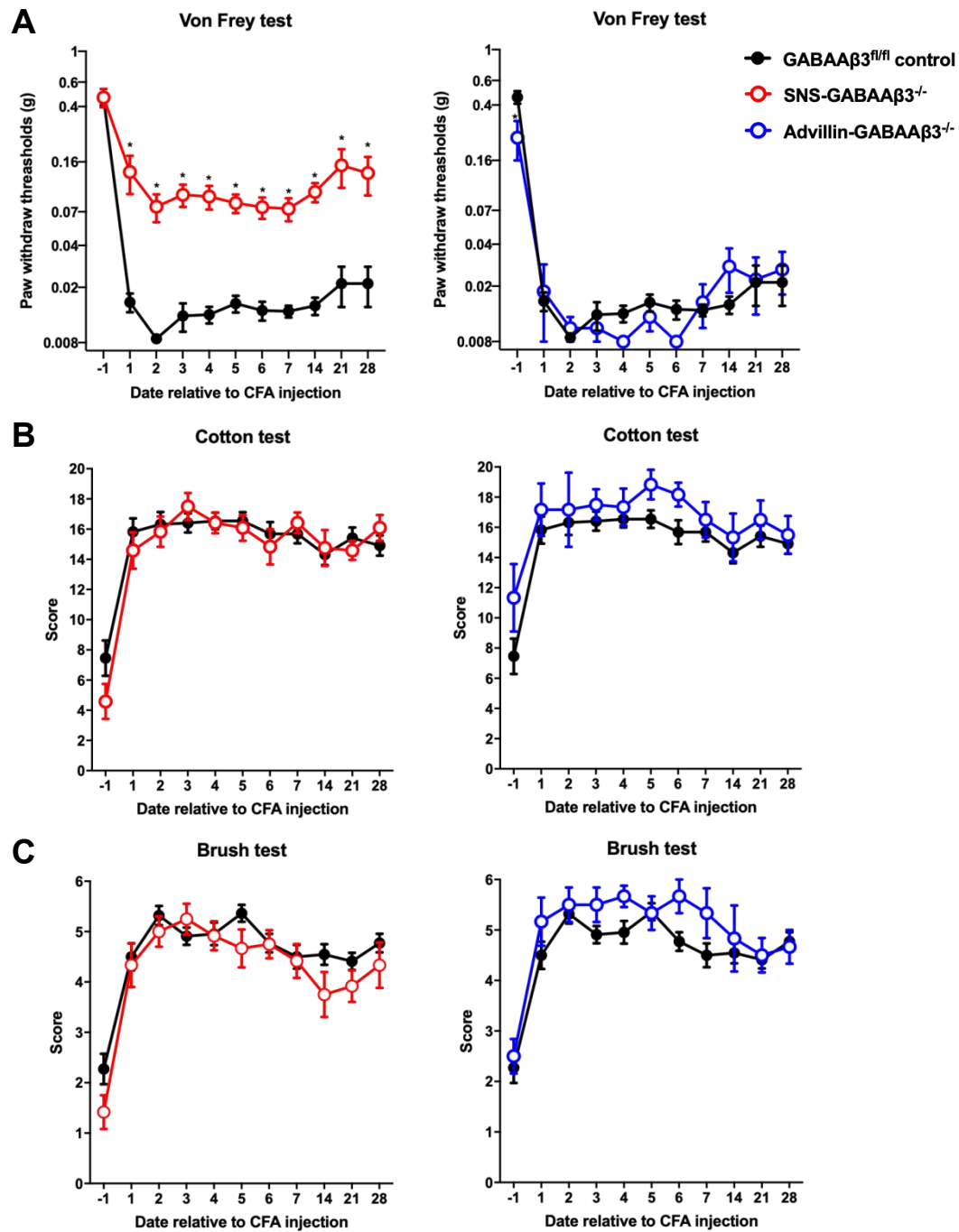


Figure 11. Mechanical pain behavior in nociceptor GABAA β 3 knock-out (KO) or DRG sensory neuron GABAA β 3 KO mice. A, SNS-GABAA β 3^{-/-}, Advillin-GABAA β 3^{-/-} and littermates control mice mechanical von Frey test after CFA injection, or B, pain related behavior score of dynamic mechanical cotton test, or C, pain related behavior score of dynamic mechanical brush test. $p < 0.05$ indicated by *, compared to littermate controls, two-way ANOVA with Bonferroni multiple comparisons, 12 mice per group. Data are represented as mean \pm SEM.

RESULTS

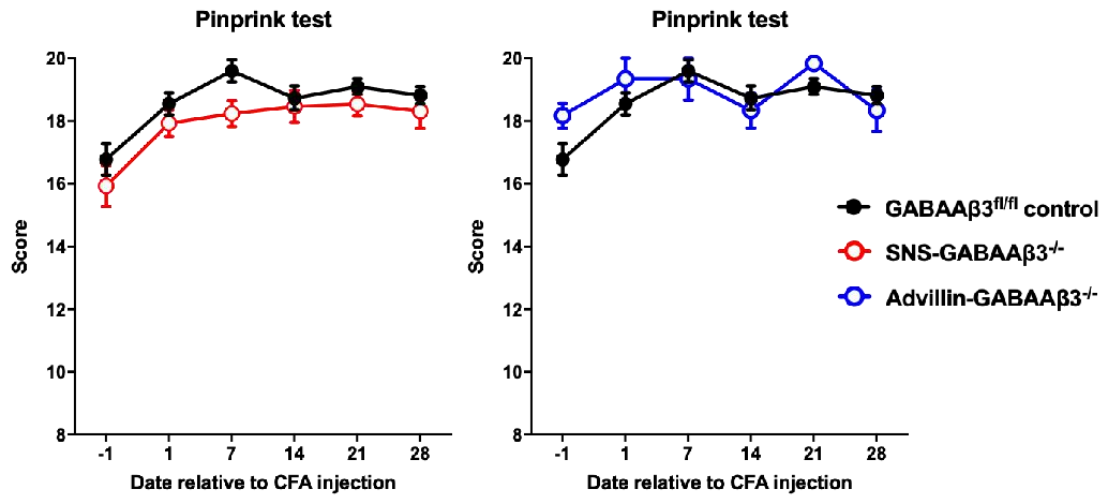


Figure 12. Nociceptive mechanical pain behavior in nociceptor GABAA β 3 knock-out (KO) mice or DRG sensory neuron GABAA β 3 KO mice. pain related behavior score of pinprick test after CFA injection in SNS-GABAA β 3^{-/-}, Advillin-GABAA β 3^{-/-} and littermates control mice. 12 mice per group, two-way ANOVA with Bonferroni multiple comparisons. Data are represented as mean \pm SEM.

RESULTS

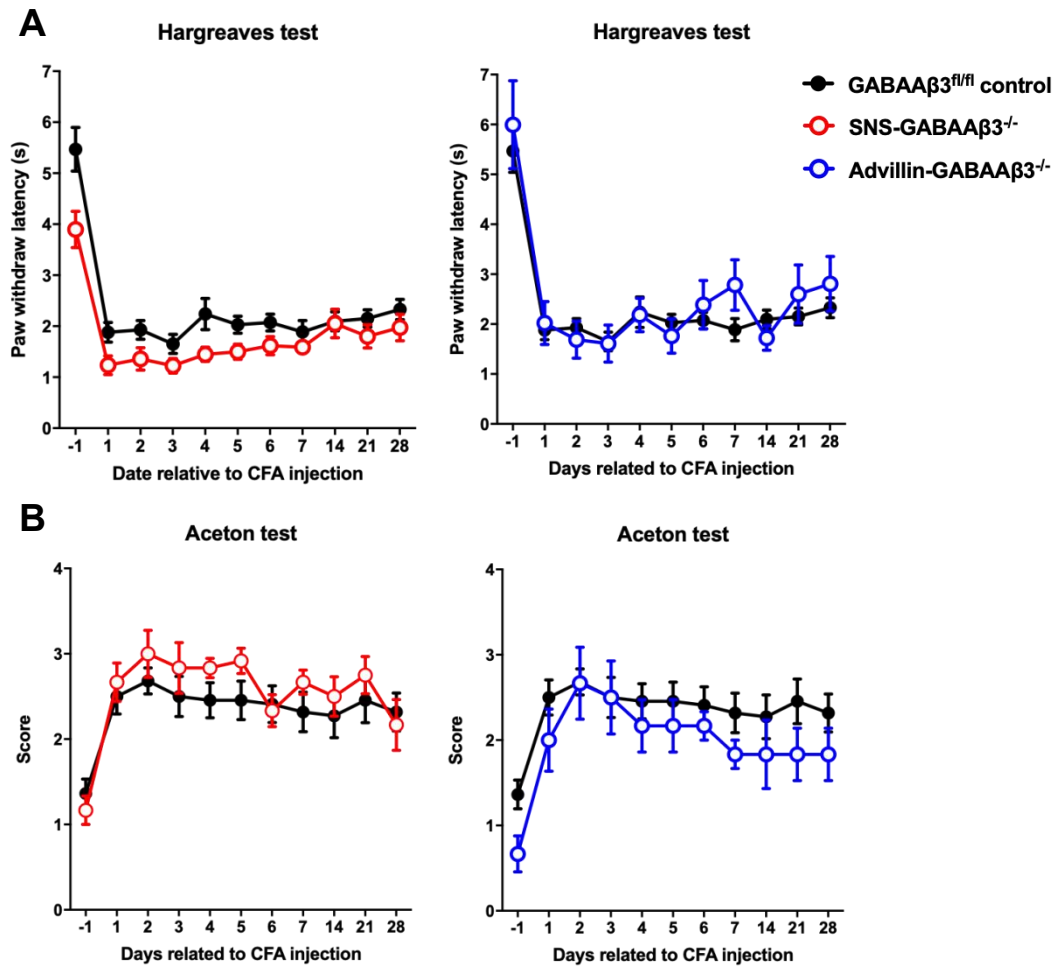


Figure 13. Thermal pain behavior in nociceptor-specific GABAAβ3 knock-out (KO) mice or DRG sensory neuron GABAAβ3 KO mice. A, hind paw withdrawal latency of Hargreaves planta test after CFA injection in SNS-GABAAβ3^{-/-}, Advillin-GABAAβ3^{-/-} and litter mate control mice. **B,** pain related behavior score of acetone test after CFA injection in SNS-GABAAβ3^{-/-}, Advillin-GABAAβ3^{-/-} and littermates control mice. 12 mice per group, two-way ANOVA with Bonferroni multiple comparisons. Data are represented as mean ± SEM.

RESULTS

3.4 Discrimination of punctate and dynamic mechanical allodynia circuits using dual-epoch mapping in spinal cord

To discriminate the circuit activity patterns in response to different kinds of mechanical stimuli (punctate or dynamic) in the spinal cord, we devised a cell labeling strategy based on the immediate early gene (IEG) *c-fos*. Cells responsive to different stimuli were identified in the spinal cord of individual mice using a double-labeling technique based on the distinct induction time course of the *c-fos* mRNA and c-Fos protein signals. According to the central dogma of molecular biology, DNA transcribes into RNA and RNA translates into protein, and once "information" has passed into protein it cannot get out again (Francis Crick, 1958). *c-fos* expression is generally low throughout the nervous system in animals at rest condition (Chan et al. 1993; Abbadie et al. 1994; Perrin-Terrin et al. 2016). However, following neuronal activation, *c-fos* mRNA increases within minutes and decays over a couple of hours, whereas its protein product appears later (approximately one hour later) and persists much longer (Greenberg and Ziff 1984; Morgan et al. 1987). Thus, when two stimuli are sequentially applied at an appropriate interval, neural circuits activated by the two stimuli can be detected by labelling *c-fos* mRNA (proportional to the second stimulus) and c-Fos protein signal (proportional to the first stimulus) using fluorescence in situ hybridization method (I-FISH) and fluorescence immunohistochemistry respectively. Furthermore, this co-labeling strategy can be combined with other neural markers to allow identification of the neuron type.

To determine the anatomical location of cells in the spinal cord responding to mechanical pain signals from the hind paw, we used pinprick stimulation and visualized the location of c-Fos expression along sagittal sections of spinal cord (Figure 14). c-Fos positive cells mostly aggregate between lumbar

RESULTS

segments 4 to 5 particularly around the lumbar 4-5 intervertebral disc (Figure 14). In the coronal plane, c-Fos positive neurons were observed in medial regions of spinal dorsal horn. This is consistent with the projection area for glabrous skin of the hindpaw and consistent with previous reports for projections of Mas-related gene product receptor D (*Mrgprd*) expression non-peptidergic nociceptors to the medial dorsal spinal cord (Olson et al. 2017).

The success of the dual-labeling approach of *c-fos* mRNA and c-Fos protein signals in the spinal cord relies on the ability to separate the mRNA and its protein signal in time. Therefore, we performed a general test of the method using a single mechanical nociceptive pinprick stimulus to determine the sequential order and temporal interval of mRNA and protein for *c-fos* (Figure 15A). After a mechanical nociceptive pinprick stimuli on the hind paw, we sacrificed mice at 5 different time points from 15 minutes to 4 hours. With the dual-labeling I-FISH staining, we counted the number of cells positive for *c-fos* mRNA and c-Fos protein. This showed that *c-fos* mRNA peaked at the 75-minute time point and was nearly below detection at the 150-minute time point, whereas c-Fos protein was not detected at the 30-minute time point, appeared at the 75-minute time point and remained elevated after 150-minutes (Figure 15B, C). Using a Gaussian regression fit, curves for the time course of dual expression were estimated (Figure 15C). To verify the validity of these estimates of time course, we stimulated mice with a pinprick either once at time point 0 or at the 120-minute time point or at both time points (Figure 16A). Using I-FISH staining, only *c-fos* mRNA expression could be detected at the 30-minute time point. In contrast, at the 150-minute time point only c-Fos protein expression could be detected and this signal reflects the translated *c-fos* mRNA induced by the first stimulus (Figure 16B, C). If stimulated at both time points, a large amount of overlap from each signal could be seen and this indicated that the two stimuli activated the same

RESULTS

neurons. These results show that this dual-epoch mapping method can be an effective way to discriminate signals in the spinal that result from different and time separated peripheral stimuli.

RESULTS

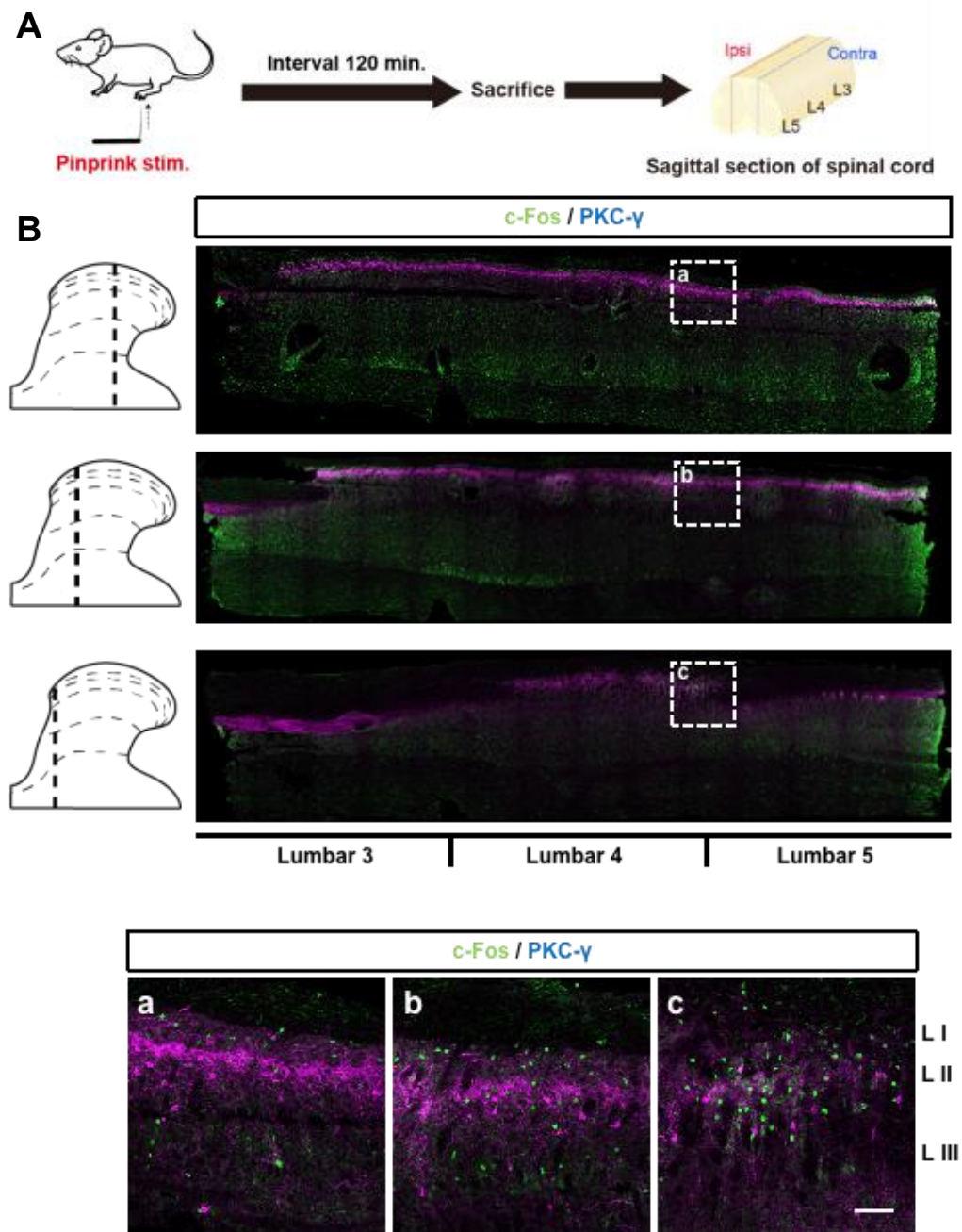


Figure 14. c-Fos expression sample image of noxious mechanical stimuli in the spinal cord. **A**, schematic showing animal sacrificed after nociceptive pinprick stimulus, following with sagittal section. **B**, c-Fos and PKC- γ fluorescent immunohistology image of spinal cord sagittal section, from lateral to medial. **a**. lateral dorsal horn, **b**. medial-lateral dorsal horn and **c**. medial dorsal horn. Scale bar represent 50 μ m.

RESULTS

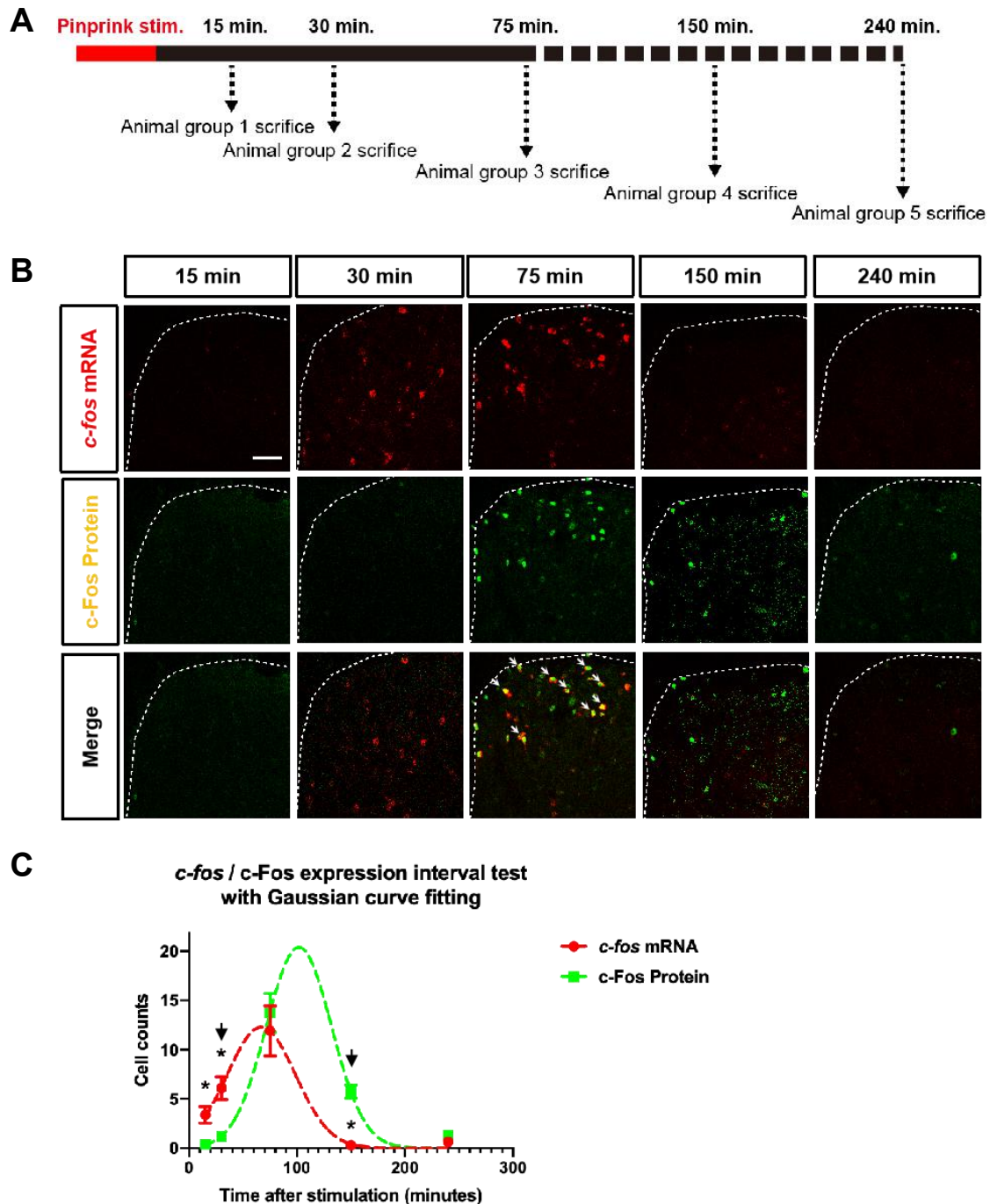


Figure 15. Time interval test for the dual-epoch mapping method. **A**, schematic showing animal groups sacrificed in sequential order on different time points, after nociceptive pinprick stimulus. **B**, dual staining sample images of medial dorsal horn from the different animal group. Arrows indicate the overlap cells. Scale bar represent 50 μ m. **C**, *c-fos* mRNA or c-Fos protein positive cell counting of different time-point and Gaussian curve fit of animal groups. Arrows indicate the 30 minutes and 150 minutes time points. Data from 12 coronal slices of lumbar 3-5 spinal cord per mouse, 3 mice per group. $p < 0.05$ indicated by *, compared to c-Fos protein positive cell counts, two-way ANOVA with Bonferroni multiple comparisons. Data are represented as mean \pm SEM.

RESULTS

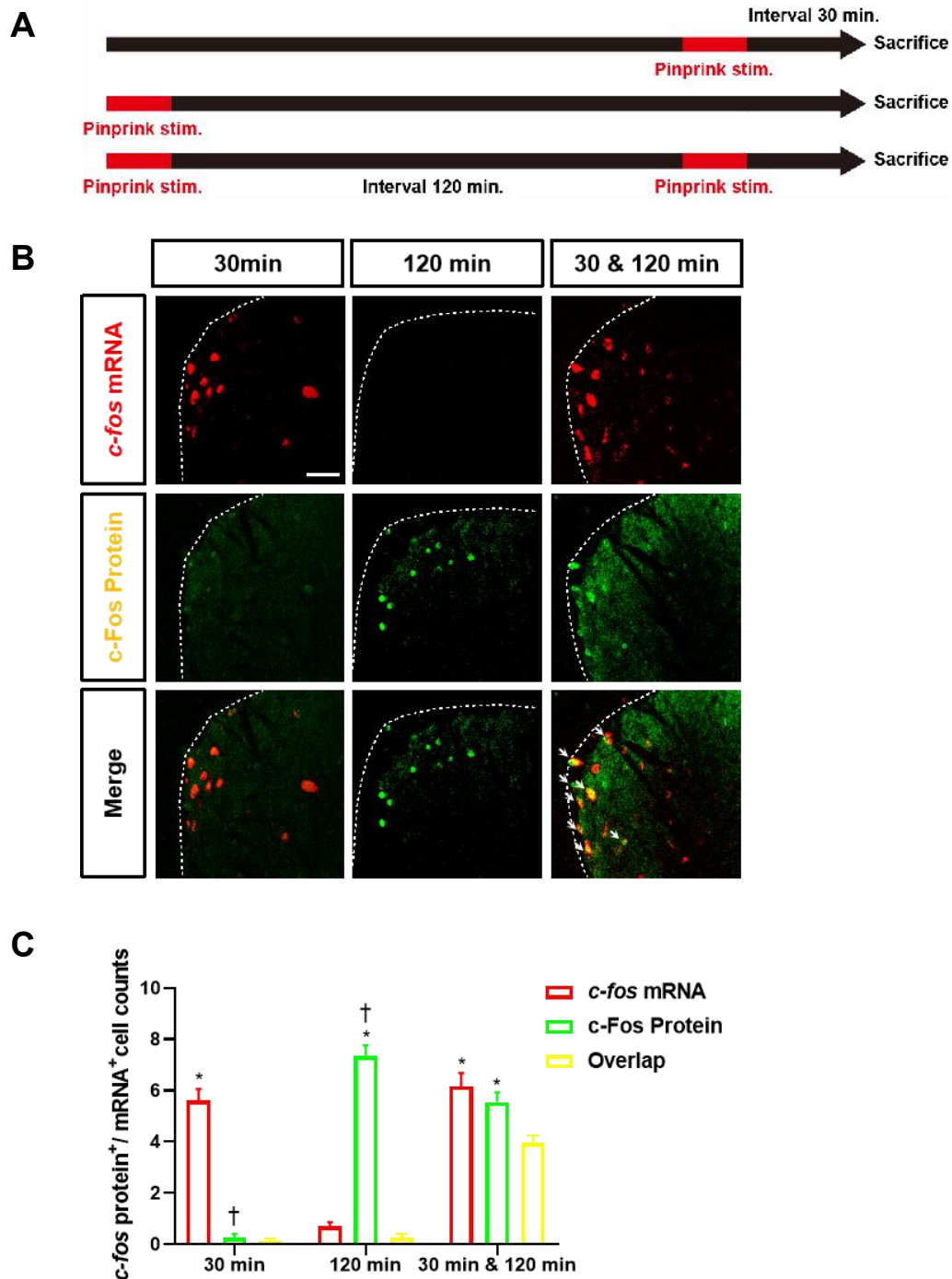


Figure 16. Activation test for dual-epoch mapping method. **A**, schematic showing animal groups sacrificed after nociceptive pinprick stimulus at different time points, or both of time points. **B**, sample image of medial dorsal horn from the different stimulate-interval animal group. Arrow heads indicate the overlap cells. **C**, cell counting of different stimulate-interval animal groups. Data from 12 coronal slices of lumbar 3-5 spinal cord per mouse, 3 mice per group. $p < 0.05$ indicated by *, compared to overlap cell counts; $p < 0.05$ indicated by †, compared between two single stimulus groups, two-way ANOVA with Bonferroni multiple comparisons. Data are represented as mean \pm SEM. Scale bar represent 50 μ m.

RESULTS

3.5 Intermingled pattern of spinal cord *c-fos* labelling following punctate and dynamic mechanical stimuli post CFA injury

Under resting conditions, the expression of *c-fos* is generally low in the mouse nervous system (Perrin-Terrin et al. 2016). Low intensity mechanical stimuli, like von Frey or cotton swab, normally do not cause substantial translation of c-Fos protein. In order to test whether punctate von Frey or dynamic cotton stimulation could induce *c-fos* mRNA or c-Fos protein expression in the spinal cord under physiological conditions, we subjected naive mice to cotton stimulation at the 30-minute time point and then to von Frey at the 150-minute time point and then performed I-FISH staining (Figure 17A). The result was that neither low-intensity von Frey or cotton stimulation were sufficient to evoke expression of *c-fos* mRNA or c-Fos protein in the spinal dorsal horn of SNS-GABAA β 3^{-/-} mice or their littermate controls (Figure 17B, 18) and this is consistent with SNS-GABAA β 3^{-/-} mice not showing mechanical hypersensitivity in the absence of inflammation.

After CFA injection, pain is usually manifest in response to low-intensity mechanical stimuli, and this is termed allodynia. In our previous results, SNS-GABAA β 3^{-/-} mice developed dynamic mechanical allodynia after CFA injury but punctate mechanical allodynia was less pronounced. Here, we applied dynamic cotton and punctate von Frey stimulation at 30-minute and 150-minute time points, 2 days after CFA and mapped cells in the spinal dorsal activated by these stimuli using the dual-epoch mapping method (Figure 19A). I-FISH staining in control mice showed robust signals for *c-fos* mRNA and c-Fos protein in the spinal dorsal horn, in particular in medial regions from lamina I to lamina III (Figure 19B). Quantitatively, there were 13 ± 2 *c-fos* mRNA positive cells per slide, 17 ± 2 c-Fos protein positive cells per slide and 7 ± 3 cells per slide that were co-labeled with *c-fos* mRNA and c-Fos

RESULTS

protein. The overlap ratio for *c-fos* mRNA positive cells was 50 ± 3 % while the overlap ratio for c-Fos protein positive cells was 70 ± 10 %. In total 396 cells were determined as double-labeled, i.e. overlapped, amongst 1380 activated cells (Figure 20C). These results suggest, that the dorsal horn pathways coding punctate and dynamic mechanical stimuli are intermingled, with approximately 30% of neurons common to both pathways. For SNS-GABAA β 3^{-/-} mice, dynamic mechanical stimuli activated a robust c-Fos protein signal, but punctate von-Frey stimuli activation of *c-fos* mRNA signal was significantly reduced compared to littermate control (Figure 19B). Compared to their littermate controls, *c-fos* mRNA positive cell counts and overlapped cell counts in spinal dorsal horn were both significantly decreased in SNS-GABAA β 3^{-/-} mice (Figure 20A). The overlap ratio for mRNA positive cells was not significantly different from controls, but the overlap ration for c-Fos protein positive cells significantly decreased (Figure 20B). This indicated that the decrease number of activated cell were not only from the von Frey punctate activated cluster but also comprised cells within the overlapping cluster that also participate in coding dynamic allodynia. The *c-fos* mRNA / c-Fos protein positive cell distribution analysis showed that *c-fos* mRNA was significantly reduced in lamina III of SNS-GABAA β 3^{-/-} mice and also that the overlapping cells were significantly reduced in lamina I and lamina III (Figure 21A, C). The c-Fos protein positive cell distribution was not significantly different from control (Figure 21B). These results suggest that punctate and dynamic allodynia circuits in spinal cord dorsal horn are partially shared, but largely retain their own unique coding patterns, resulting in a hybrid intermingled coding pattern (Figure 20C).

As the location of neurons is crucial to the role they play in the spinal cord (Moehring et al. 2018; Todd 2010b), we were curious about the location in the spinal cord where these populations were distributed. Traditional counting methods do not provide anatomically based information on the spatial

RESULTS

distribution of neurons. Here we standardized the location of positive cells across all mouse spinal cord sections using a mathematical transformation of the images based on the dividing line between white matter and gray matter as the landmark. Using the dual epoch method, we generated spatial distributions of *c-fos* positive cells based upon their activation by dynamic and punctate mechanical stimuli. We observed that cells activated by mechanical stimulation of the plantar surface of the hindpaw were located medially in the spinal dorsal from lamina I to III. The cells activated by punctate and dynamic stimuli were similar (Figure 22, 23), indicating they share the same anatomical location to code or relay information. Consistent with our previous finding, SNS-GABAA β 3^{-/-} mice showed an abundant reduction of *c-fos* mRNA expression in the medial dorsal horn. From the heat map indicating region specific cell activation, we observed that both punctate and dynamic mechanical circuits were prominent within a triangular core region (Figure 23). In SNS-GABAA β 3^{-/-} mice cells activated by punctate stimuli after CFA deviated from this core pattern, which is consistent with behavioral evidence that punctate allodynia was less pronounced in these mice (Figure 11A). However, in SNS-GABAA β 3^{-/-} mice, the density of overlapping cells was reduced, possibly indicating a reduction in peripheral punctate stimulus input signal (Figure 22). All of these data indicate a reduction of excitatory signals from the periphery under inflammatory conditions and thus a loss of GABA inhibition. This is also consistent with our previous study using two-photon imaging in SNS-Ai38 mice, that recombine the fluorescent calcium indicator GCaMP3 in SNS-Cre neurons. In spinal slices from CFA injected SNS-Ai38 mice, GABA did not evoke calcium transients in primary afferent terminals (Guo, D. 2017).

RESULTS

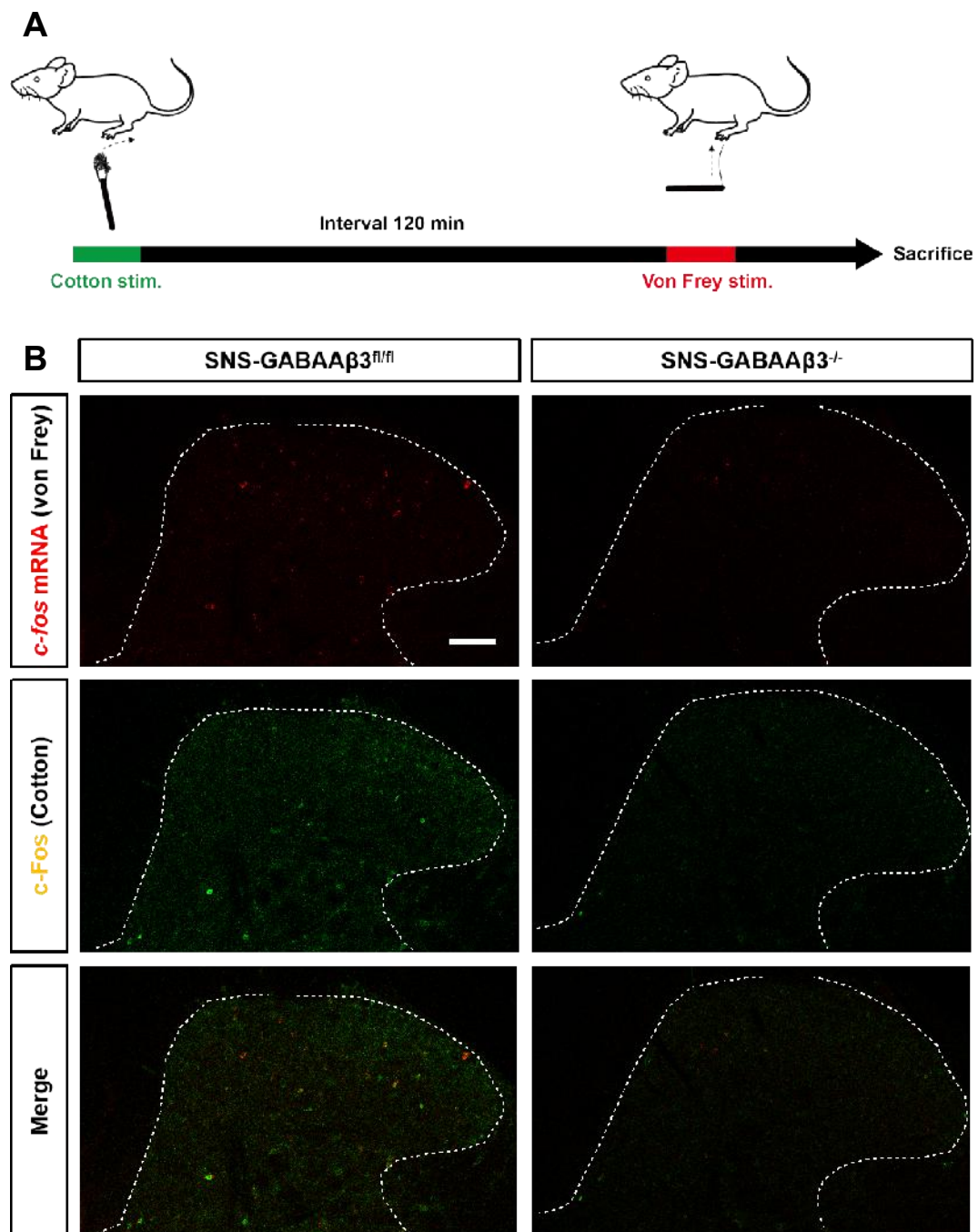


Figure 17. Spinal neural activate representations of punctate and dynamic mechanical stimulation under physiological conditions. A, schematic showing animals were performed von Frey stimuli and cotton stimuli with sequential order and temporal intervals. **B**, I-FISH staining sample image of spinal cord dorsal horn from the SNS-GABAA β ^{-/-}, and littermate control mice. Scale bar represents 100 μ m.

RESULTS

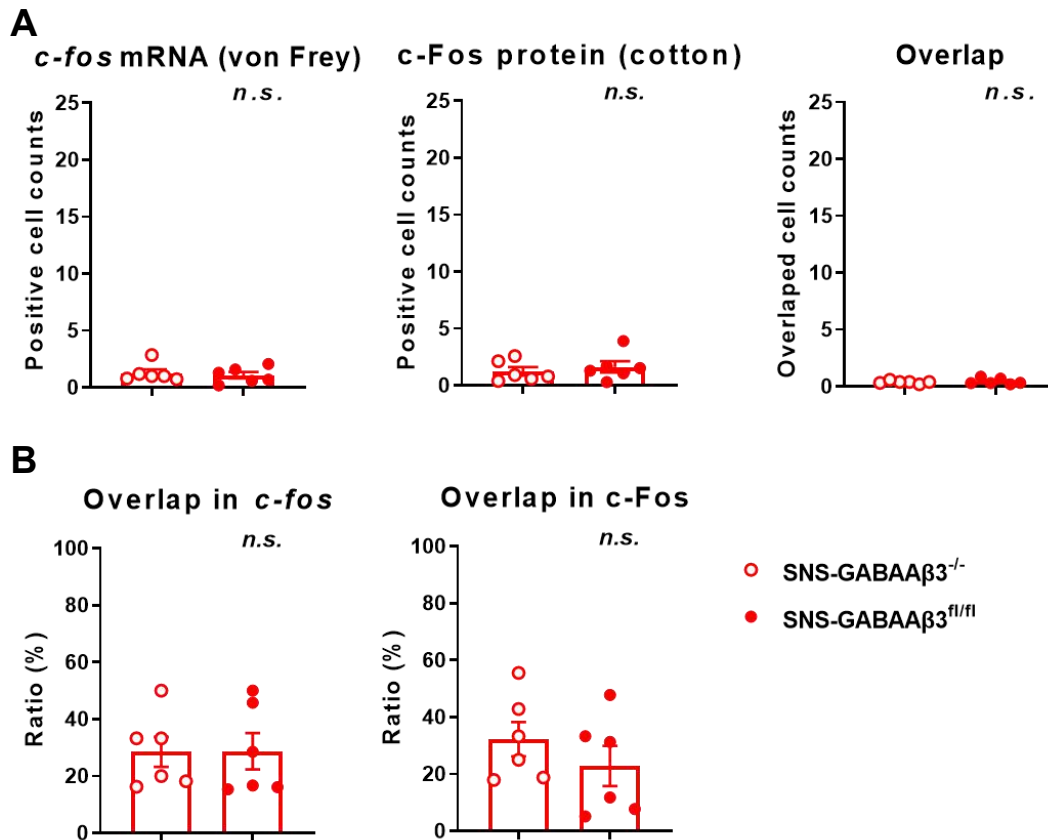


Figure 18. Spinal neurons activated by punctate and dynamic mechanical stimulation under physiological conditions. A, Counting of von Frey and cotton stimuli-induced *c-fos* mRNA positive, c-Fos protein positive, and the overlapping cells. **B,** Overlap ratio of cell counts over *c-fos* mRNA positive cell counts, and overlapping cell counts over c-Fos protein-positive cell counts. Counting data from 12 coronal slices of lumbar 3-5 spinal cord per mouse, 6 mice per group. Unpaired t-test adjusted by Benjamini-Hochberg procedure controlling for false discovery rate. Data are represented as mean \pm SEM.

RESULTS

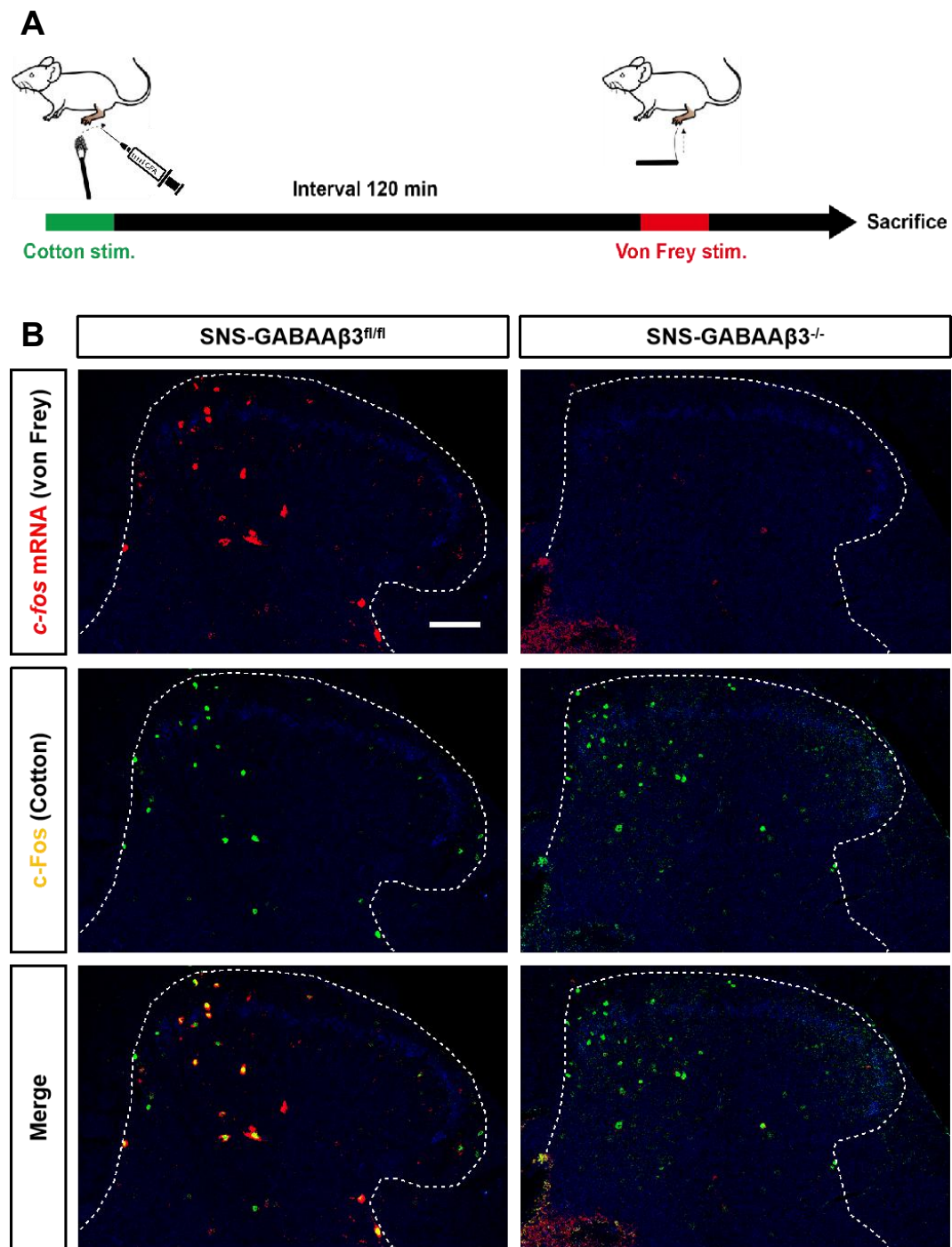


Figure 19. Spinal neuronal activation representations of punctate and dynamic mechanical stimulation under inflammation. **A**, schematic showing animals have performed cotton stimuli and von Frey stimuli with sequential order and temporal interval post CFA injury. **B**, I-FISH staining example image of spinal cord dorsal horn from SNS-GABAA β ^{-/-} mice, and littermate control mice. The blue channel is IB-4 immunofluorescence co-staining as the marker of lamina II. Scale bar represent 100 μ m.

RESULTS

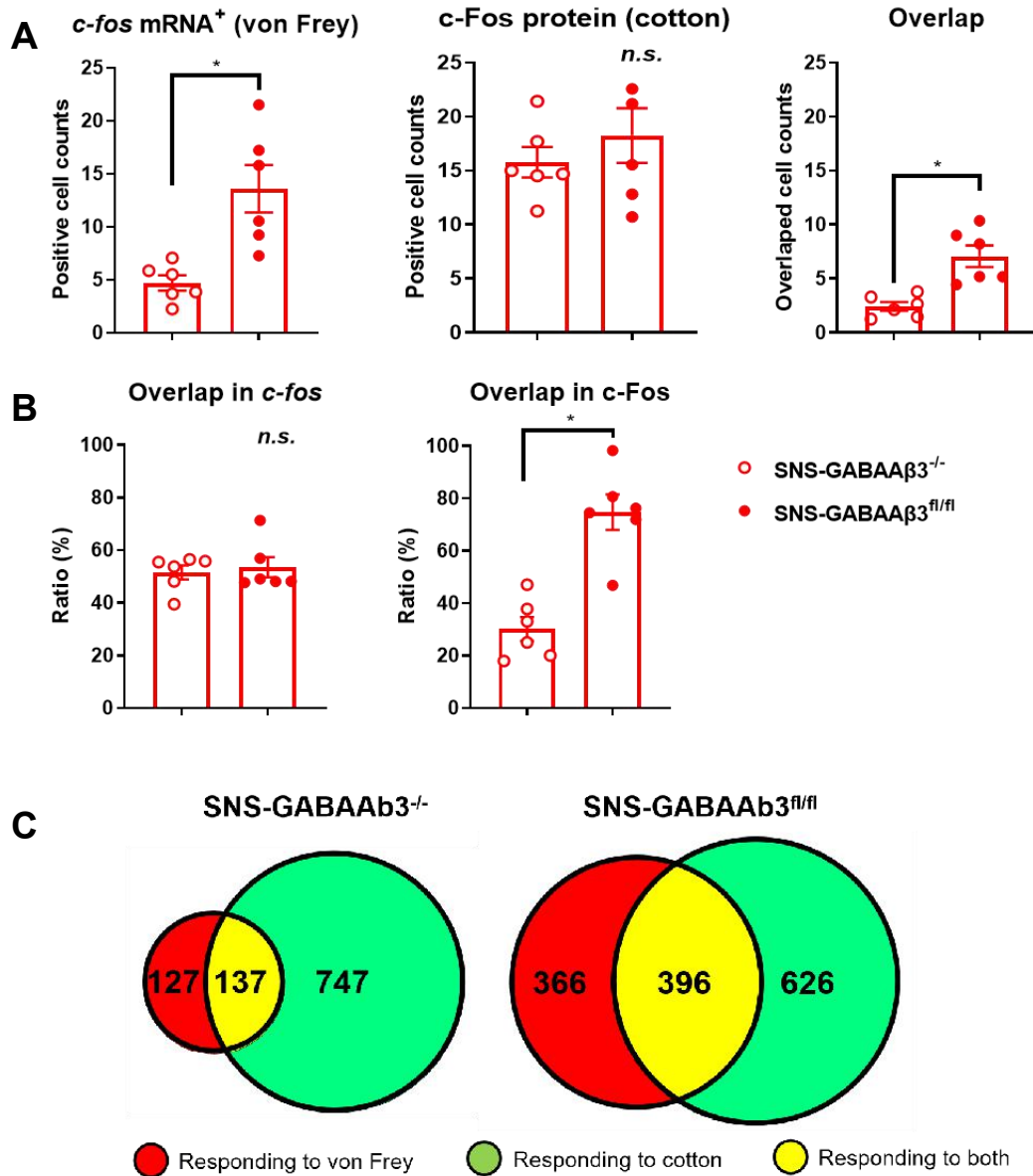


Figure 20. Spinal neurons activated by punctate and dynamic mechanical stimulation following hindpaw inflammation. **A**, Counting of von Frey and cotton stimuli-induced *c-fos* mRNA positive, c-Fos protein positive, and the overlapping cells. **B**, Overlap ratio of cell counts over *c-fos* mRNA positive cell counts, and overlapping cell counts over c-Fos protein-positive cell counts. **C**, scaled Venn diagrams showing the number of *c-fos* mRNA positive (red), c-Fos protein positive (green), and the overlapping cell (yellow). Counting data from 12 coronal slices of lumbar 3-5 spinal cord per mouse, 6 mice per group. $p < 0.05$ indicated by *, compared to littermate control, unpaired t-test adjusted by Benjamini-Hochberg procedure controlling for false discovery rate. Data are represented as mean \pm SEM.

RESULTS

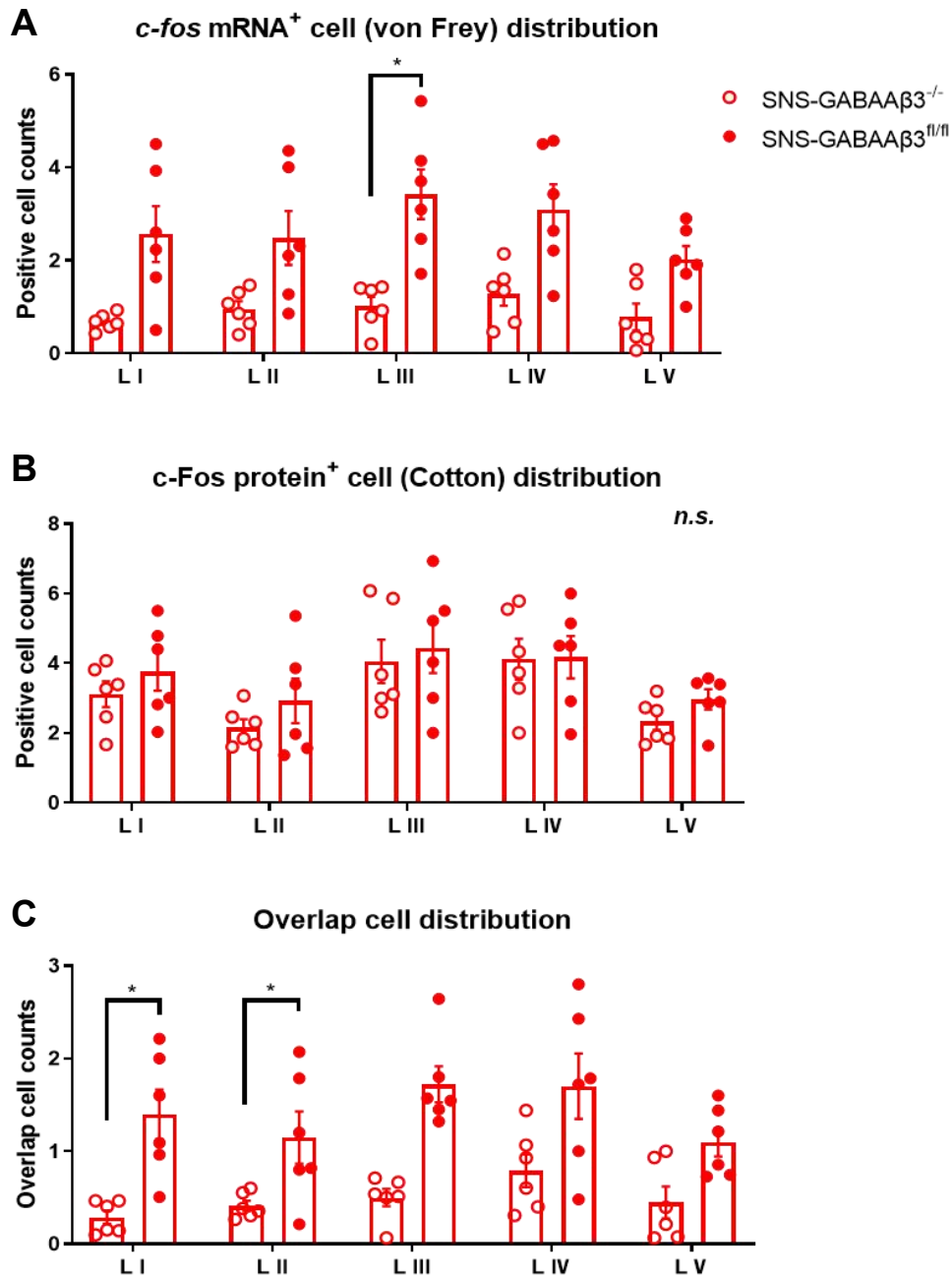


Figure 21. Laminal distribution of spinal neurons activated by punctate and dynamic mechanical stimulation following hindpaw inflammation. **A**, Counting of von Frey and cotton stimuli-induced *c-fos* mRNA positive, c-Fos protein positive, and the overlapping cells, **B**, c-Fos protein positive cell counts, and **C**, the overlapping cell counts from spinal cord lamina I-V. Counting data from 12 coronal slices of lumbar 3-5 spinal cord per mouse, 6 mice per group. $p < 0.05$ indicated by *, compared to littermate control, one-way ANOVA with Tukey's post-hoc test for multiple comparisons. Data are represented as mean \pm SEM.

RESULTS

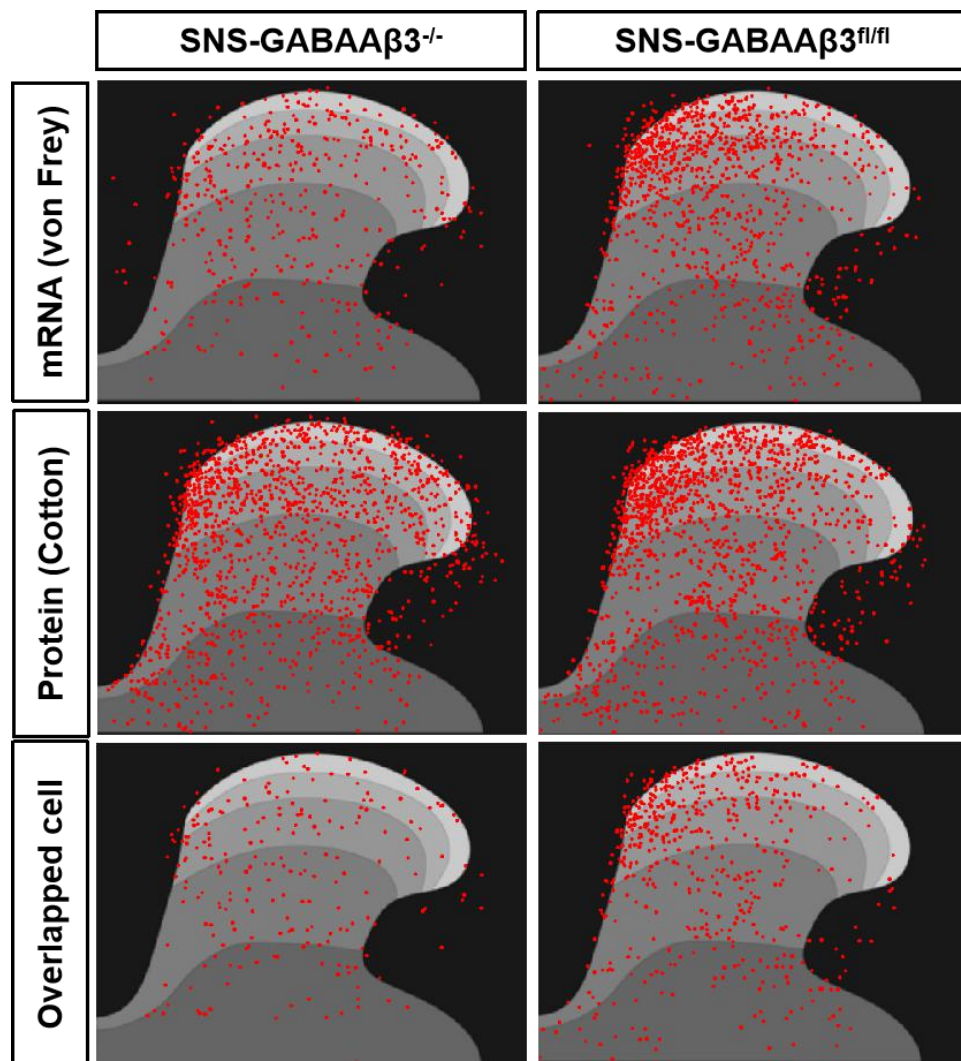


Figure 22. Plotting distribution of spinal neurons activated by punctate and dynamic mechanical stimulation following hindpaw inflammation. Plots of the distribution of *c-fos* mRNA- or c-Fos protein-labeled cells in laminae I–IV, following dynamic cotton and punctate von Frey stimulation. The relative location of individual *c-fos* or c-Fos positive cells in representative sections from each experimental group is depicted and transformed into a standard spinal cord lamina anatomy distribution image. Single red dots represent relevant locations of *c-fos*- or c-Fos-positive cells. Plotting data from 12 coronal slices of lumbar 3-5 spinal cord per mouse, 6 mice per group.

RESULTS

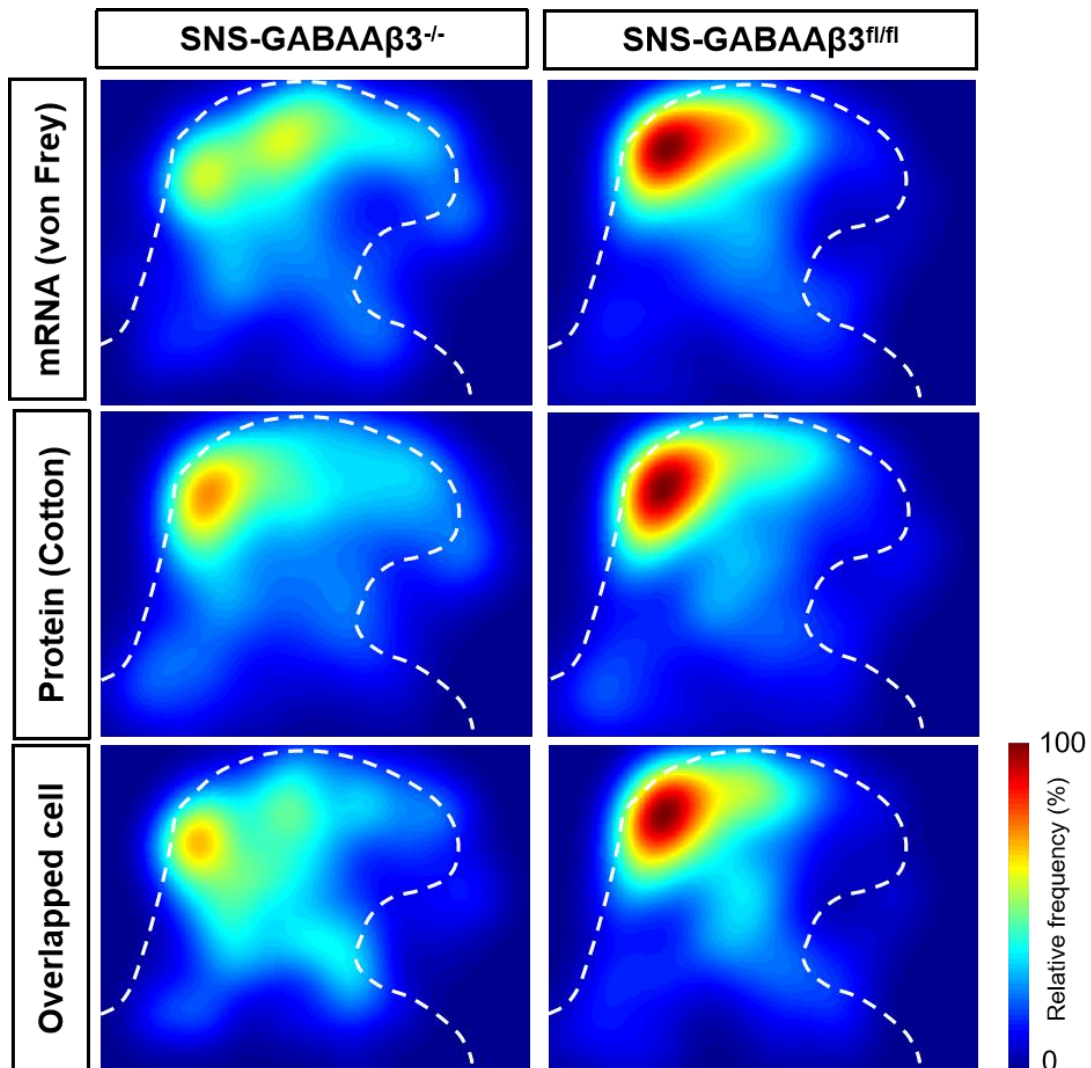


Figure 23. Regionally specific of the dynamic and punctate mechanical nociception under inflammation. Heat map showing the value of relative frequency of occurrence of *c-fos* mRNA or c-Fos protein labeled cells in spinal cord dorsal horn, following dynamic cotton and punctate von Frey stimulation. Plotting location data from 12 coronal slices of lumbar 3-5 spinal cord per mouse, 6 mice per group.

RESULTS

3.6 Conditional deletion of GABAA β 3 in nociceptors reduced activation of CR neurons for punctate but not dynamic mechanical allodynia

Excitatory populations in the dorsal horn, which comprise a vast heterogeneous population distributed throughout lamina I to deeper III. In lamina II, neurons that produce calretinin (CR), are crucial for transmitting mechanical allodynia. (Peirs et al. 2020). Using *c-fos* labeling and pharmacogenetics activation, Peirs et al. demonstrated that CR neurons play a specific role in mechanical allodynia in the context of persistent inflammatory pain. While it has been well established that mechanical allodynia is mediated by neural circuits that differ by injury type (Peirs et al. 2015b), these experiments were the first to suggest that the circuitry in the dorsal horn also differs in the inflammatory to injury model.

In a previous study, we found that in mice lacking GABAA β 3^{-/-} a specific loss of punctate allodynia development was evident after an inflammatory injury with reduced signals in the spinal cord from punctate stimuli (Guo and Hu 2014; Guo, D. 2017). To investigate whether the SNS-GABAA β 3^{-/-} knock out also affected activation of CR-positive neurons under inflammatory conditions, CR was immunolabeled in parallel with I-FISH staining in order to compare the CR expression pattern in response to punctate and dynamic mechanical stimuli after CFA inflammation (Figure 24). The results showed that for SNS-GABAA β 3^{-/-} mice *c-fos* mRNA⁺CR⁺ co-labeling but not c-Fos protein⁺CR⁺ neuron counts decreased significantly compared to their littermate controls (Figure 25). These results indicates that von-Frey punctate activated CR neurons in the context of allodynia after CFA injury. This is consistent with Peirs et al. proposal that CR neuron in lamina II are important for conveying mechanical allodynia in inflammatory pain models but not in neuropathic pain models. Analogously, in the carrageenan inflammatory model,

RESULTS

chemogenetic inhibition of CR neurons caused a significant increase in von Frey thresholds but not a significant change in the responsiveness to a cotton swab, which was consistent with our observation (Peirs et al. 2020). With respect to the types of primary afferent input, 80% of CR neurons receive A δ input while all CR neurons receive C-fiber input (Smith et al. 2019; Peirs et al. 2020). These results suggest that GABA β 3 knockout in nociceptors could be reduced downstream CR excitatory neuron activity and thus abrogated the development of allodynia. In addition, peripheral GABA β 3 receptor knockout affects information flow for punctate but not dynamic mechanical stimuli indicating that there are additional mechanisms involved in the development of mechanical allodynia.

RESULTS

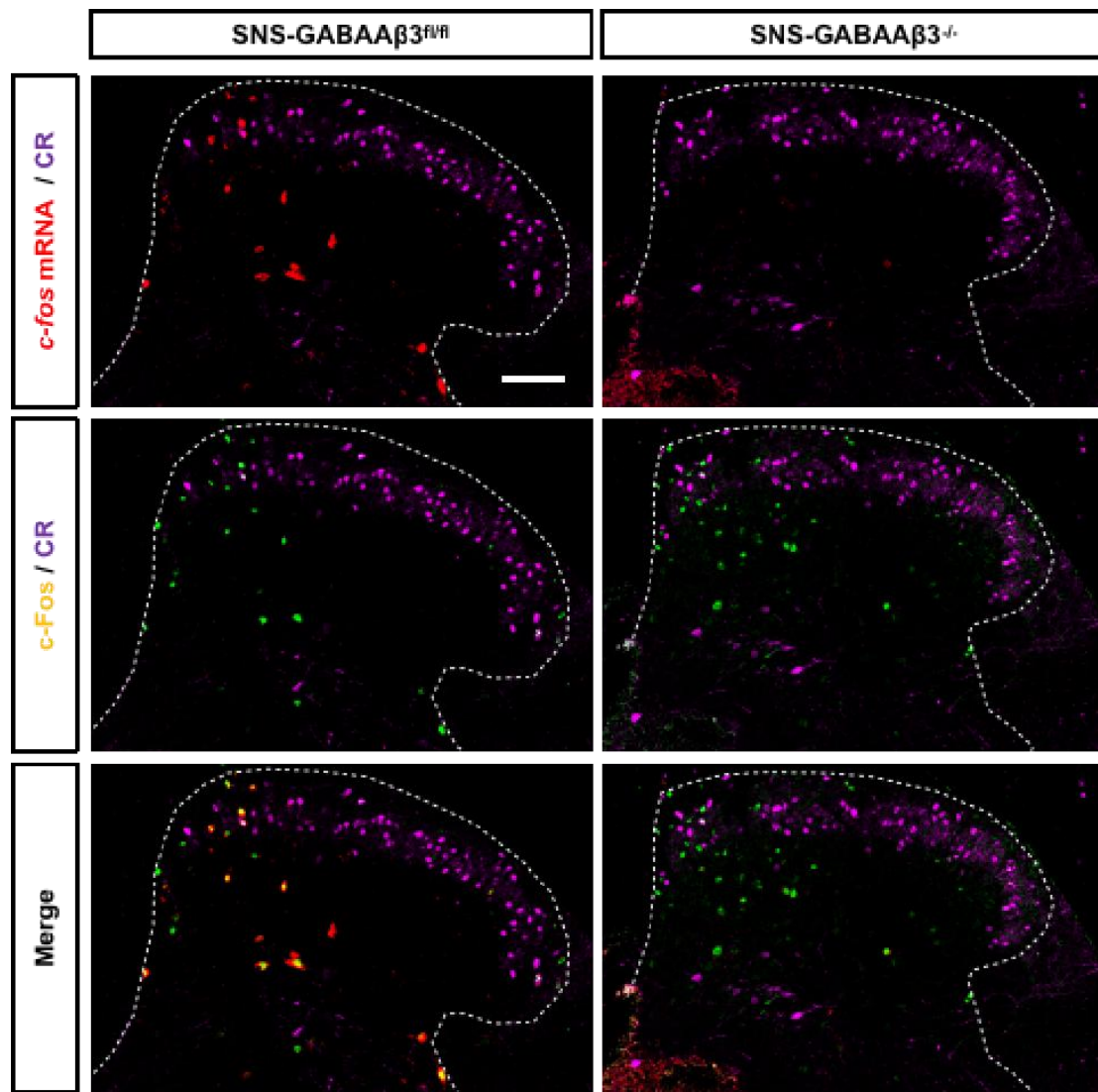


Figure 24. Spinal CR neuron activate representations of punctate and dynamic mechanical stimulation under inflammation. I-FISH and CR co-staining sample image of spinal cord dorsal horn from the SNS-GABAA β 3^{-/-}, and littermate control mice. Scale bar represent 100 μ m.

RESULTS

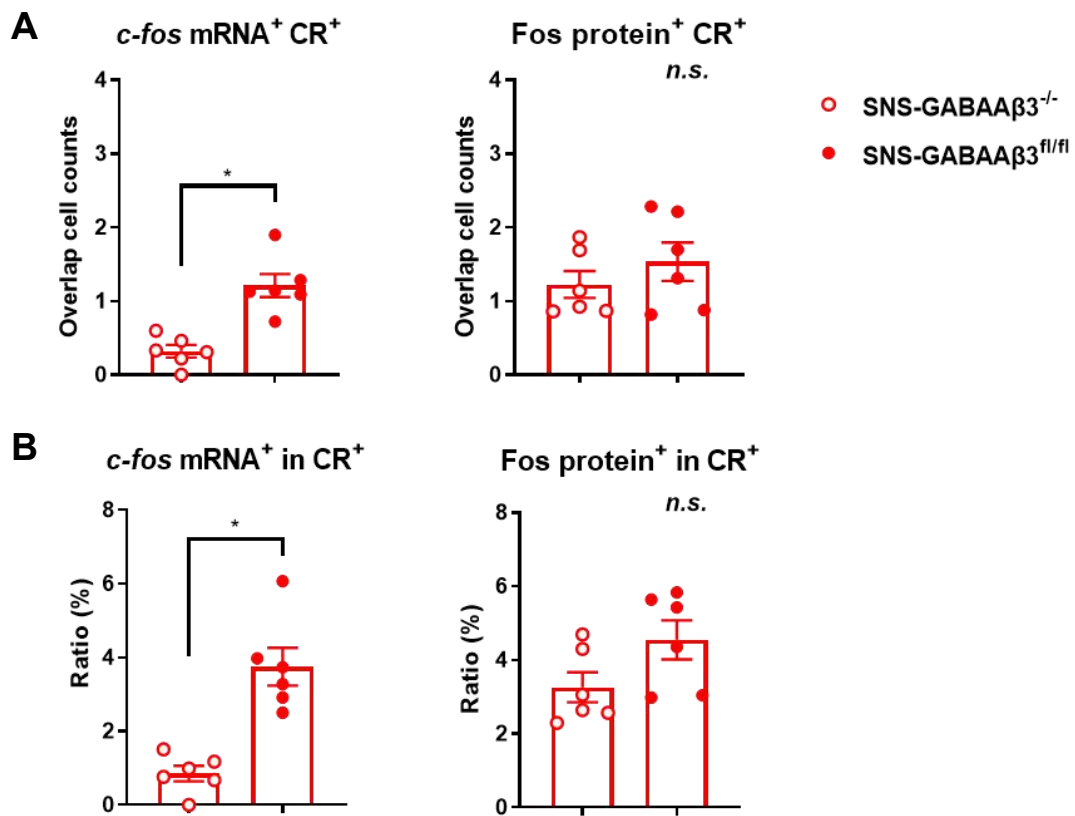


Figure 25. Spinal CR neuron counting of of punctate and dynamic mechanical stimulation under inflammation of nociceptor GABAAβ3 KO mice. A, double-positive cell counting of CR with *c-fos* mRNA or c-Fos protein. **B,** overlap ratio of CR⁺ *c-fos* mRNA⁺ cells over CR⁺ cells, and CR⁺c-Fos protein⁺ cells over CR⁺ cells. Data from 12 coronal slices of lumbar 3-5 spinal cord per mouse, 6 mice per group. $p < 0.05$ indicated by *, compare to littermate control, unpaired t-test adjusted by Benjamini-Hochberg procedure controlling the false discovery rate. Data are represented as mean ± SEM.

RESULTS

3.7 Conditional deletion of GABAA β 3 in nociceptors reduced activation of PV neurons for punctate mechanical allodynia

Presynaptic inhibition of primary afferent central terminals is thought to be mediated by GABA release at axoaxonic synapses (Todd et al. 1996; Hughes et al. 2005). Hughes et al. have demonstrated that a significant proportion of axoaxonic synapses on the central terminals of myelinated afferents are derived from inhibitory interneurons that express the calcium-binding protein parvalbumin (PV), and that axoaxonic synapses are the predominant form of synaptic output from these cells (Hughes et al. 2012). PV cells have since been shown to play a key role in mechanical sensitivity in normal and chronic pain condition (Petitjean et al. 2015). Here we aimed to investigate whether PV neurons were involved in the coding of punctate mechanical allodynia. To this end, c-Fos signals in response to von Frey filament after CFA injury were co-stained against PV in control and GABAA β 3^{-/-} mice (Figure 26). However, the number of c-Fos⁺PV⁺ cells was not significantly altered compared to littermate controls (Figure 27A). But the overlap ratio of cell counts / PV⁺ cells decreased significantly indicating von Frey punctate stimuli post CFA injection activated less PV cells (Figure 27B).

RESULTS

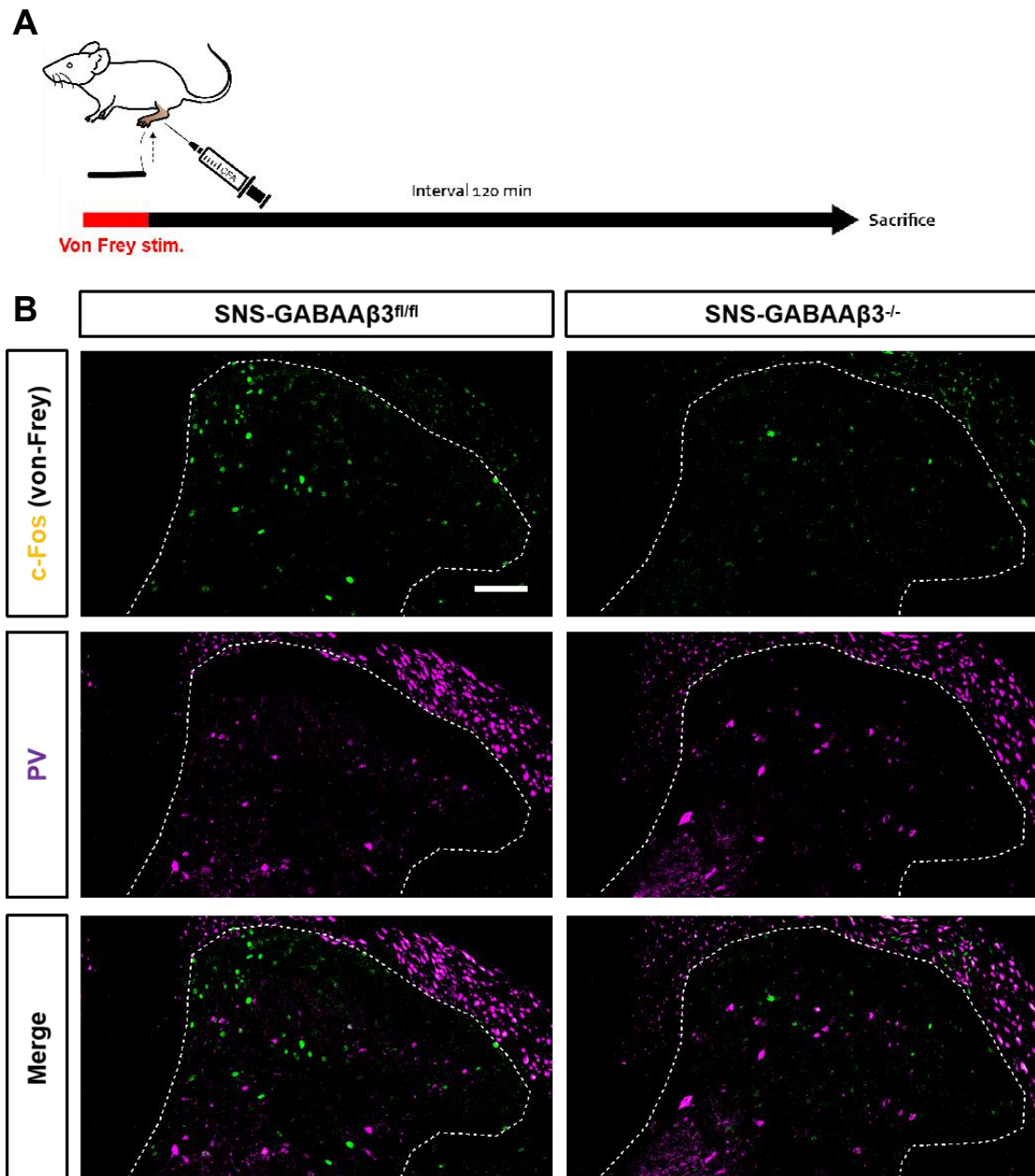


Figure 26. Spinal PV neuron activate representations of punctate mechanical stimulation under inflammation. A, schematic showing animals were performed single von Frey stimuli. **B,** PV and c-Fos co-staining sample image of spinal cord dorsal horn from the SNS-GABA β 3^{-/-}, and littermate control mice. Scale bar represent 100 μ m.

RESULTS

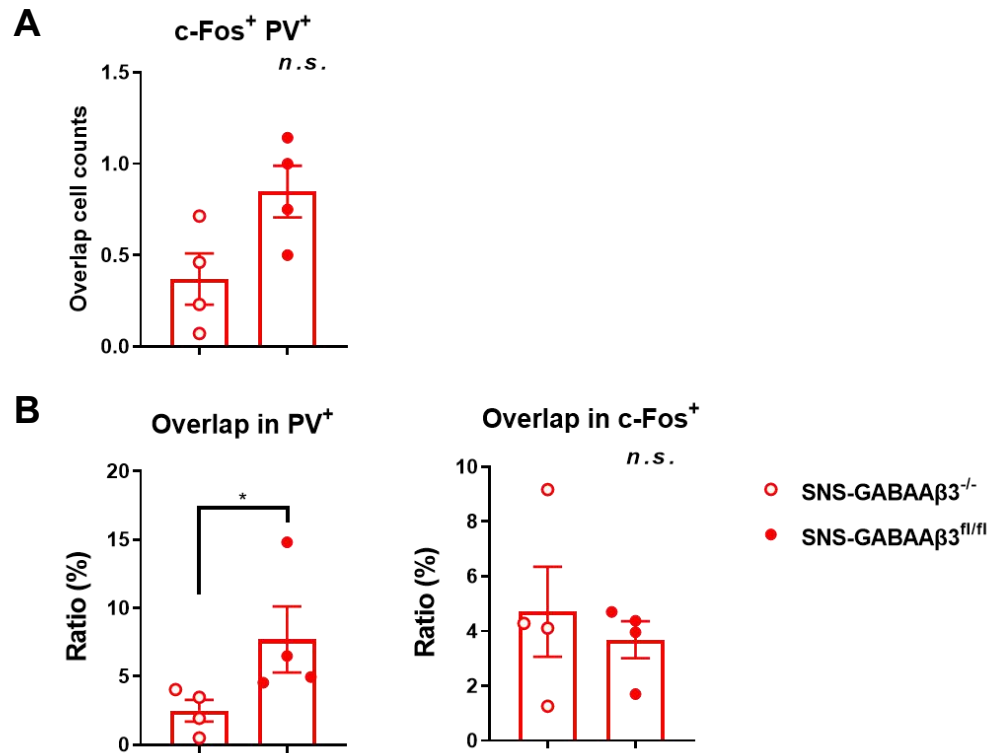


Figure 27. Spinal PV neuron activate representations and distribution of punctate mechanical stimulation under inflammation. A, von Frey stimuli in inflammatory condition caused c-Fos and PV positive overlapped cell counting. **B,** overlap ratio of overlapped cell counts over PV positive cell counts, and overlap ratio of overlapped cell counts over c-Fos protein positive cell counts. Counting data from 12 coronal slices of lumbar 3-5 spinal cord per mouse, 4 mice per group. $p < 0.05$ indicated by *, compare to littermate control, unpaired t-test adjusted by Benjamini-Hochberg procedure controlling the false discovery rate.

RESULTS

3.8 Analysis of relation between fear-associated and pain-associated neurons under baseline and inflammatory condition

Ground-breaking recent work has uncovered the cellular basis of acute (recent) and long-term (remote) fear memory induced by aversive stimuli, including pain (Restivo et al. 2009; Liu et al. 2012; Kitamura et al. 2017; Frankland and Bontempi 2005; Ehrlich et al. 2009; Do-Monte et al. 2015). Recent analysis from our lab colleague revealed a small subset of neurons that are common to both pain and fear engrams in the prelimbic cortex. Functional analysis showed that this interaction between fear and pain at the level of commonly activated prelimbic neurons is sufficient to drive positive modulation of tonic pain by long-term fear independently of aversive or appetitive encoding. Here, we further aimed to investigate whether prelimbic neurons are involved in pain coding and interactions with fear in inflammatory pain conditions.

First, we aimed to investigate whether thermal pain activates populations of prelimbic neurons. We stimulated mice in the Hargraves setup, then identified activated neurons with IEG *c-fos* via immunohistochemistry. After counting the cell number of the prelimbic area, we found that heat stimuli increased the c-Fos expression significantly, compared to the control group that was treated in the same manner but not stimulated with heat (Figure 28). This confirmed that heat pain stimuli can activate prelimbic neurons.

Next, we sought to identify prelimbic assemblies that are selectively recruited during fearful anticipation or heat pain. To specifically label prelimbic neurons activated in states of heat pain or fear recall with tight spatio-temporal control, we employed a binary, tetracycline-inducible activity

RESULTS

mapping system that enables label and manipulating the activated neuron of population in a specific behavior condition (Figure 29A) (Dogbevia et al. 2015). This binary system includes an activation-dependent IEG *c-fos*, promoted transactivator (tTA) regulatory fusion protein, and another tetracycline-response element (TRE) promoted expression of ArchT optical neural silencer and Venus fluorescent protein expression. In the absence of doxycycline, tTA dimers bind TRE sequences and promote downstream ArchT and Venus gene expression. For contrast, otherwise in the presence doxycycline (Dox), these effector molecules preclude tTA binding to the TRE, thus silencing downstream gene expression. Thus, keeping the mice on Dox (Dox ON) represses IEG *c-fos* background expression, otherwise taking the mice off Dox (Dox OFF) opens a finite time window to label neuronal populations with fluorescent protein in response to a given stimulus. In order to utilize this system, we performed a bilateral injection of adeno-associated virus (AAV) particles which served as the vector to deliver the binary system to prelimbic neurons in mouse brain (Figure 28A). Mice were on Dox again to close the time window and the cells that are activated by a second stimulus can be identified via anti-Fos immunohistochemistry (Figure 29B). In order to label the fear engram in the prelimbic cortex, we put the mice through the classical fear conditioning paradigm with Dox ON, in which they learned to associate a given random auditory tone with succeeding acutely painful foot shocks (Figure 29C). Upon opening a 48-hour time window via Dox OFF, we then presented the auditory tone cue to these mice without the foot shock, to activate the fear engram coding neurons during pain anticipation. Indeed, a neuron population of approximate 3000/mm³ density were observed to express Venus yellow fluorescent in the prelimbic cortex. In contrast nearly no Venus expressing-neurons present in the Dox ON control group (Figure 30). We then sought to discern cells specifically activated in fearful anticipation from those selectively recruited during heat pain under inflammatory condition within the same prelimbic area in the same animal. Towards this

RESULTS

end, after labeling fear memory engram with Venus, the neuron population activated by heat were detected by anti-Fos immunofluorescence. For doing so, we compared mice that had received intraplantar injection of CFA to mimic inflammatory pain condition or saline injection as a control. We observed that the both groups showed c-Fos expression after heat stimulus. The heat-induced c-Fos expression did not show a significant difference in the CFA injected mice, compare to the sham control group. However, compared to the sham control group with saline injection, the group with CFA injection showed a larger overlap between the fear engram and heat engram (Figure 31A). Furthermore, we found that the proportion of fear recruited ArchT positive neurons that were overlap with the heat-induced c-Fos positive neurons in mice of CFA injection was significantly higher than sham control mice, and vice versa (Figure 31B). Taken together, our results showed the heat-engram did not show a significant expansion in the inflammatory pain condition, but showed increased overlap with the fear engram in the prelimbic cortex.

RESULTS

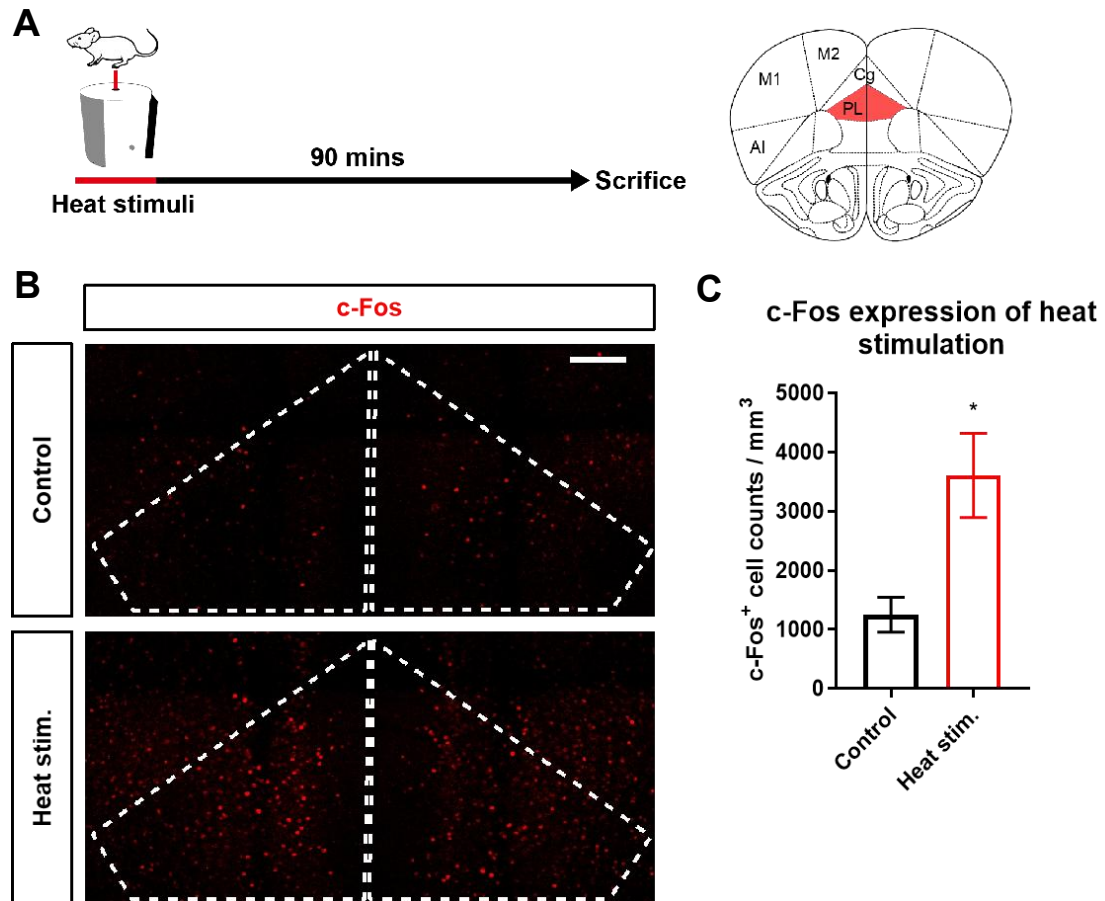
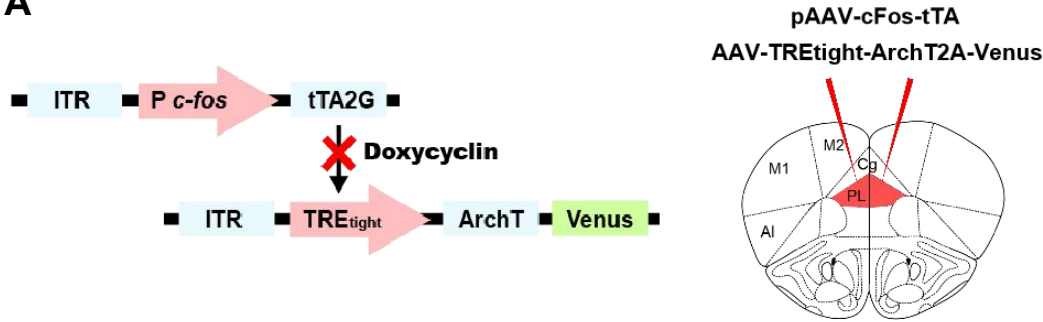


Figure 28. Prelimbic c-Fos expression upon hindpaw heat stimulation. **A**, schematic showing animals have performed heat stimuli via Hargreaves setup, then sacrificed after 90 minutes interval for c-Fos expression. **B**, c-Fos staining sample images of the prelimbic cortex. Scale bar represents 100 μ m. **C**, c-Fos positive cell counting analysis of the prelimbic cortex. $p < 0.05$ indicated by *, compared to the control group with unpaired t-test. Counting data from 4 coronal slices of mouse brain prelimbic cortex, 4 mice per group. Data are represented as mean \pm SEM.

RESULTS

A



B



C

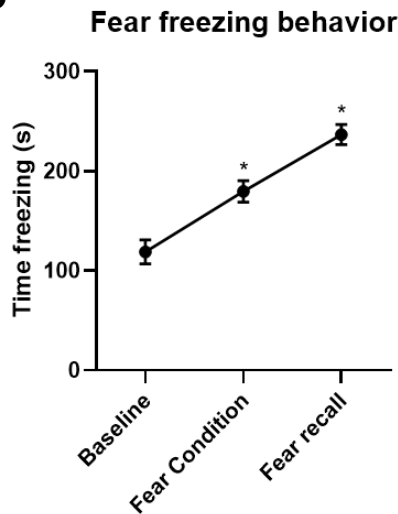


Figure 29. Prelimbic fear labeling and heat c-Fos expression post-CFA. **A**, schematic showing the design of the doxycycline-inducible activity mapping system and bilateral injection of virus combination into prelimbic cortex. **B**, experimental schematic showing the timeline of dual labeling of neuronal activity via Venus (first stimulus given by fear recall after a Dox OFF window) and c-Fos immunohistochemistry (second stimulus given by heat stimulus) under inflammatory pain condition. Control group was only injected with the virus and CFA. **C**, Freezing behavior analysis of fear condition and fear recall. Data from 10 mice, $p < 0.05$ indicated by *, compare to baseline, unpaired t-test adjusted by Benjamini-Hochberg procedure controlling for false discovery rate.

RESULTS

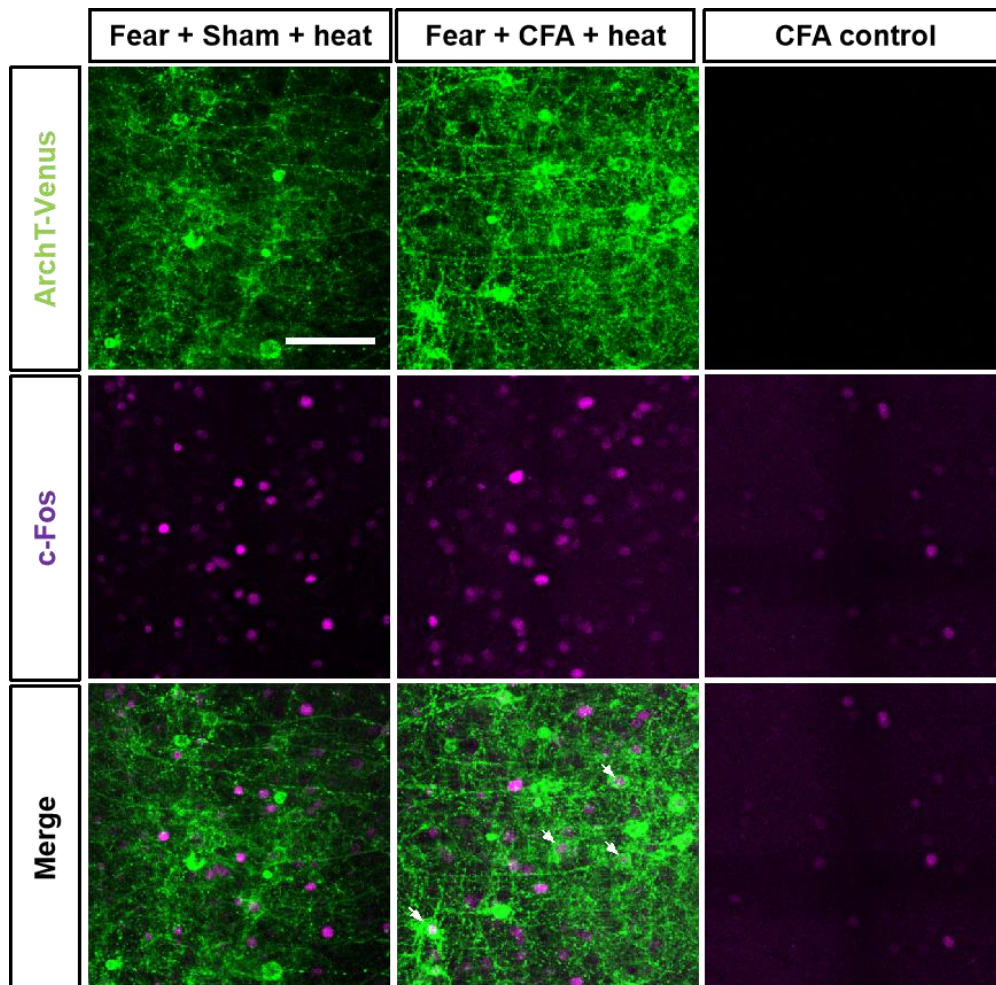


Figure 30. Prelimbic ArchT-Venus and c-Fos expression upon fear recall labeling and heat stimulus. Sample image of fear engram labeling via fear recall and c-Fos expression upon heat stimulation via immunohistochemistry. Arrows indicate overlapping cells. Scale bar represents 100 μ m.

RESULTS

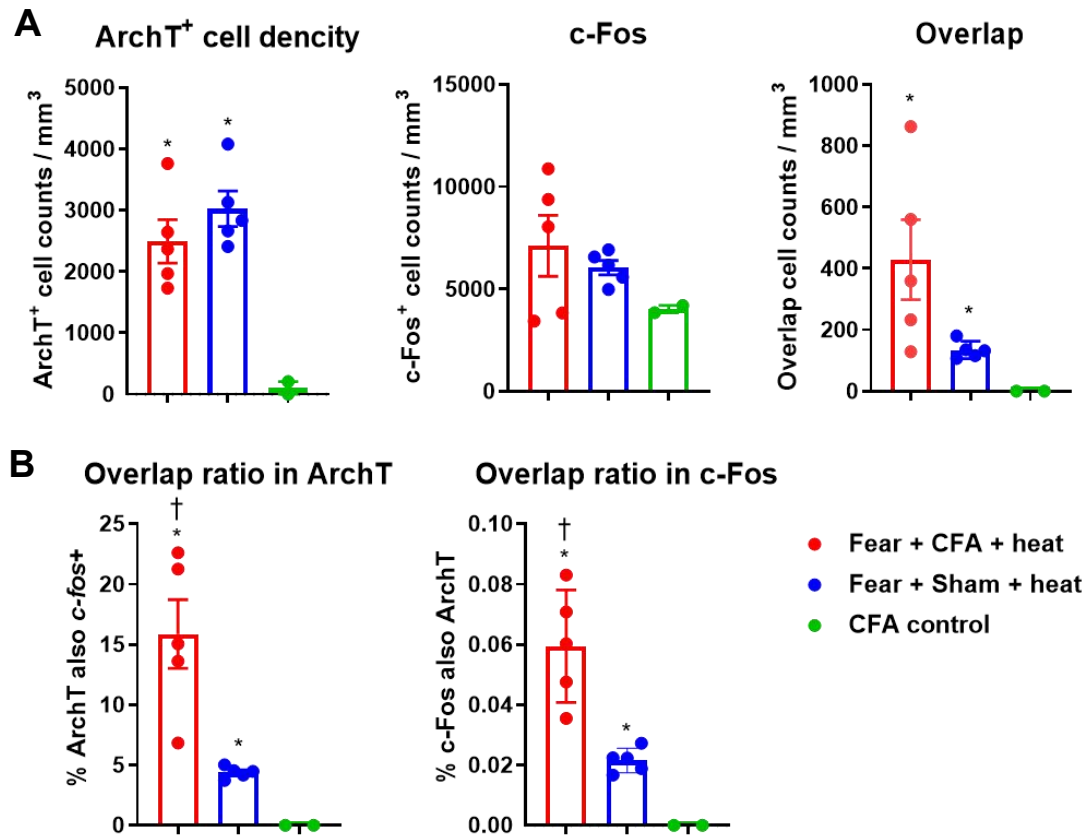


Figure 31. Labeling of the prelimbic fear engram and heat engram under inflammatory pain conditions. **A**, Counting cells positive for of ArchT (fear), c-Fos (heat), and overlapping cells in the prelimbic cortex. **B**, overlap ratio of ArchT positive cell also c-Fos positive, and c-Fos positive cell also ArchT positive. $p < 0.05$ indicated by *, compared to the CFA control group with unpaired t-test; $p < 0.05$ indicated by †, compared to the sham group with unpaired t-test. Counting data from 5 mice per experimental group. Data are represented as mean \pm SEM.

RESULTS

3.9 Suppression of PL fear engram coding neuron decreases heat post-inflammatory hypersensitivity

Next, we sought to identify the functional implications of these neuronal assemblies associated with prospective fear engram and heat hypersensitivity post-inflammation. Here, we are aimed to perform optogenetic inhibition of prefrontal neurons which recruited during remote fear recall. By employing next generation versions of the binary labelling system (Tre Tight), we engineered cells active during remote fear recall to express the inhibitory opsin ArchT, which silences neuronal activity upon illumination with yellow light (Figure 32A). To verify ArchT-mediated neuron silencing *in vivo*, we first analysed the freezing behavior during the fear recall after the fear conditioning and labelling of the fear engram in the PL (Figure 32B). As a control experiment, there was no significant difference in fear behavior between the virus injection group and the sham group (Figure 32C). As reported previously freezing behavior is associated with the fear-coding neuron of population in PL during fear recall (Kitamura et al. 2017). Recall population suppressed effect on the emergence of freezing behavior significantly, thus verifying the experimental design (Figure 33A). We then performed Opto-suppression 2 days post-CFA injection, when mice exhibit a pronounced heat hypersensitivity with Hargreaves infrared radiation stimulus. Upon Optogenetic inhibition of the remote fear engram population in PL mice with inflamed hind paw significant lesser inflammatory heat hypersensitivity than sham mice (Figure 33B). As the heat hypersensitivity in CFA-induced chronic inflammatory pain usually lasts 2-4 weeks in mice, we next addressed whether heat hypersensitivity is also chronically affected by remote fear engram inhibition. The ArchT expression of remote fear engram neuron normally decays within 2 weeks post-labelling. To enable manipulating the remote fear engram in the chronic state 2 weeks after CFA injection, we repeated the fear conditioning and fear recall to re-labelled the fear engram

RESULTS

with Dox ON/OFF manipulation. In the fear recall test, mice post-injury day 13 shows a similar suppression effect on the emergence of freezing behavior as post-injury day 1, which that the effect of re-labeling the fear engram had worked (Figure 32B, 33A). Similar to the early state, we observed that the heat hypersensitivity was also significantly decreased at day 14 after CFA injection by suppressing the fear recall engram (Figure 33B).

Indeed, pain is a multidimensional experience integrating nociceptive processing with aversive and cognitive-motivational components (Baliki and Apkarian 2015; Wiech and Tracey 2013). Considering that pain and fear behavioral states share a common aversive component, we also addressed the possible scenario that suppressing behaviors associated with pain perception by inhibiting the fear recall method, is linked to aversion. In order to test this hypothesis, we designed experiments testing optogenetic silencing of the prefrontal fear engram with respect to aversion in the absence of nociceptive component. We established a task employing aversive white noise in a modified real-time place avoidance paradigm, in which mice increasingly avoided a chamber coupled with aversive white noise, spending more time in the chamber with less noise. We observed although CFA-injected mice showed a slightly enhanced tendency toward aversive-freezing behavior, the mice with optogenetic suppression of the PL remote fear engram population exhibited a similar noise-related avoidance as control mice (Figure 34A). Similarly, we sought to determine whether the suppression of pain perception by silencing of the fear recall engram is specific to pain or also reflects modulation of anxiety, which is also seen in pain states but is not specific to pain. We employed two classical anxiety behavioral tests, namely open field (OP) and elevated plus maze (EPM). Mice with optogenetic suppression of the prefrontal remote fear recall population did not show significant differences from control ArchT-expressing mice without illumination in all parameters of anxiety testing (Figure 34B, C). Thus, unlike the suppression of pain, this

RESULTS

optogenetic inhibition of the PL remote fear memory engram did not generally affect aversion or anxiety encoding.

To further verify the expression and functionality of fear recall labeling and ArchT expression, we analyzed c-Fos as a marker for neuronal excitation. In mice with ArchT expression with laser illumination, c-Fos expression in the PL was significantly decreased (Figure 35A). Simultaneously, the overlap population labeled both by formal fear recall engram (Venus) and fear recall stimulus were also decreased in sham mice and CFA-injected mice (Figure 35B). The same tendency was observed with overlap ratio which overlap population counts divided by fear recall engram labelled population or fear recall stimulus activated population (Figure 35C). This evidence confirms the efficiency of optogenetic inhibition, with the same inhibition of remote fear engram populations in both inflammation pain mouse model and physiological sham control.

RESULTS

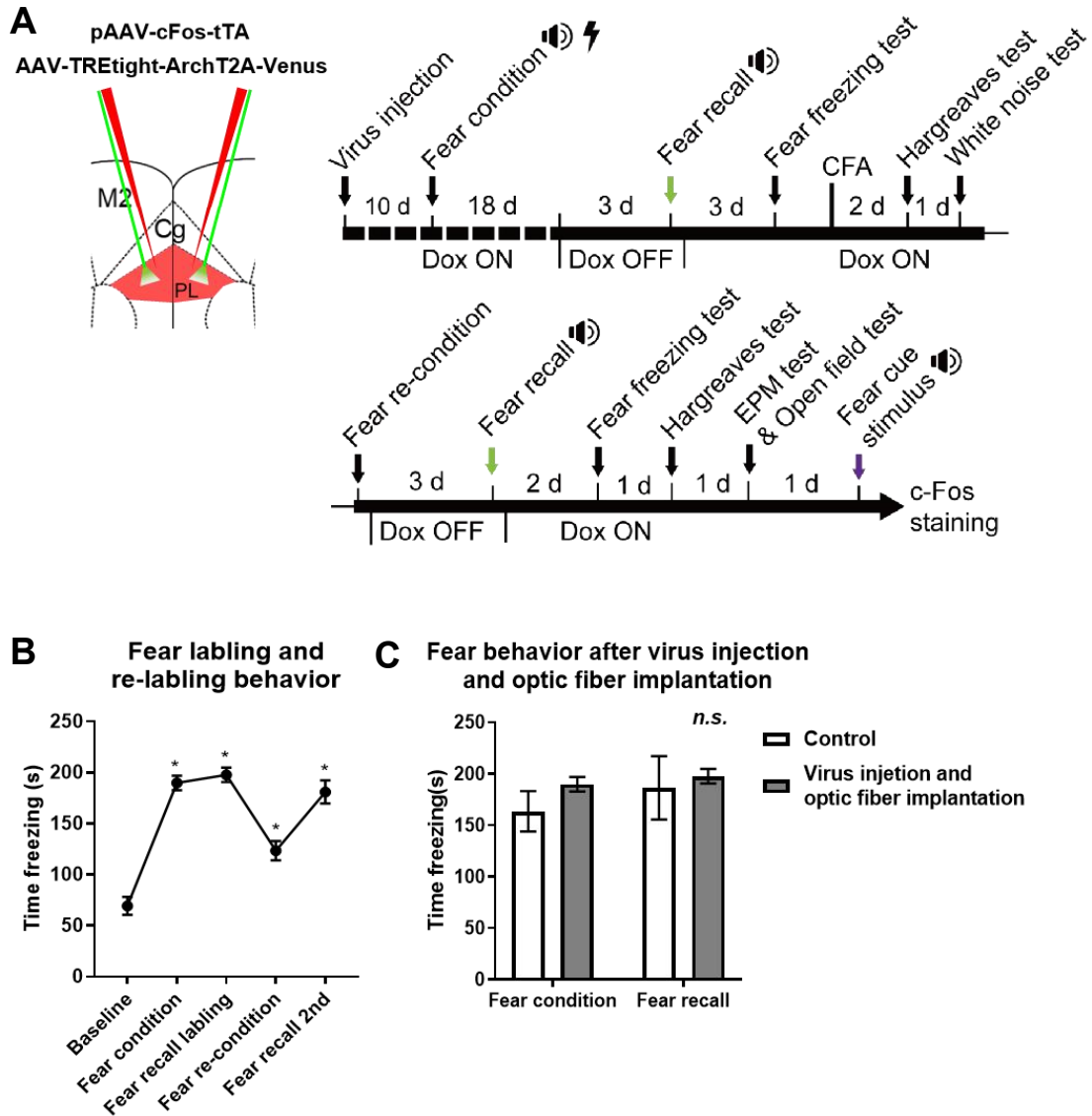
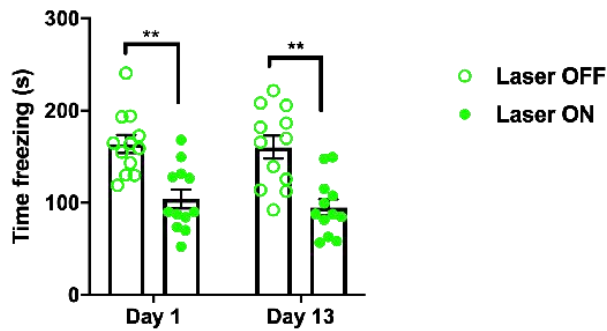


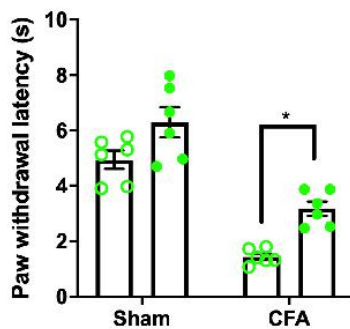
Figure 32. Optogenetic suppression of PL fear engram under inflammatory pain conditions. **A**, schematic showing the bilateral injection of virus combination and optic fiber implate into the prelimbic cortex. Experimental schematic showing the timeline of two-times (acute stage or chronic stage) fear labeling and behavior tests with ArchT suppression. **B**, Freezing behavior analysis of first and second fear condition and fear recall labeling. Data from 12 mice, $p < 0.05$ indicated by *, compare to baseline, one-way ANOVA with Bonferroni correction. **C**, Freezing behavior analysis between non-surgery control mice and the mice took virus injection and optic fiber implantation. Control group $n = 4$, virus injection and optic fiber implantation group $n = 12$. Unpaired t test was performed.

RESULTS

A Fear recall test with optogenetic suppression post-CFA day 1 or day 13



B Hargreaves test with optogenetic suppression post-CFA day 2 and day 3



Hargreaves test with optogenetic suppression post-CFA day 14 and day 15

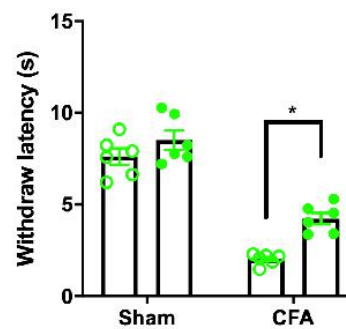
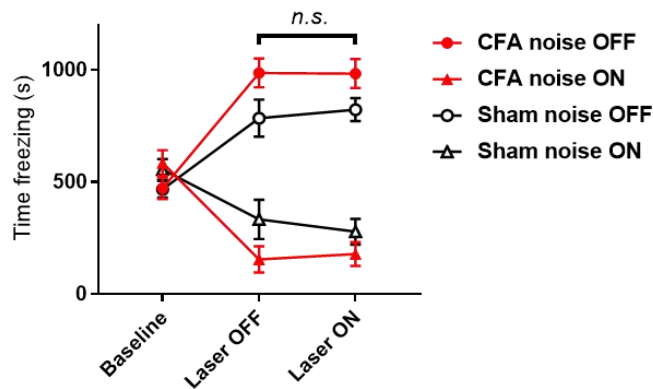


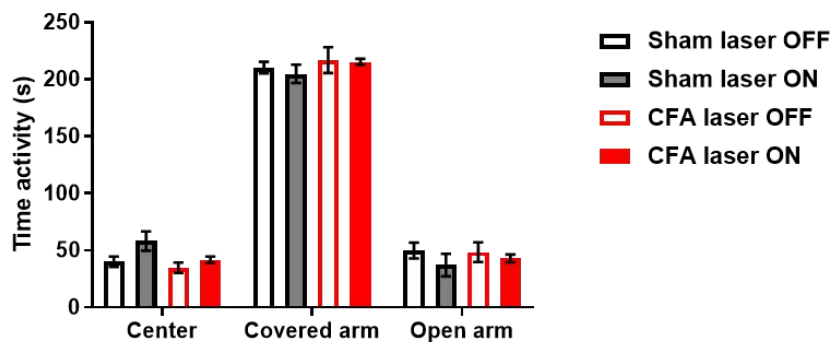
Figure 33. Analysis of fear and pain behavior upon optogenetic suppression of the PL fear engram. **A**, quantification of fear freezing behavior with or without ArchT-induced suppression before CFA injection. $p < 0.05$ indicated by *, based on two-tailed paired t-test. Counting data from 12 mice of both groups. **B**, quantification of heat hypersensitivity behavior test with or without ArchT-induced suppression after CFA injection, in the acute stage (2-3 days after CFA injection) or chronic stage (14-15 days after CFA injection). $p < 0.05$ indicated by *, based on two-tailed paired t-test. Data from 6 mice per group. All data are represented as mean \pm SEM.

RESULTS

A White noise test with optogenetic suppression of PL fear engram post-CFA injury



B EPM test with optogenetic suppression of PL fear engram post-CFA injury



Open field test with optogenetic suppression of PL fear engram post-CFA injury

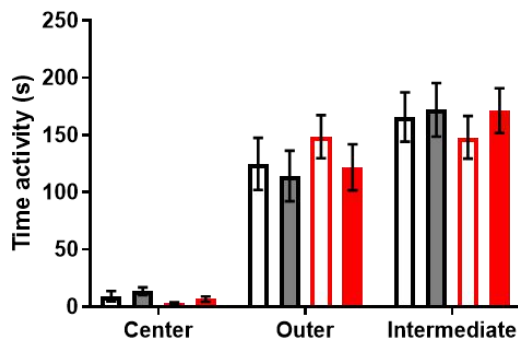


Figure 34. Analysis of non-painful aversion behavior upon optogenetic suppression of PL fear engram. **A**, quantification of freezing behavior in CFA-injected mice or sham mice in the chamber associated with white noise or in the quiet chamber, with or without ArchT-mediated optogenetic suppression. **B**, quantification of anxiety-related behavior in the elevated plus maze (EPM) and open field behavior test in CFA-injected or sham mice, with or without ArchT-mediated suppression of PL fear engram. All the comparison above was between laser ON or laser OFF in each group, based on two-tailed paired t-test. Data from 6 mice per group. All data are represented as mean \pm SEM.

RESULTS

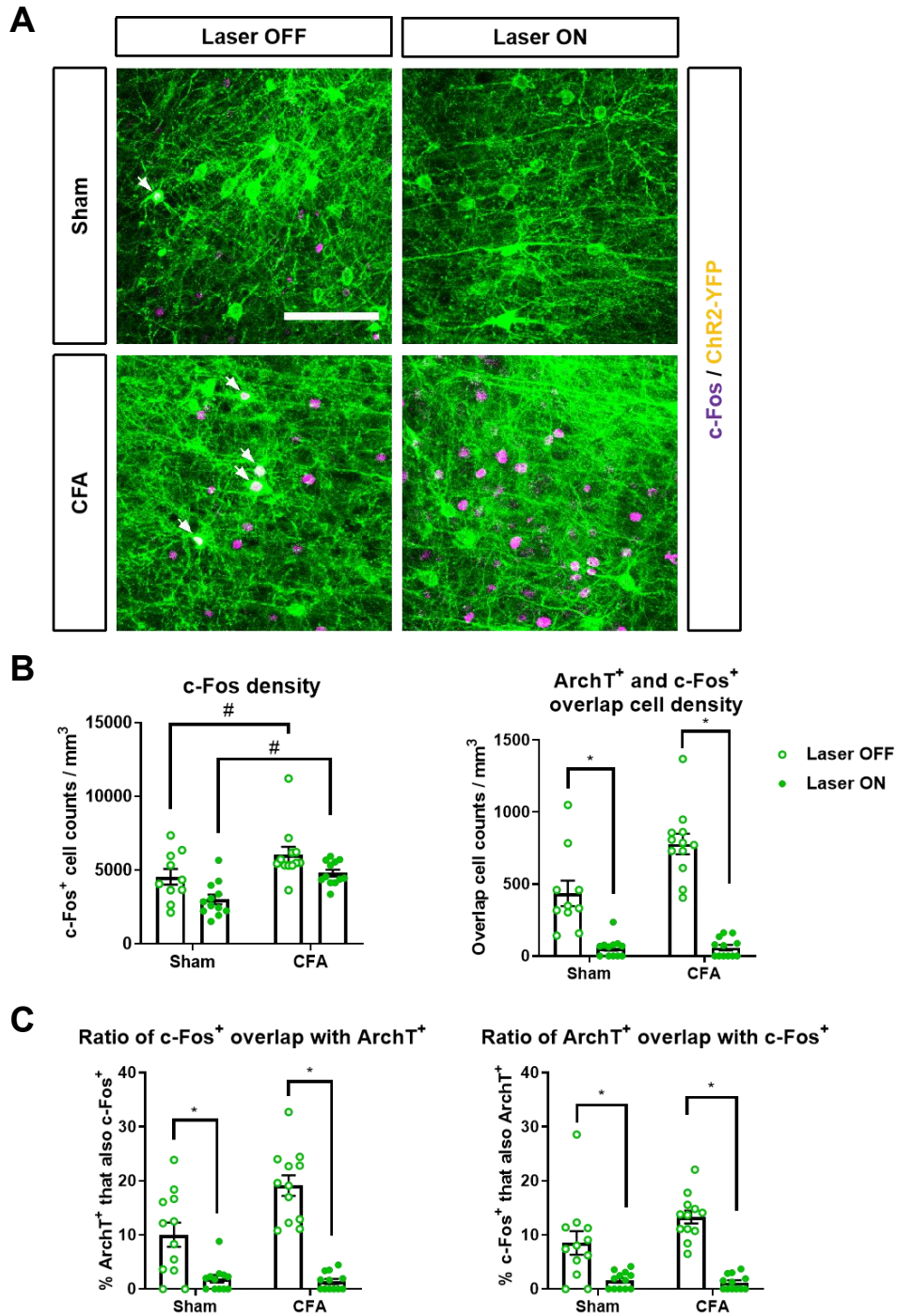


Figure 35. Analysis of fear cue stimulus-activated c-Fos expression upon optogenetic suppression of PL fear engram. **A**, Sample image of fear engram labeling via fear recall and c-Fos expression via fear cue stimulation, in CFA injected mice or sham mice. Arrows indicate overlapping cells. Scale bar represent 100 μm . **B**, quantification of c-Fos positive cells, or ArchT and c-Fos overlapping cells in the prelimbic cortex after fear cue stimulation in CFA injected mice or sham mice. **C**, overlap ratio of ArchT positive cell also c-Fos positive, and c-Fos positive cell also ArchT positive. $p < 0.05$ indicated by #, compared between CFA and sham group; $p < 0.05$ indicated by *, compared between Laser OFF and Laser On in each group, based on two-tailed paired t-test. Counting data from 4 slice per mice, 3 mice per group. Data are represented as mean \pm SEM.

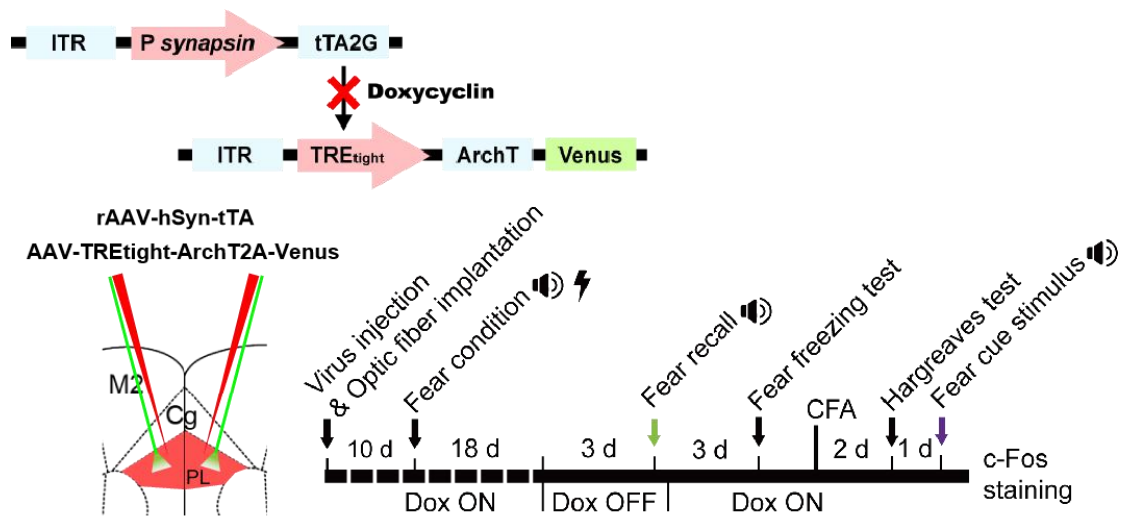
RESULTS

3.10 Suppression of random neurons in the prelimbic cortex does not impact on post inflammatory heat hypersensitivity

To further investigate the specificity of this modulation of pain by the remote fear memory ensemble, we next engineered cells to express the inhibitory opsin ArchT randomly under the synapsin promoter, which enable expression across all neuronal population (Figure 36A). Upon random expression of ArchT followed fear conditioning and labelling, optogenetic suppression did not show the difference in fear recall behavior (Figure 36B). In the Hargreaves test post-CFA, we did not observe any change upon laser illumination in pain perception (Figure 36C). Following optogenetic suppression of the random PL population investigated c-Fos expression in the PL. Optogenetic suppression did not impact on c-Fos expression and overlap ratio between fear and pain engram in the PL (Figure 37), which indicates that unspecific expression of ArchT in random PL neuron population could not suppress the fear engram in the PL. These experiments demonstrate that modulation of pain population is specific to the fear recall engram and not caused unspecifically by random neurons of the PL.

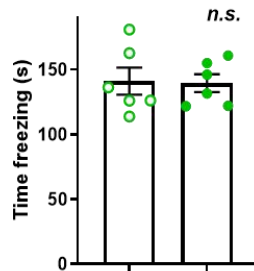
RESULTS

A



B

Freezing test with optogenetic suppression of random PL neuron



C

Hargreaves test with optogenetic suppression of random PL neurons post-CFA injection

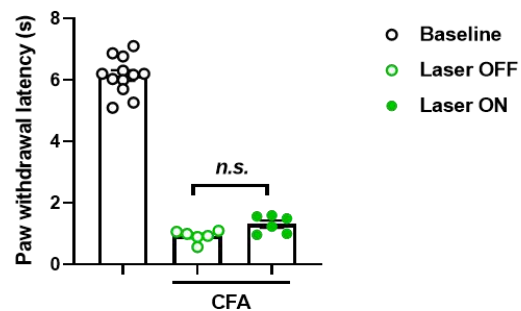


Figure 36. Optogenetic (ArchT) suppression of random prelimbic population and associated behavioral tests. **A**, Schematic showing the design of synapsin-based sparse labeling of random prelimbic neuronal population and the timeline of behavioral tests after ArchT-induced suppression and fear cue stimulation. **B**, quantification of fear freezing behavior with or without ArchT-induced suppression of random PL neuron before CFA injection. **C**, quantification of heat hypersensitivity behavior test with or without ArchT-induced suppression of random PL neuron after 2 days of CFA injection. All test analysis based on two-tailed paired t-test, data from 6 mice per group. Baseline data from both paw of the mice. All data are represented as mean \pm SEM.

RESULTS

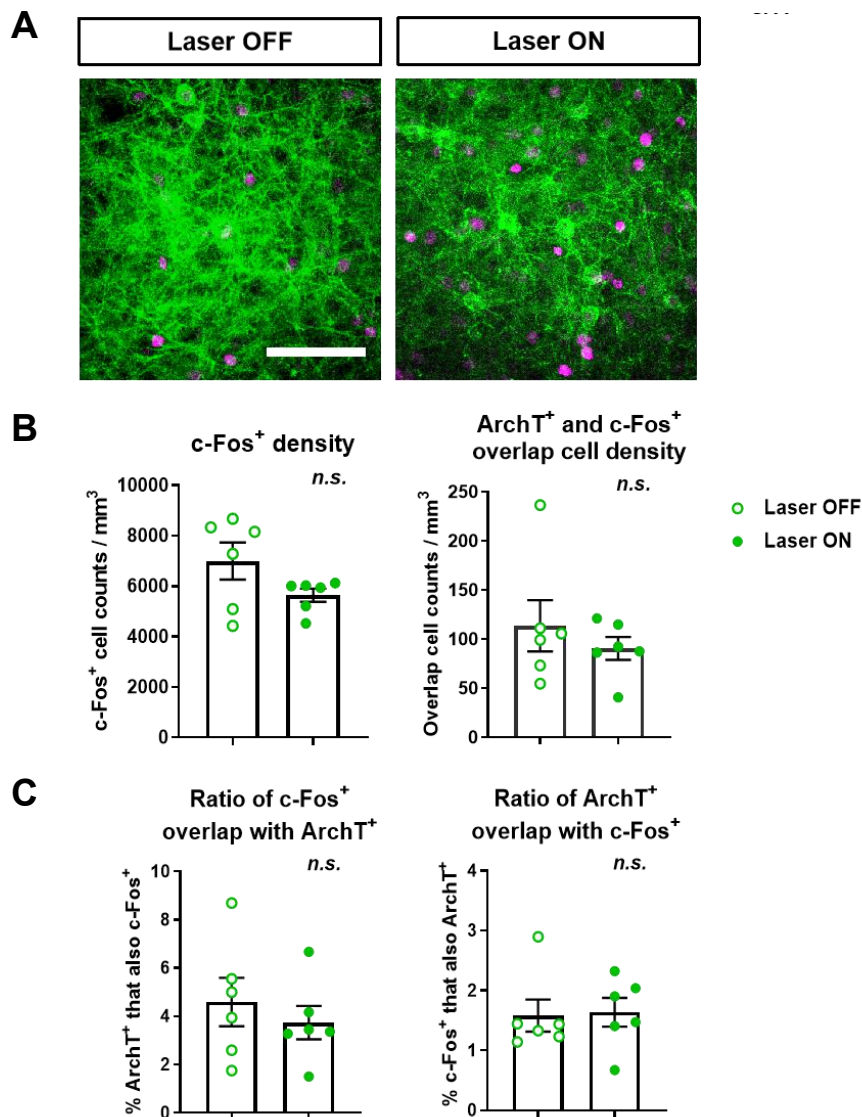


Figure 37. Analysis of fear cue stimulus-activated c-Fos expression upon optogenetic suppression of PL random neurons. **A**, Sample image of PL random neuron labeling via ArchT and c-Fos expression via fear cue stimulation, post CFA injection. Scale bar represent 100 μm . **B**, quantification of c-Fos positive cells, or ArchT and c-Fos overlapping cells in the prelimbic cortex after random neuron labeling and fear cue stimulation, post CFA injection. **C**, overlap ratio of ArchT-positive cells that are also c-Fos positive, and c-Fos-positive cells that are also ArchT-positive. All analyses based on two-tailed paired t-test. Counting data from 4 slice per mice, 6 mice per group. Data are represented as mean \pm SEM.

RESULTS

3.11 Activation of PL fear engram coding neuron deteriorating acute pain behavior post capsaicin injection

Our work thus far suggested that suppressing the fear engram in the PL attenuates pain. This raised the question as to whether activation of the PL fear engram is involved perception and facilitates it. Therefore, we engineered PL neurons engineered cells active during remote fear recall to express the classical excitatory opsin Channelrhodopsin-2(ChR2), which stimulates neuron electrical excitability upon illumination with blue light (Figure 38A). To verify specific labelling of the fear engram and ChR2-mediated neuronal activation in vivo, we first tested freezing behavior during fear recall after labelling the fear engram labelling with YFP-tagged ChR2. Upon blue light illumination of the PL fear engram, mice show an increase in freezing behavior in the absence of any fear cues, which consistent previous reports (Figure 38B). Next, we tested heat sensitivity of these mice upon optogenetic activation the PL fear engram. We observed that upon activating the fear recall engram, mice showed an increased sensitivity to thermal stimuli which was evident as a drop in latency to infrared heat in the Hargreaves test (Figure 38D). Furthermore, mice with ChR2-mediated activation of the fear recall population in PL spent significantly more time in exhibiting nocifensive behaviors upon hind paw capsaicin injection, such as licking, flicking, and lifting, as compared to capsaicin-evoked responses in the other paw upon absence of blue illumination (Figure 38E). To further investigate the specificity of this fear recall engram-dependent modulation, we also tested anxiety and conditioned fear in an open field. Mice did not show a significant change in anxiety or immobility behavior after optogenetic activation of the fear recall engram (Figure 38C). Last, we investigated c-Fos expression in these mice post-capcaisin injection (Figure 39A). In mice with laser illumination, c-Fos positive cells in the PL were significantly higher in number than in mice without laser illumination of the PL fear engram (Figure 39B).

RESULTS

Capcaisin injected mice did not show a further increase upon optogenetic activation, which could be because capsaicin injection is a strong nociceptive stimulus and activates a large number of cells in the PL (Figure 39B). We also analyzed c-Fos expression in cells labeled by fear recall. Mice with optogenetic activation of the fear engram showed a large overlap with the neurons expressing c-Fos upon capsaicin stimulation (Figure 39B, C) Overall, these result indicate that modulation of the remote fear engram in the PL exhibits a bivariate regulatory nature, which affects acute pain perception in both positive and negative dimensions upon excitation or inhibition of fear memory.

RESULTS

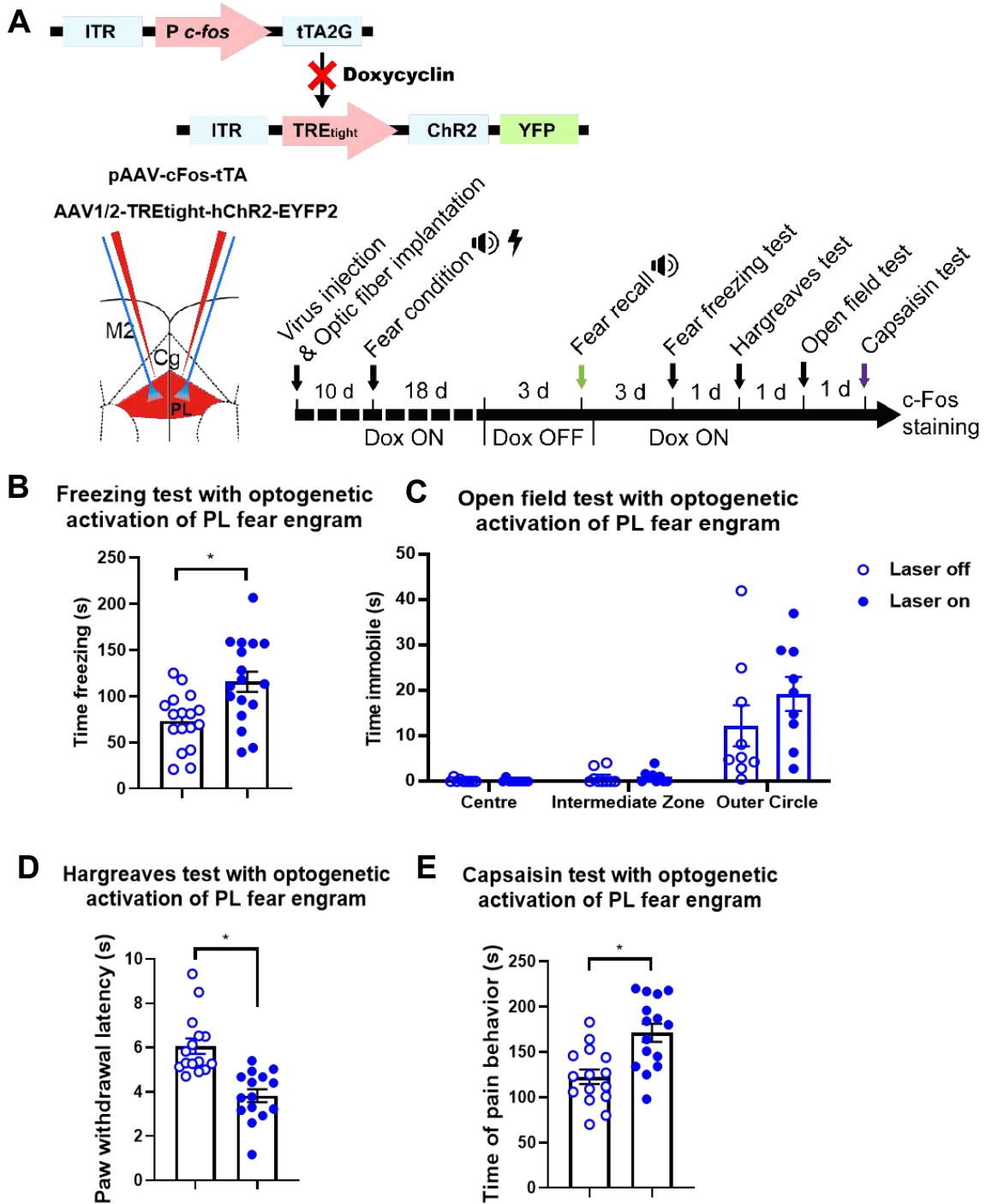


Figure 38. Impact of optogenetic activation of PL fear engram on capsaicin-mediated tonic pain. **A**, schematic showing the experimental design, virus combination injection and optic fiber implantation into the prelimbic cortex. Experimental schematic showing the timeline of fear labeling and behavioral tests with ChR2 activation after a capsaicin injection. **B**, quantification of fear freezing behavior, or **C**, aversion open field test, or **D**, heat hypersensitivity behavior test with or without ChR2 activation before capsaicin injection. **E**, quantification of pain related behavior with or without ChR2 activation after capsaicin injection. $p < 0.05$ indicated by *, all the analysis based on two-tailed paired t-test. Data from 15-17 mice. All data are represented as mean \pm SEM.

RESULTS

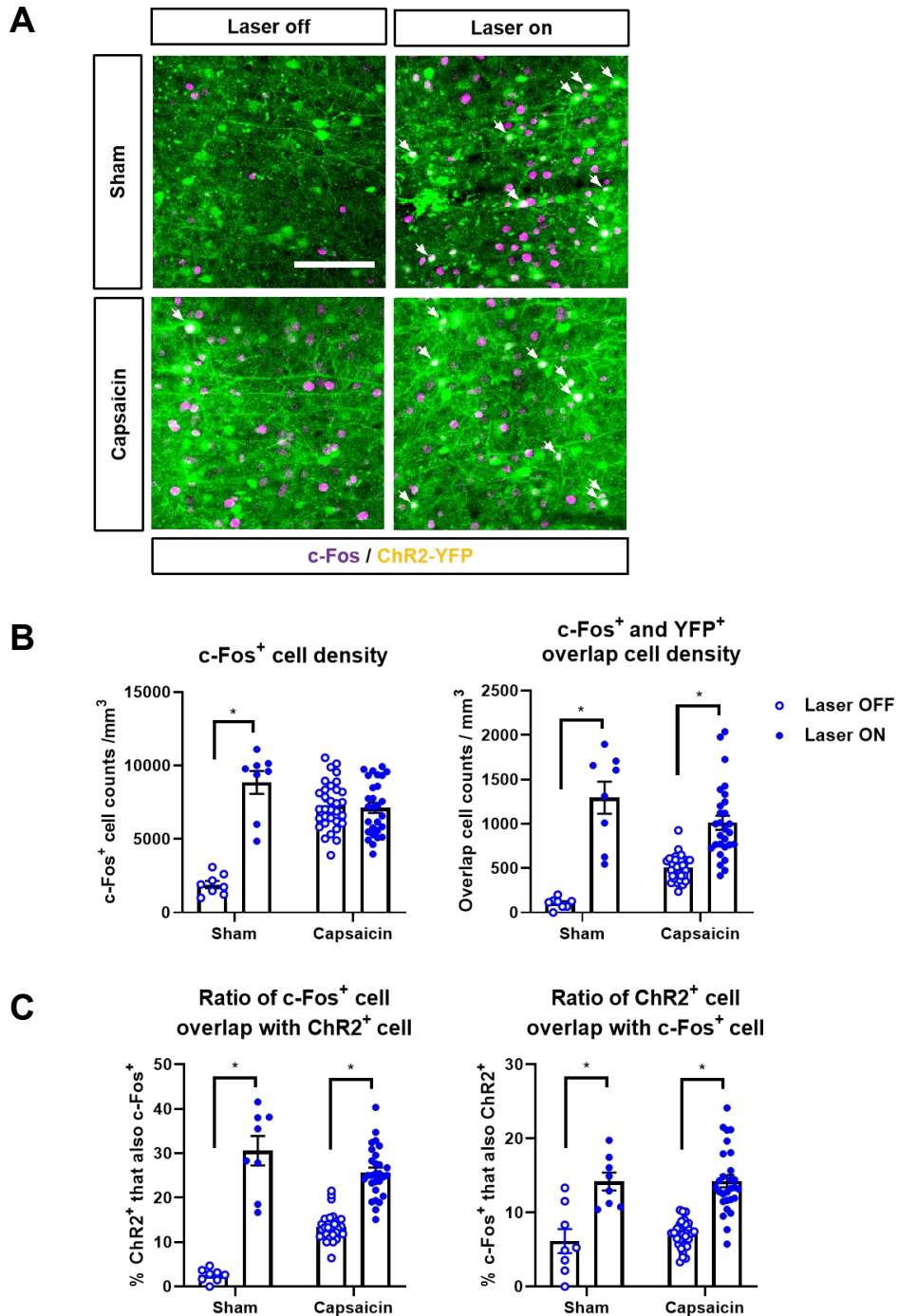


Figure 39. Analysis of c-Fos expression after optogenetic activation of PL fear engram or capsaicin injection. **A**, Sample image of fear engram labeling neurons and c-Fos expression with or without fear engram optogenetic activation and capsaicin injection to induce tonic pain. Arrows indicate overlapping cells. Scale bar represents 100 μ m. **B**, quantification of c-Fos positive cells, or ChR2 and c-Fos overlapping cells with or without fear engram optogenetic activation. **C**, overlap ratio of ChR2 positive cell also c-Fos positive, and c-Fos positive cell also ChR2 positive. $p < 0.05$ indicated by *, compared between Laser OFF and Laser On in each group, based on two-tailed paired t-test. Counting data from 4 slice per mice, 7-8 mice of each capsaicin injection group and 2 mice of each sham group. Data are represented as mean \pm SEM.

DISCUSSION

4 Discussion

The modulation of pain perception involves different levels of peripheral versus central regulation, including selective spinal cord processing-mediated regulation or brain integration of input signals. Here, we first generated conditional knock out mice for a key GABA_A receptor subunit in all DRG sensory neurons or specifically in nociceptors and investigated the influence of spinal presynaptic GABAergic inhibition on mechanical punctate allodynia as well as dynamic allodynia. Next, we identified underlying spinal circuits using IEG expression time interval based dual-epoch method. In a second study we continued the theme of inflammatory pain modulation by exploring interaction between fear memory and inflammatory and tonic pain using IEG-based cell-tagging, optogenetic approaches and a large number of behavioral readouts, revealing that prefrontal fear engrams facilitate tonic and inflammatory pain perception.

4.1 Motor function of GABA_Aβ₃ knock out functions of PSI in mechanosensation and behavior

GABAergic presynaptic inhibition correlates to sensory-motor control. GABAergic inhibitory interneurons that make axo-axonic connections with sensory terminals vary from other spinal GABAergic neurons. Fink et al. reported that Presynaptic inhibition at sensory-motor synapses is mediated by GABAergic Gad2-expressing interneurons, and their selective elimination causes motor vibrations during goal-directed reaching (Fink et al. 2014). Presynaptic inhibition operates in various relays of the somatosensory systems. A study showed that loss of GABA_ARs in somatosensory neurons after weaning led to tactile hypersensitivity and impaired tactile information processing and responsiveness during development, resulting in abnormal anxiety and social interactions in adult mice (Orefice et al. 2016). The motor function of sensory neuron GABA_Aβ₃ knock-out mice shows that GABA has a

DISCUSSION

slight impact on the fine movement in different ways. Advillin-GABAA β 3 knock-out mice were observed to exhibit an over movement in the home cage test, with loss of GABAARs in somatosensory neurons leading to anxiety-like and exploratory behavioral alterations. This result is consistent with a recent study that concluded that somatosensory neuron-specific GABAA β 3 conditional knock-out mice show increased exploratory behavior, spend more time in the center chamber of the open field test and display less aversion to the open arms of the elevated plus-maze test. This may be owing to GABAAR-dependent presynaptic inhibition underlying the glabrous skin innervating A β - low-threshold mechanoreceptor (LTMR) terminals, thus giving a substrate for acuity control (Orefice et al. 2016; Zimmerman et al. 2019).

4.2 Pain-related sensation change of GABAA β 3 knock out

Our deletion of GABAA β 3 in sensory neuron mimics punctate mechanical hypersensitivity upon previously upon embryonic or adult deletion of these subunits (Pagadala et al. 2013; Orefice et al. 2016; Zimmerman et al. 2019), showing that these receptors play an important function in regulating punctate mechanosensation. To investigate the presynaptic GABAA effect on different sensations, we further performed several basal sensation behavior tests. Advillin-GABAA β 3 mice did not cause deficits in D-hair-related innocuous touch sensation or sensorimotor function or exhibited thermal or dynamic mechanical hypersensitivity. In contrast, we did not observe a punctate mechanical but heat hypersensitivity phenotype on the mouse line in which the GABAA β 3 is knocked out selectively in primary nociceptors in this study. In the previous study, the amplitude of GABAA receptor current was significantly reduced in these mice compared to wild-type mice, demonstrating that a functional loss of presynaptic GABAA receptors might cause a reduction of the threshold of nociceptive sensation. Considering that

DISCUSSION

injurious heat information is generally mediated by TRPV1-positive nociceptor (Mandadi and Roufogalis 2008), whereas punctate mechanical sensation is mediated more by A β sensory neurons (Cheng et al. 2017; Sakai and Akiyama 2020), such results may reflect the heterogeneity of these two different sensory modalities.

4.3 GABAA β 3 deletion from nociceptors impacts on punctate, but not dynamic, inflammatory allodynia

Brush-evoked dynamic and filament-evoked punctate hypersensitivities are two types of mechanical hypersensitivity that may be debilitating for millions of people suffering from chronic pain. Cheng et al. first reported a mice phenotype with a reduction in dynamic mechanical hypersensitivity induced in SNI nerve injury or CFA inflammation mice model (Cheng et al. 2017). The mice lost the brush-evoked nocifensive responses through ablation of VGLUT3 and Lbx1 co-expression in spinal neurons throughout development (VT3^{Lbx1} neurons). In this study, SNS-GABAA β 3^{-/-} and Advillin-GABAA β 3^{-/-} mice were challenged in different pain-related sensation behaviors, post-inflammatory injury. However, the SNS-GABAA β 3^{-/-} mice did not develop punctate allodynia but showed preservation of dynamic hypersensitivity, having an opposite phenotype with VT3^{Lbx1} mice. However, each of these two contrasting phenotypes is due to a different mechanism. In humans study, brush-evoked dynamic allodynia is considered to be transmitted via myelinated A β or A δ mechanoreceptors (Campbell et al. 1988; Torebjörk et al. 1992; Ochoa and Yarnitsky 1993; Koltzenburg et al. 1992). Under the inflammatory condition, punctate or dynamic mechanical allodynia activates the targeted CR neurons in lamina II by engaging CCK or tVGLUT3-expressing neurons in lamina III. To evoke mechanical allodynia, these CR neurons subsequently activate projection neurons (PNs) directly or indirectly through vertical cells. (Peirs et al. 2021). In DRG, after

DISCUSSION

inflammatory injury, an increased G^{GABA} after inflammatory injury would convert presynaptic inhibition to excitation (Chen et al. 2014); hence, enhancing a cross activation of the pain pathway by non-nociceptive input, with $A\beta$ mechanoreceptors contributing to the C-fiber input (Da Guo, 2017). Since CR neurons receive both A-fiber and C-fiber inputs from DRG, the enhanced activation of nociceptive pathways could also contribute to allodynia. Here, we only observed a dynamic hypersensitivity but not punctate allodynia, suggesting that this presynaptic modulation to some extent can influence distinct mechanoreceptive modalities. Among other sensations, we did not observe significant differences in the formation of hypersensitivity after injury in knockout and control mice, which also suggests that loss of GABA uniquely affects the formation of punctate mechanical allodynia.

GABA is an important transmitter that induces presynaptic inhibition via generating the primary afferent depolarization (PAD), which prevents the production of excitatory transmitters by a primary afferent central terminal (Gradwell et al. 2020). Depolarization of the central terminals of nociceptors can inactivate voltage-gated calcium channels, reducing calcium inflow and transmitter release. PAD may also inactivate voltage-gated sodium channels, as well as have a shunting effect by opening the GABA_A receptor; as a result, action potential propagation towards primary afferent terminals may be hampered. It was previously reviewed that GABA_A receptor agonists had analgesic benefits in neuropathic pain situations were previously evaluated, but their effects in inflammatory pain were debatable (Guo and Hu 2014). Analgesia effect has been attributed to both agonists and antagonists of the GABA_A receptor. This ambiguous impact of the GABAergic system might be explained by a distinct event known as the dorsal root reflex (DRR), which occurs exclusively after inflammation but not after nerve damage. (Willis 1999). Here, a paw edema reduction was observed post inflammation in SNS-GABA β 3^{-/-} mice. In a summary, DRR is caused by a strong form of PAD

DISCUSSION

capable of evoking an action potential. PAD now has an excitatory rather than an inhibitory effect, and the mechanical allodynia induced by inflammation is most likely owing to the excitatory switch of the GABA effect, which is triggered by increased PAD strong enough to activate action potentials. (Da Guo, 2017; Price et al. 2009; Garcia-Nicas et al. 2001; Cervero et al. 2003).

4.4 An intermingled pattern of punctate and dynamic allodynia post-inflammation

It has been previously demonstrated that 2 days after CFA injection, GABA fails to suppress high Cl^- Ringer's solution generated calcium transition in the mouse spinal cord tissue slice; however, GABA alone could generate calcium influx in more presynapses in the spinal cord from CFA-injected mice (Da Guo, 2017). Here, a distinct punctate allodynia circuit deactivation was observed in nociceptor GABAA receptor knock mice in the spinal cord dorsal horn laminae I–III. This is consistent with the earlier hypothesis, where an excitation effect of GABA generated by peripheral inflammation, suggested a presynaptic inhibition effect of GABA switch to excitation in peripheral inflammation (Guo and Hu 2014). The circuit of punctate and dynamic mechanical allodynia was well discussed in a previous study. However, most studies have emphasized the postsynaptic disinhibition function of interneurons in laminae III-IV and correlated excitatory neurons in laminae II. In the present study, we demonstrated another aspect of inhibition - presynaptic inhibition, involved in the regulation of the mechanical allodynia circuit. Despite this, we further discriminated the punctate and dynamic allodynia circuit, uncovering an intermingled activation pattern post-inflammation. In our results, after inflammation, punctate and dynamic stimuli activated cells formed an intertwined neural network in spinal cord laminae I–III, where some cells contributed to a distinct modality of mechanical allodynia circuit; however, a few others responded to both. In particular, in mice with deleted GABA,

DISCUSSION

neurons that should have been activated by punctate stimulation did not show an expression response of c-Fos. This indicated that punctate stimulation due to GABA absence did not occur in response to excitation switch after inflammation.

Recently, a study showed that Blocking glycinergic transmission in the spine can cause transitory dynamic allodynia but not punctate allodynia. (Lee et al. 2013; Miraucourt et al. 2009), when glycine receptor inhibitor, strychnine, was administered intrathecally. In contrast, Only punctate, but not dynamic allodynia was produced by bicuculline, a GABAA receptor inhibitor (Shi et al. 2019). These findings imply that dynamic allodynia is more susceptible to glycinergic transmission failure than punctate allodynia, and that inhibiting spinal glycinergic transmission causes dynamic allodynia exclusively. Dynamic allodynia, on the other hand, may be more susceptible to GABAergic transmission regulation than punctate mechanical allodynia. This is consistent with the study observations. First, the neuron population encoding the response to punctate or dynamic mechanical allodynia shows separate but partial overlap. Second, the GABAA receptor loss could reduce the population response to punctate mechanical allodynia, but not dynamic allodynia. Third, the reduced population is not only from the punctate allodynia coding specific cells; however, the overlapping ones also show a response to dynamic allodynia.

Although activation of GABAA receptors is commonly recognized as a major factor in the presynaptic inhibition of both nociceptors and LTMRs, glutamatergic N-methyl-D-aspartate receptor (NMDAR) could also regulates sensory inputs presynaptically on sensory neuron terminals in the dorsal horn. (Zimmerman et al. 2019). Zimmerman et al. defined two distinct circuits of presynaptic inhibition of cutaneous somatosensory neuron inputs to the spinal cord. Low-threshold cutaneous afferents elicit a GABAA

DISCUSSION

receptor-dependent presynaptic inhibition, whereas small-diameter afferents elicit an NMDAR-dependent presynaptic inhibition that inhibits large-diameter fibers. This evidence suggests these different modes of presynaptic inhibition play different roles in distinct forms of allodynia. To provide an integrated understanding of the mechanisms of allodynia circuit switching, a differentiated study of the effects of different peripheral neuron types on presynaptic inhibition, coupled with the mechanisms of postsynaptic inhibition in the spinal cord, will be required in the future.

4.5 Calretinin neurons participate in the punctate allodynia formation in the spinal cord

The primary relay point for innocuous and noxious sensory information is the spinal dorsal horn. This location integrates sensory inputs via a complex neural circuit that includes both excitatory and inhibitory interneurons, ultimately recruiting projection neurons to transmit the touch or pain information to the brain (Bohlen et al. 2011; Todd 2010a). Changes in the activity of these interneurons have a substantial impact on touch and pain perception (Petitjean et al. 2015; Peirs et al. 2015a; Cui et al. 2016). Calretinin-expressing (CR) interneurons form up a substantial population in the dorsal horn's superficial layers. Anatomical and electrophysiological evidence (Smith et al. 2016; Smith et al. 2015), as well as behavioral studies including specific neuron ablation methods (Duan et al. 2014) or pharmacogenetic activation of CR neuron (Peirs et al. 2015b), all point to CR neurons being involved in the processing of noxious inputs and the production of mechanical allodynia, or pain induced by innocuous stimuli. Petitjean et al. demonstrated that CR neuron stimulation can elicit nocifensive responses in addition to acting as amplifiers of incoming sensory signals, which mice show indications of spontaneous pain, such as facial grimacing, shortly after chemogenetic stimulation of CR neurons (Petitjean et al. 2019). About half of

DISCUSSION

the excitatory inputs to these projection neurons come from CR neurons, which have a direct connection to ascending pathway. These evidence highlights that the CR neurons are important for the activation of nociceptive circuits. Our c-Fos data show both punctate and dynamic mechanical stimuli activated cell partial expression CR in control mice, reaching a ratio of 19.8% and 20.8% in lamina I–II, respectively. This is consistent with the study by Peirs et al., who reported that after activation of hM3Dq in VGLUT3^{Cre} mice, the c-Fos was costained with 28% of calretinin⁺ neuron in lamina I–II (Peirs et al. 2015b). Furthermore, further c-Fos studies for mechanical allodynia in the setting of chronic pain models revealed that CR neurons had a greater number of c-Fos⁺ cells following inflammatory injury than after nerve injury. Moreover, from a recent study, Peirs et al. showed in inflammatory pain models, but not in neuropathic pain models, targeted CR neurons are important for conveying mechanical allodynia, while inhibition of the CR neurons in the CFA model caused a statistically significant reversal of punctate mechanical allodynia. (Peirs et al. 2020). CR neurons are highly interconnected, as demonstrated by an in vitro electrophysiology study, which showed that CR-ChR2 neurons exhibit diverse functional excitatory synaptic connections within the dorsal horn. This study showed that CR neurons establish an excitatory network when participating in chronic pain networks based on both intrinsic and extrinsic properties; thus, producing persistent activation after intense stimulation and acting as pain amplifiers (Smith et al. 2019). Our data are in line with these observations that CR neurons represent a mechanism for the role of presynaptic GABAA receptor involvement in punctate mechanical allodynia post-CFA. We therefore suggest that not only the postsynaptic input from the interneuron of deep III–IV lamina, but also the excitation of the presynaptic terminal from nociceptors in lamina I–II, may modulate inflammatory pain processing via CR neurons. CR neurons simultaneously receive high threshold excitatory inputs and also mediate low threshold afferents. This is not contradictory but suggests that inflammatory

DISCUSSION

allodynia consists of additional factors and that the enhancement of high threshold nociceptive signals also influences the formation of nociceptive sensitization, while low threshold touch signals pass through postsynaptic gating in deep laminae.

4.6 PV neurons participate in the punctate allodynia formation in the spinal cord

Unlike CR neurons, spinal cord parvalbumin-expressing (PV) inhibitory interneurons, which predominate in lamina III - IV, have recently been shown to be involved in axo-axonic synapses with non-nociceptive A δ afferents, or larger myelinated fibers. (Hughes et al. 2012). These Axo-axonic synapses on the primary afferent fiber central terminals regulate sensory input and anatomical correlates of presynaptic inhibition. Consequently, PV expressing neurons play a crucial role in the development of tactile allodynia and central sensitization. GABA release at axo-axonic synapses mediates presynaptic inhibition, which leading to GABA-mediated PAD (Kullmann et al. 2005). Boyle et al. reported PV-expressing interneurons as a source of presynaptic inputs onto several classes of myelinated LTMRs from both hairy and glabrous skin, where individual PV interneurons can mediate two distinct forms of inhibition, namely, presynaptic inhibition of LTMR afferents and postsynaptic inhibition of vertical cell dendrites (Boyle et al. 2019). A recent study has established that virtually all central terminals from myelinated afferent fibers arborizing in the LTMR-recipient zone (LTMR-RZ; laminae Iii-IV) are associated with inhibitory axon terminals (Abraira et al. 2017) and that a significant proportion of these inhibitory inputs express PV. This implies that all LTMRs are under presynaptic control and that many of these axoaxonic synaptic inputs are derived from PV cells. Selective ablation of spinal PV interneurons leads to the development of mechanical hypersensitivity, whereas the chemogenetic activation of these cells in

DISCUSSION

allodynic mice restores normal mechanical thresholds (Petitjean et al. 2015). Boyle et al. showed that selectively blocking synaptic transmission from PV cells, innocuous peripheral manipulation produced robust c-Fos immunolabeling throughout laminae I–IV of the spinal cord dorsal horn (Boyle et al. 2019). Here, our result showed that GABAA receptor knockout from the nociceptor reduces the ratio of activation of PV cells, while excitation loss also reduces the PV cell leading to presynaptic inhibition. This further suggests that there are multiple modes of presynaptic inhibition. A possible explanation is that after inflammation, presynaptic inhibition transfer to excitation not only activates the excitatory neuron located in lamina II but also reduces the inhibitory interneuron in laminae III–IV, which opens the gate of LTMR, producing allodynia.

4.7 Dual-epoch mapping method to discriminate punctate and dynamic allodynia circuits in spinal cord

There are limitations to existing mainstream neuroscience research methods for distinguishing between two distinct neurobehavioral pathways. Traditional electrophysiological recordings can record only a small number of neurons at a time; while calcium imaging recordings can only be made in spinal cord sections, and even two-photon microscopy can detect signals in the more superficial layers of the dorsal horn of the spinal cord. Thus, behavioral neuroscience requires a molecular imaging technique that can compare activity patterns of different physiological states at the cellular level. Several innovative functional imaging methods of IEG-based genetic mouse models such as TetTag, TRAP, or CANE mice have been developed to examine the neural correlates of two distinct stimuli (Zhang et al. 2015; Guenther et al. 2013; Sakurai et al. 2016). However, these methods require waiting for the expression of the secondary signal and switching off the expression of the reporter after the first stimulus is applied. For transient stimuli such as

DISCUSSION

mechanical pain, all the aforementioned methods take too long to open and close the behavioral recording channel. The spinal cord regularly receives signals from peripheral sensations; thus, would generate excessive background noise to obtain a reasonable signal-to-noise ratio. Therefore, to investigate the activity pattern of dynamic and punctate mechanical allodynia post inflammation, we chose to perform the IEG gene-based dual-epoch method to discriminate the population involved. The strengths of this method are as follows. After the first stimulation, it does not require any intervention with the animal; therefore, the second stimulation can be performed directly. Moreover, the interval between the first and second stimulation is only 2–3 h, which minimizes the possibility of the animal being affected by other factors. As with the techniques aforementioned, we can characterize the type of neuron by co-staining with other markers and obtain a spatial representation of the population by post-processing the image transformation. However, there are still limitations to such a technique. It is unable to detect neurons below the detection threshold or inhibited by a stimulus; this poses difficulties for our understanding of the spinal pathway of touch sensation in the physiological state. As normally low threshold neural activity does not result in high expression of c-Fos genes; therefore, we cannot use this technique to understand the population of non-pain sensations in the spinal cord before the injury. In conclusion, this method permits a dual-activity mapping of neuronal activation in mice with single-cell resolution. It provides a powerful methodology, complementing electrophysiological and other functional imaging methods, for identifying neural circuits responsible for the internal representations of different behavioral and sensation modalities.

4.8 Partial colocalization of the fear engram with neuronal ensemble activated in heat pain in the murine

DISCUSSION

prelimbic cortex

The medial prefrontal cortex (mPFC) is implicated in processing sensory-discriminative and affective pain and undergoes marked remodelling in chronic pain patients (Kummer et al. 2020; Kuner and Kuner 2021). Nonetheless, the underlying mechanisms are poorly understood. In our labortoty, we previously demonstrated the role of fear-activated neurons in the PL cortex, a sub-region of mPFC, in the regulation of tonic pain sensation behaviors. In that study, we injected capsaicin, TRPV1 agonist activating nociceptors acutely, as an tonic pain model. This study established a prefrontal cellular basis of pain perception, which partly overlapped with prefrontal fear memory recall engrams, revealing a powerful synergism between the prefrontal circuitries for retrieval of learned fear and pain. It also suggests that persistent pain has a major component associated with a fearful memory. Here, we demonstrated that in chronic inflammatory pain conditions, the overlap between the fear engram and the heat pain engram in the prelimbic cortex undergoes marked expansion, suggesting that the interaction between fear and pain is accentuated in chronic pain conditions. This evidence provides a cellular-level understanding of the clinically observed interaction between anticipatory fear states and enhanced pain perception (Labrenz et al. 2016; Wiech and Tracey 2013), and partly elucidate the mechanism by which chronic fear perpetuates pain and leads to its chronicity (Rusu et al. 2014; Vlaeyen and Linton 2000).

4.9 PL fear engram coding neuron activation increase the acute pain perception

According to the cellular basis above, we the asked whether a direct manipulation of prefrontal fear memory engrams at chronic stages after fear conditioning can facilitate pain perception. Further, it would be an aid for understanding whether the extinction of fear memory can clinically alleviate

DISCUSSION

chronic pain, in the context of cognitive-behavioral therapy (Meulders et al. 2015; Meulders et al. 2017; Greenwald and Shafritz 2018). Previously, optogenetic suppression of fear engram was observed in capsaicin-induced acute pain context, possibly reducing the pain duration. Here, optogenetic activation of PL fear engram in acute pain perception led to an increase of pain-related behavior, which demonstrates a key role of fear engram neurons in the regulation of acute pain-coping behavior (Huang et al. 2019). Both activation and inhibition of PL fear memory component neurons can positively or negatively affect pain perception, which is reflected in behavioral observations of increased or decreased protective behavior towards injury. This suggests that the neurons involved in the consolidation of cued fear memory composition or modulation in PL are also involved in acute pain modulation by some mechanism. Dale et al. reported that acute pain raises prefrontal cortex neuron firing rates, and raising basal prefrontal firing rates can improve cortical pain control gain. (Dale et al. 2018). However, their findings do not necessarily indicate that the PFC contains distinct pain-processing or pain-regulatory neurons. Rather, these results more indicate that one of the most important functions of PFC neurons is to respond to nociceptive inputs. This evidence complements the findings before, in which the fear-pain regulation population in PL could have a bi-directional regulation to assessing the positive or negative effects of anticipation on pain perception. Furthermore, throughout diverse behavioral tasks, prefrontal neurons have been shown to have mixed selectivity (Rigotti et al. 2013). Our evidence implicates the prefrontal cortical circuitry as a causally relevant entity in mediating these interactions, which could be influencing pain perception by judging fear expectations positively or negatively.

4.10 PL fear engram suppression decrease the heat

DISCUSSION

hypersensitivity in chronic inflammatory pain

Previously, we have confirmed that optogenetic inhibition of PL remote fear engram could reduce tonic pain behavior induced by capsaicin injection. This implies that perception of ongoing pain causally entails a major component of fear memory that is encoded in prefrontal circuits by prior exposure to a painful stimulus. Not only can these insights provide a cellular understanding for well-known interactions between anticipatory states and heightened pain sensation (Labrenz et al. 2016; Wiech and Tracey 2013), but also mechanistically explain why long-term fear can perpetuate pain and predispose towards pain chronicity (Rusu et al. 2014; Vlaeyen and Linton 2000). In this study, we further presented evidence that direct suppression of prefrontal fear memory engrams at chronic time points after fear conditioning can decrease heat pain perception in an inflammatory pain setting. This result indicates that chronic inflammatory pain can be partly disrupted by inhibition of the prefrontal cellular substrates of fear memory, which provides a further understanding of whether the suppression or distinction of fear memory could clinically alleviate chronic pain. In the context of cognitive-behavioral therapy, the mPFC is assumed to be involved in the alteration of the default mode network and to be a major driving force in the process of central sensitization. In terms of cellular mechanisms, the mPFC may form new neural circuits through long-term potentiation that may cause the extinction of pre-existing pain pathways found within fear-related brain circuits (Greenwald and Shafritz 2018; Meulders et al. 2015; Meulders et al. 2017).

The interactions between pain and fear are complicated and multifaceted. Fear of pain has been related to exaggerated pain experiences in the ‘fear-avoidance model,’ which matches clinical results in patients with chronic pain. In contrast, this study specifically tested how suppression of a long-term fear ensemble influences pain sensitivity independent of the fear-inducing

DISCUSSION

context. Here, we observed that indicators of both avoidance and aversion were not included in this distinct pain-fear interaction, simulating a clinical scenario in which pain is exaggerated by fear, ruling out other possible cognitive effects on this pathway in mPFC.

Our study describes a mechanism that long-term fear instilled by pain can perpetuate pain and further predispose towards pain chronicity, and the prefrontal cortical circuitry as a causally relevant entity in mediating these interactions. Overall, our findings suggest that overcoming anticipated fear by inhibiting prefrontal circuits can reduce acute versus chronic inflammatory pain perception. These findings provide a cellular mechanism for establishing and optimizing closed-loop interventions that target the activity of prefrontal circuits. Treatment of inflammatory pain in patients with fear and pain comorbidities using prefrontal neural stimulation or modulation would be promising and shape the way for individualized future pain therapies.

4.11 Conclusion

From the study of spinal cord microcircuits activated in dynamic and punctate allodynia under inflammatory pain conditions, a distinct presynaptic GABAergic excitatory modulation of punctate mechanical allodynia and underlying spinal circuits was depicted. In conclusion,

1. Nociceptor-specific GABAA β 3 knock-out mice did not show obvious changes in motor function; however, GABAAR knockout in all peripheral sensory neurons had a slight impact on fine movement.
2. Nociceptor-specific GABAA β 3 knock-out mice did not develop punctate mechanical allodynia, but showed preserved dynamic mechanical allodynia under inflammatory pain conditions.
3. Under inflammatory pain conditions, punctate and dynamic mechanical

DISCUSSION

stimuli shaped intermingled neuronal activation patterns in the spinal cord dorsal horn.

4. Nociceptor-specific GABAA β 3 knock-out mice showed significantly reduced activation of spinal neurons upon punctate mechanical stimulus post-inflammation.

5. Nociceptor-specific presynaptic GABAA β 3 knock-out mice showed significantly reduced activation of spinal Calretinin-expressing and Parvalbumin-expressing neurons in response to punctate mechanical stimuli post-inflammation.

From the study of the cellular prefrontal basis for modulation of inflammatory pain by fear, we have unraveled a remote fear engram enhancing tonic pain perception, and demonstrated that inhibition of this population reduces the inflammatory thermal pain perception.

In conclusion,

1. In the mouse prelimbic cortex, the remote fear neuronal engram was largely distinct with the population activated by heat pain; however, a small degree of overlap in activated neurons was seen, which expanded significantly in inflammatory pain conditions.

2. Optogenetic activation of the prelimbic remote fear engram enhanced heat pain perception.

3. Optogenetic suppression of the prelimbic remote fear engram reduced heat hypersensitivity in chronic inflammatory pain.

Thus, the contributions made by these studies is anticipated to be useful to the scientific community in understanding and developing novel treatment strategies for inflammatory pain.

SUMMARY

5 Summary

One of the characteristics of inflammatory pain is mechanical allodynia, which occurs in distinct forms, including dynamic and punctate mechanical allodynia. Although the spinal cord circuitry of mechanical allodynia is well understood in terms of postsynaptic inhibition, the contribution of presynaptic inhibition to these distinct forms is not clear. Here, we used an IEG-based dual epoch method to simultaneously visualize the population correlates and the circuitry involved in these two contrasting types of mechanical allodynia in the spinal cord dorsal horn at a single-cell resolution. To investigate the role of presynaptic inhibition in these circuits, we also generated mice conditionally lacking GABAA receptors in DRG sensory neurons (Advillin-GABAA β 3^{-/-}) or nociceptive neurons (SNS-GABAA β 3^{-/-}). In conditions of inflammatory pain induced by paw inflammation, SNS-GABAA β 3^{-/-} mice did not develop punctate mechanical allodynia, while dynamic mechanical allodynia was still preserved. We observed that punctate and dynamic mechanical stimuli shape distinct activation patterns of intermingled neurons in the spinal cord dorsal horn under inflammatory pain conditions. Only the neuronal population activated by punctate mechanical stimuli was significantly reduced in SNS-GABAA β 3^{-/-} mice as compared to control littermates. The activation of spinal neurons expressing Calretinin and Parvalbumin activated by punctate mechanical stimuli was significantly reduced in SNS-GABAA β 3^{-/-} mice. Collectively with previous studies, these results support the hypothesis that presynaptic GABAergic inhibition switches to excitation in nociceptors under inflammatory pain conditions, and particularly modulates punctate mechanical allodynia. Moreover, this study is amongst the first to visualize the circuit population of these two distinct forms of mechanical allodynia and demonstrates the distinct, but intermingled, patterns shared between them. This work has significant impact on the current consideration of GABA-modulating drugs as analgesics and suggests

SUMMARY

that the switch from inhibition to excitation may be a hindrance.

Fear has a significant impact on one's subjective perception of pain and is involved in the development of chronic pain. However, mechanistic understanding and causal investigation of the underlying cellular substrates are lacking. Formerly, we observed silencing the remote fear retrieval engram specifically inhibited subsequent tonic pain without eliciting a generalized impairment of associative learning or aversion. Here, to further address whether directly activating prefrontal fear memory engrams after fear conditioning can facilitate tonic pain perception, we employed activity-based cell-tagging and optogenetic approaches to activate the neuronal assemblies for remote fear recall. Furthermore, to investigate whether established chronic inflammatory pain perception can be reduced by inhibition of these prefrontal cellular substrates of fear memory, we performed similar approaches to identify and inhibit the neuronal assemblies for remote fear recall in the mouse prefrontal cortex under chronic inflammatory pain conditions. We report that cell assemblies representing long-term fear retrieval and inflammatory heat pain are largely distinct, but a smaller overlapping subset also exists in the prefrontal cortex. Activation of the remote fear retrieval engram specifically promoted subsequent tonic pain perception and pain-related behavior. Under inflammatory pain conditions, suppression of remote fear engram reduced inflammatory heat hypersensitivity, without causing an associative avoidance or aversion deficiency. These findings provide a further understanding about how long-term fear prospectively shapes the experience of tonic pain and inflammatory pain. Moreover, our data reveal the fundamental cellular mechanism in the prefrontal cortex causally mediating this synergistic interaction, thereby laying a basis for future interventional therapies in patients with chronic pain and fear.

SUMMARY

5 Zusammenfassung

Eines der Merkmale entzündlicher Schmerzen ist die mechanische Allodynie, die in verschiedenen Formen auftritt, darunter die dynamische und punktuelle mechanische Allodynie. Obwohl die spinalen Schaltkreise, die an der mechanischen Allodynie beteiligt sind, im Hinblick auf die postsynaptische Hemmung bereits weitgehend untersucht sind, ist der Beitrag der präsynaptischen Hemmung zu diesen unterschiedlichen Formen noch nicht eindeutig geklärt. Hier haben wir eine IEG-basierte duale Methode verwendet, um die Populationskorrelate und die Schaltkreise, die an diesen beiden unterschiedlichen Arten mechanischer Allodynie im dorsalen Horn des Rückenmarks beteiligt sind, gleichzeitig auf der Ebene einzelner Zellen darzustellen. Um die Rolle der präsynaptischen Hemmung in diesen Schaltkreisen zu untersuchen, haben wir Mäuse gezüchtet, denen GABAA-Rezeptoren in sensorischen Neuronen des DRG (Advillin-GABAA β 3^{-/-}) oder in nozizeptiven Neuronen (SNS-GABAA β 3^{-/-}) fehlen. Unter den Bedingungen inflammatorischer Schmerzen, die durch eine Entzündung der Pfote ausgelöst wurden, entwickelten SNS-GABAA β 3^{-/-} Mäuse keine punktuelle mechanische Allodynie, während die dynamische mechanische Allodynie weiterhin auftrat. Nur die Neuronenpopulation, die durch punktuelle mechanische Reize aktiviert wurde, war in SNS-GABAA β 3^{-/-} Mäusen im Vergleich zu Kontrollmäusen signifikant reduziert. Die Aktivierung von spinalen Neuronen, die Calretinin und Parvalbumin exprimieren, die durch punktuelle mechanische Reize aktiviert werden, war bei SNS-GABAA β 3^{-/-} Mäusen signifikant reduziert. Zusammen mit früheren Studien stützen diese Ergebnisse die Hypothese, dass präsynaptische GABAerge Hemmung in Nozizeptoren unter entzündlichen Schmerzbedingungen auf Erregung umschaltet und insbesondere punktuelle mechanische Allodynie moduliert. Darüber hinaus ist diese Studie eine der ersten, die die Schaltkreise dieser beiden unterschiedlichen Formen der

SUMMARY

mechanischen Allodynie aufzeigt und die individuellen, aber dennoch zusammenhängenden Muster aufzeigt, die zwischen ihnen bestehen. Diese Arbeit hat erhebliche Auswirkungen auf die derzeitige Betrachtung von GABA-modulierenden Medikamenten als Analgetika und legt nahe, dass die Umstellung von Hemmung auf Erregung ein Hindernis sein kann.

Angst hat einen erheblichen Einfluss auf das subjektive Schmerzempfinden und ist an der Entstehung chronischer Schmerzen beteiligt. Es fehlt jedoch ein mechanistisches Verständnis und eine kausale Untersuchung der zugrunde liegenden zellulären Substrate. In der Vergangenheit haben wir beobachtet, dass die Inhibition eines Angstgedächtnis-Engramms spezifisch den nachfolgenden tonischen Schmerz hemmt, ohne eine allgemeine Beeinträchtigung des assoziativen Lernens oder der Aversion hervorzurufen. Um herauszufinden, ob die direkte Aktivierung dieses Angstgedächtnisses die tonische Schmerzwahrnehmung verstärken kann, setzten wir aktivitätsbasierte Zellmarkierungen und optogenetische Ansätze ein, um die neuronalen Korrelate für ein Angstgedächtnisses zu aktivieren. Um zu untersuchen, ob die Wahrnehmung von chronisch entzündlichen Schmerzen durch die Hemmung dieser präfrontalen zellulären Substrate des Angstgedächtnisses reduziert werden kann, haben wir ähnliche Ansätze zur Identifizierung und Hemmung dieser Neurone im präfrontalen Kortex der Maus auch unter chronisch entzündlichen Schmerzbedingungen durchgeführt. Es zeigt sich, dass die Zellverbände, die für den langfristigen Furchtabruf und den entzündlichen Hitzeschmerz verantwortlich sind, weitgehend voneinander getrennt sind, aber darüber hinaus auch eine kleinere, sich überschneidende Untergruppe im präfrontalen Kortex existiert. Die Aktivierung des Engramms zum Abrufen von Angst förderte spezifisch die anschließende tonische Schmerzwahrnehmung und das schmerzassoziierte Verhalten. Unter entzündlichen Schmerzbedingungen verringerte die Unterdrückung des Angst-Engramms die entzündliche

SUMMARY

Hitzeüberempfindlichkeit, ohne dass es zu einem Mangel an assoziierter Vermeidung oder Aversion kam. Diese Ergebnisse liefern weitere Erkenntnisse darüber, wie langfristige Angst das Erleben von tonischem Schmerz und Entzündungsschmerz prospektiv prägt. Darüber hinaus enthüllen unsere Daten den grundlegenden zellulären Mechanismus im präfrontalen Kortex, der diese synergistische Interaktion kausal vermittelt, und schaffen damit eine Grundlage für künftige interventionelle Therapien bei Patienten mit chronischen Schmerzen und Angst.

REFERENCE

6 Reference

Abbadie, C., Besson, J. M. and Calvino, B. (1994). **c-Fos expression in the spinal cord and pain-related symptoms induced by chronic arthritis in the rat are prevented by pretreatment with Freund adjuvant.** *J Neurosci* *14(10)*, 5865-5871, doi: 10.1523/jneurosci.14-10-05865.1994.

Abraira, V. E., Kuehn, E. D., Chirila, A. M., Springel, M. W., Toliver, A. A., Zimmerman, A. L., Orefice, L. L., Boyle, K. A., Bai, L., Song, B. J., Bashista, K. A., O'Neill, T. G., Zhuo, J., Tsan, C., Hoynoski, J., Rutlin, M., Kus, L., Niederkofler, V., Watanabe, M., Dymecki, S. M., Nelson, S. B., Heintz, N., Hughes, D. I. and Ginty, D. D. (2017). **The Cellular and Synaptic Architecture of the Mechanosensory Dorsal Horn.** *Cell* *168(1-2)*, 295-310 e219.

Agarwal, N., Offermanns, S. and Kuner, R. (2004). **Conditional gene deletion in primary nociceptive neurons of trigeminal ganglia and dorsal root ganglia.** *Genesis* *38(3)*, 122-129.

Alvarez-Leefmans, F. J., León-Olea, M., Mendoza-Sotelo, J., Alvarez, F. J., Antón, B. and Garduño, R. (2001). **Immunolocalization of the Na(+)-K(+)-2Cl(-) cotransporter in peripheral nervous tissue of vertebrates.** *Neuroscience* *104(2)*, 569-582, doi: 10.1016/S0306-4522(01)00091-4.

An, X., Bandler, R., Ongür, D. and Price, J. L. (1998). **Prefrontal cortical projections to longitudinal columns in the midbrain periaqueductal gray in macaque monkeys.** *J Comp Neurol* *401(4)*, 455-479.

Anderson, D. J. and Adolphs, R. (2014). **A framework for studying emotions across species.** *Cell* *157(1)*, 187-200, doi: 10.1016/j.cell.2014.03.003.

Anderson, M. A., Akshintala, V., Albers, K. M., Amann, S. T., Belfer, I., Brand, R., Chari, S., Cote, G. and Davis, B. M. (2016). **Mechanism, assessment and management of pain in chronic pancreatitis: Recommendations of a multidisciplinary study group.** *Pancreatology* *16(1)*, 83-94, doi: 10.1016/j.pan.2015.10.015.

Apkarian, A. V., Bushnell, M. C., Treede, R. D. and Zubieta, J. K. (2005). **Human brain mechanisms of pain perception and regulation in**

REFERENCE

health and disease. Eur J Pain 9(4), 463-484, doi: 10.1016/j.ejpain.2004.11.001.

Arruda-Carvalho, M. and Clem, R. L. (2014). **Pathway-selective adjustment of prefrontal-amygdala transmission during fear encoding.** J Neurosci 34(47), 15601-15609, doi: 10.1523/jneurosci.2664-14.2014.

Baliki, M. N. and Apkarian, A. V. (2015). **Nociception, Pain, Negative Moods, and Behavior Selection.** Neuron 87(3), 474-491, doi: 10.1016/j.neuron.2015.06.005.

Bartel, D. P., Sheng, M., Lau, L. F. and Greenberg, M. E. (1989). **Growth factors and membrane depolarization activate distinct programs of early response gene expression: dissociation of fos and jun induction.** Genes Dev 3(3), 304-313, doi: 10.1101/gad.3.3.304.

Basbaum, A. I., Bautista, D. M., Scherrer, G. and Julius, D. (2009). **Cellular and molecular mechanisms of pain.** Cell 139(2), 267-284, doi: 10.1016/j.cell.2009.09.028.

Benarroch, E. E. (2016). **Dorsal horn circuitry: Complexity and implications for mechanisms of neuropathic pain.** Neurology 86(11), 1060-1069, doi: 10.1212/wnl.0000000000002478.

Bennett, D. L., Clark, A. J., Huang, J., Waxman, S. G. and Dib-Hajj, S. D. (2019). **The Role of Voltage-Gated Sodium Channels in Pain Signaling.** Physiol Rev 99(2), 1079-1151, doi: 10.1152/physrev.00052.2017.

Beyeler, A., Namburi, P., Glober, G. F., Simonnet, C., Calhoon, G. G., Conyers, G. F., Luck, R., Wildes, C. P. and Tye, K. M. (2016). **Divergent Routing of Positive and Negative Information from the Amygdala during Memory Retrieval.** Neuron 90(2), 348-361, doi: 10.1016/j.neuron.2016.03.004.

Bohlen, C. J., Chesler, A. T., Sharif-Naeini, R., Medzihradzsky, K. F., Zhou, S., King, D., Sánchez, E. E., Burlingame, A. L., Basbaum, A. I. and Julius, D. (2011). **A heteromeric Texas coral snake toxin targets acid-sensing ion channels to produce pain.** Nature 479(7373), 410-414, doi: 10.1038/nature10607.

Bourane, S., Duan, B., Koch, S. C., Dalet, A., Britz, O., Garcia-Campmany, L., Kim, E., Cheng, L., Ghosh, A., Ma, Q. and Goulding, M. (2015). **Gate control**

REFERENCE

of mechanical itch by a subpopulation of spinal cord interneurons. *Science* 350(6260), 550-554, doi: 10.1126/science.aac8653.

Boyle, K. A., Gradwell, M. A., Yasaka, T., Dickie, A. C., Polgár, E., Ganley, R. P., Orr, D. P. H., Watanabe, M., Abaira, V. E., Kuehn, E. D., Zimmerman, A. L., Ginty, D. D., Callister, R. J., Graham, B. A. and Hughes, D. I. (2019). **Defining a Spinal Microcircuit that Gates Myelinated Afferent Input: Implications for Tactile Allodynia.** *Cell Rep* 28(2), 526-540.e526, doi: 10.1016/j.celrep.2019.06.040.

Buldyrev, I. and Taylor, W. R. (2013). **Inhibitory mechanisms that generate centre and surround properties in ON and OFF brisk-sustained ganglion cells in the rabbit retina.** *J Physiol* 591(1), 303-325, doi: 10.1113/jphysiol.2012.243113.

Bushnell, M. C., Ceko, M. and Low, L. A. (2013). **Cognitive and emotional control of pain and its disruption in chronic pain.** *Nat Rev Neurosci* 14(7), 502-511, doi: 10.1038/nrn3516.

Butler, R. K., Nilsson-Todd, L., Cleren, C., Léna, I., Garcia, R. and Finn, D. P. (2011). **Molecular and electrophysiological changes in the prefrontal cortex-amygdala-dorsal periaqueductal grey pathway during persistent pain state and fear-conditioned analgesia.** *Physiol Behav* 104(5), 1075-1081, doi: 10.1016/j.physbeh.2011.05.028.

Campbell, J. N., Raja, S. N., Meyer, R. A. and Mackinnon, S. E. (1988). **Myelinated afferents signal the hyperalgesia associated with nerve injury.** *Pain* 32(1), 89-94, doi: 10.1016/0304-3959(88)90027-9.

Caterina, M. J., Leffler, A., Malmberg, A. B., Martin, W. J., Trafton, J., Petersen-Zeitz, K. R., Koltzenburg, M., Basbaum, A. I. and Julius, D. (2000). **Impaired nociception and pain sensation in mice lacking the capsaicin receptor.** *Science* 288(5464), 306-313, doi: 10.1126/science.288.5464.306.

Cavanaugh, D. J., Lee, H., Lo, L., Shields, S. D., Zylka, M. J., Basbaum, A. I. and Anderson, D. J. (2009). **Distinct subsets of unmyelinated primary sensory fibers mediate behavioral responses to noxious thermal and mechanical stimuli.** *Proc Natl Acad Sci U S A* 106(22), 9075-9080, doi: 10.1073/pnas.0901507106.

Cervero, F., Laird, J. M. and García-Nicas, E. (2003). **Secondary hyperalgesia and presynaptic inhibition: an update.** *Eur J Pain* 7(4), 345-351, doi: 10.1016/s1090-3801(03)00047-8.

REFERENCE

Chan, R. K., Brown, E. R., Ericsson, A., Kovács, K. J. and Sawchenko, P. E. (1993). **A comparison of two immediate-early genes, c-fos and NGFI-B, as markers for functional activation in stress-related neuroendocrine circuitry.** *J Neurosci* *13*(12), 5126-5138, doi: 10.1523/jneurosci.13-12-05126.1993.

Chaplan, S. R., Bach, F. W., Pogrel, J. W., Chung, J. M. and Yaksh, T. L. (1994). **Quantitative assessment of tactile allodynia in the rat paw.** *Journal of Neuroscience Methods* *53*, 55-63.

Chaudhuri, A., Nissanov, J., Larocque, S. and Rioux, L. (1997). **Dual activity maps in primate visual cortex produced by different temporal patterns of zif268 mRNA and protein expression.** *Proc Natl Acad Sci U S A* *94*(6), 2671-2675, doi: 10.1073/pnas.94.6.2671.

Chen, J. T., Guo, D., Campanelli, D., Frattini, F., Mayer, F., Zhou, L., Kuner, R., Heppenstall, P. A., Knipper, M. and Hu, J. (2014). **Presynaptic GABAergic inhibition regulated by BDNF contributes to neuropathic pain induction.** *Nat Commun* *5*, 5331.

Cheng, L., Duan, B., Huang, T., Zhang, Y., Chen, Y., Britz, O., Garcia-Campmany, L., Ren, X., Vong, L., Lowell, B. B., Goulding, M., Wang, Y. and Ma, Q. (2017). **Identification of spinal circuits involved in touch-evoked dynamic mechanical pain.** *Nat Neurosci* *20*(6), 804-814, doi: 10.1038/nn.4549.

Cole, A. J., Saffen, D. W., Baraban, J. M. and Worley, P. F. (1989). **Rapid increase of an immediate early gene messenger RNA in hippocampal neurons by synaptic NMDA receptor activation.** *Nature* *340*(6233), 474-476, doi: 10.1038/340474a0.

Colloca, L., Ludman, T., Bouhassira, D., Baron, R., Dickenson, A. H., Yarnitsky, D., Freeman, R., Truini, A., Attal, N., Finnerup, N. B., Eccleston, C., Kalso, E., Bennett, D. L., Dworkin, R. H. and Raja, S. N. (2017). **Neuropathic pain.** *Nat Rev Dis Primers* *3*, 17002, doi: 10.1038/nrdp.2017.2.

Corcoran, K. A. and Quirk, G. J. (2007). **Activity in prelimbic cortex is necessary for the expression of learned, but not innate, fears.** *J Neurosci* *27*(4), 840-844, doi: 10.1523/jneurosci.5327-06.2007.

Coull, J. A., Beggs, S., Boudreau, D., Boivin, D., Tsuda, M., Inoue, K., Gravel, C., Salter, M. W. and De Koninck, Y. (2005). **BDNF from microglia causes**

REFERENCE

the shift in neuronal anion gradient underlying neuropathic pain. *Nature* 438(7070), 1017-1021.

Courtin, J., Chaudun, F., Rozeske, R. R., Karalis, N., Gonzalez-Campo, C., Wurtz, H., Abdi, A., Baufreton, J., Bienvenu, T. C. and Herry, C. (2014). **Prefrontal parvalbumin interneurons shape neuronal activity to drive fear expression.** *Nature* 505(7481), 92-96, doi: 10.1038/nature12755.

Cui, L., Miao, X., Liang, L., Abdus-Saboor, I., Olson, W., Fleming, M. S., Ma, M., Tao, Y. X. and Luo, W. (2016). **Identification of early RET+ deep dorsal spinal cord interneurons in gating pain.** *Neuron* 91(6), 1413, doi: 10.1016/j.neuron.2016.09.010.

Dale, J., Zhou, H., Zhang, Q., Martinez, E., Hu, S., Liu, K., Urien, L., Chen, Z. and Wang, J. (2018). **Scaling Up Cortical Control Inhibits Pain.** *Cell Rep* 23(5), 1301-1313, doi: 10.1016/j.celrep.2018.03.139.

Davis, R. E., Knappenberger, P. C., Michaels, P. J. and Novicoff, W. M. (2003). **Changing heat-related mortality in the United States.** *Environ Health Perspect* 111(14), 1712-1718, doi: 10.1289/ehp.6336.

Do-Monte, F. H., Manzano-Nieves, G., Quiñones-Laracuenta, K., Ramos-Medina, L. and Quirk, G. J. (2015). **Revisiting the role of infralimbic cortex in fear extinction with optogenetics.** *J Neurosci* 35(8), 3607-3615, doi: 10.1523/jneurosci.3137-14.2015.

Dogbevia, G. K., Marticorena-Alvarez, R., Bausen, M., Sprengel, R. and Hasan, M. T. (2015). **Inducible and combinatorial gene manipulation in mouse brain.** *Front Cell Neurosci* 9, 142, doi: 10.3389/fncel.2015.00142.

Duan, B., Cheng, L., Bourane, S., Britz, O., Padilla, C., Garcia-Campmany, L., Krashes, M., Knowlton, W., Velasquez, T., Ren, X., Ross, S., Lowell, B. B., Wang, Y., Goulding, M. and Ma, Q. (2014). **Identification of spinal circuits transmitting and gating mechanical pain.** *Cell* 159(6), 1417-1432, doi: 10.1016/j.cell.2014.11.003.

Ehrlich, I., Humeau, Y., Grenier, F., Cioocchi, S., Herry, C. and Lüthi, A. (2009). **Amygdala inhibitory circuits and the control of fear memory.** *Neuron* 62(6), 757-771, doi: 10.1016/j.neuron.2009.05.026.

Ferguson, C., Hardy, S. L., Werner, D. F., Hileman, S. M., Delorey, T. M. and Homanics, G. E. (2007). **New insight into the role of the beta3 subunit of the GABAA-R in development, behavior, body weight regulation,**

REFERENCE

and anesthesia revealed by conditional gene knockout. BMC Neurosci 8, 85, doi: 10.1186/1471-2202-8-85.

Fink, A. J., Croce, K. R., Huang, Z. J., Abbott, L. F., Jessell, T. M. and Azim, E. (2014). **Presynaptic inhibition of spinal sensory feedback ensures smooth movement.** Nature 509(7498), 43-48, doi: 10.1038/nature13276.

Finnerup, N. B., Kuner, R. and Jensen, T. S. (2021). **Neuropathic Pain: From Mechanisms to Treatment.** Physiol Rev 101(1), 259-301, doi: 10.1152/physrev.00045.2019.

Frankland, P. W. and Bontempi, B. (2005). **The organization of recent and remote memories.** Nat Rev Neurosci 6(2), 119-130, doi: 10.1038/nrn1607.

Froger, A. and Hall, J. E. (2007). **Transformation of plasmid DNA into E. coli using the heat shock method.** J Vis Exp(6), 253, doi: 10.3791/253.

Garcia-Nicas, E., Laird, J. M. A. and Cervero, F. (2001). **Vasodilatation in hyperalgesic rat skin evoked by stimulation of afferent A beta-fibers: further evidence for a role of dorsal root reflexes in allodynia.** Pain 94(3), 283-291, doi: 10.1016/s0304-3959(01)00365-7.

Garrison, S. R., Dietrich, A. and Stucky, C. L. (2012). **TRPC1 contributes to light-touch sensation and mechanical responses in low-threshold cutaneous sensory neurons.** J Neurophysiol 107(3), 913-922.

Giustino, T. F. and Maren, S. (2015). **The Role of the Medial Prefrontal Cortex in the Conditioning and Extinction of Fear.** Front Behav Neurosci 9, 298, doi: 10.3389/fnbeh.2015.00298.

Gödde, K., Gschwend, O., Puchkov, D., Pfeffer, C. K., Carleton, A. and Jentsch, T. J. (2016). **Disruption of Kcc2-dependent inhibition of olfactory bulb output neurons suggests its importance in odour discrimination.** Nat Commun 7, 12043, doi: 10.1038/ncomms12043.

Gold, M. S. and Gebhart, G. F. (2010). **Nociceptor sensitization in pain pathogenesis.** Nat Med 16(11), 1248-1257, doi: 10.1038/nm.2235.

Goldman-Rakic, P. S. (1996). **The prefrontal landscape: implications of functional architecture for understanding human mentation and the central executive.** Philos Trans R Soc Lond B Biol Sci 351(1346), 1445-1453, doi: 10.1098/rstb.1996.0129.

REFERENCE

Golmohammadi, M. G., Blackmore, D. G., Large, B., Azari, H., Esfandiary, E., Paxinos, G., Franklin, K. B., Reynolds, B. A. and Rietze, R. L. (2008). **Comparative analysis of the frequency and distribution of stem and progenitor cells in the adult mouse brain.** *Stem Cells* 26(4), 979-987, doi: 10.1634/stemcells.2007-0919.

Gossen, M. and Bujard, H. (1992). **Tight control of gene expression in mammalian cells by tetracycline-responsive promoters.** *Proc Natl Acad Sci U S A* 89(12), 5547-5551, doi: 10.1073/pnas.89.12.5547.

Gradwell, M. A., Callister, R. J. and Graham, B. A. (2020). **Reviewing the case for compromised spinal inhibition in neuropathic pain.** *J Neural Transm (Vienna)* 127(4), 481-503, doi: 10.1007/s00702-019-02090-0.

Graham, B. and Redman, S. (1994). **A simulation of action potentials in synaptic boutons during presynaptic inhibition.** *J Neurophysiol* 71(2), 538-549, doi: 10.1152/jn.1994.71.2.538.

Greenberg, M. E. and Ziff, E. B. (1984). **Stimulation of 3T3 cells induces transcription of the c-fos proto-oncogene.** *Nature* 311(5985), 433-438, doi: 10.1038/311433a0.

Greenwald, J. D. and Shafritz, K. M. (2018). **An Integrative Neuroscience Framework for the Treatment of Chronic Pain: From Cellular Alterations to Behavior.** *Front Integr Neurosci* 12, 18, doi: 10.3389/fnint.2018.00018.

Grewe, B. F., Gründemann, J., Kitch, L. J., Lecoq, J. A., Jercog, P. E., Grenier, F., Li, J. Z., Lüthi, A. and Schnitzer, M. J. (2017). **Neural ensemble dynamics underlying a long-term associative memory.** *Nature* 543(7647), 670-675, doi: 10.1038/nature21682.

Guenther, C. J., Miyamichi, K., Yang, H. H., Heller, H. C. and Luo, L. (2013). **Permanent genetic access to transiently active neurons via TRAP: targeted recombination in active populations.** *Neuron* 78(5), 773-784, doi: 10.1016/j.neuron.2013.03.025.

Guo, D. (2017). **Presynaptic Gate of Pain Control: Malfunctioning Presynaptic GABAergic Inhibition in Neuropathic and Inflammatory Pain.** . Naturwissenschaften Dissertation
Eberhard-Karls-Universität Tübingen.

Guo, D. and Hu, J. (2014). **Spinal presynaptic inhibition in pain control.** *Neuroscience* 283, 95-106.

REFERENCE

- Hameed, S. (2019). **Na(v)1.7 and Na(v)1.8: Role in the pathophysiology of pain.** *Mol Pain* 15, doi: 10.1177/1744806919858801.
- Hardy, S. G. and Leichnetz, G. R. (1981). **Cortical projections to the periaqueductal gray in the monkey: a retrograde and orthograde horseradish peroxidase study.** *Neurosci Lett* 22(2), 97-101, doi: 10.1016/0304-3940(81)90070-7.
- Hope, B., Kosofsky, B., Hyman, S. E. and Nestler, E. J. (1992). **Regulation of immediate early gene expression and AP-1 binding in the rat nucleus accumbens by chronic cocaine.** *Proc Natl Acad Sci U S A* 89(13), 5764-5768, doi: 10.1073/pnas.89.13.5764.
- Hopman, A. H., Ramaekers, F. C. and Speel, E. J. (1998). **Rapid synthesis of biotin-, digoxigenin-, trinitrophenyl-, and fluorochrome-labeled tyramides and their application for In situ hybridization using CARD amplification.** *J Histochem Cytochem* 46(6), 771-777, doi: 10.1177/002215549804600611.
- Huang, T., Lin, S. H., Malewicz, N. M., Zhang, Y., Zhang, Y., Goulding, M., LaMotte, R. H. and Ma, Q. (2019). **Identifying the pathways required for coping behaviours associated with sustained pain.** *Nature* 565(7737), 86-90, doi: 10.1038/s41586-018-0793-8.
- Hübner, C., Bosch, D., Gall, A., Lüthi, A. and Ehrlich, I. (2014). **Ex vivo dissection of optogenetically activated mPFC and hippocampal inputs to neurons in the basolateral amygdala: implications for fear and emotional memory.** *Front Behav Neurosci* 8, 64, doi: 10.3389/fnbeh.2014.00064.
- Hughes, D. I., Mackie, M., Nagy, G. G., Riddell, J. S., Maxwell, D. J., Szabó, G., Erdélyi, F., Veress, G., Szucs, P., Antal, M. and Todd, A. J. (2005). **P boutons in lamina IX of the rodent spinal cord express high levels of glutamic acid decarboxylase-65 and originate from cells in deep medial dorsal horn.** *Proc Natl Acad Sci U S A* 102(25), 9038-9043, doi: 10.1073/pnas.0503646102.
- Hughes, D. I., Sikander, S., Kinnon, C. M., Boyle, K. A., Watanabe, M., Callister, R. J. and Graham, B. A. (2012). **Morphological, neurochemical and electrophysiological features of parvalbumin-expressing cells: a likely source of axo-axonic inputs in the mouse spinal dorsal horn.** *J Physiol* 590(16), 3927-3951, doi: 10.1113/jphysiol.2012.235655.

REFERENCE

- Iwamura, Y., Tanaka, M., Iriki, A., Taoka, M. and Toda, T. (2002). **Processing of tactile and kinesthetic signals from bilateral sides of the body in the postcentral gyrus of awake monkeys.** *Behav Brain Res* 135(1-2), 185-190, doi: 10.1016/s0166-4328(02)00164-x.
- Jarvis, M. F., Honore, P., Shieh, C. C., Chapman, M., Joshi, S., Zhang, X. F., Kort, M., Carroll, W., Marron, B., Atkinson, R., Thomas, J., Liu, D., Krambis, M., Liu, Y., McGaraughty, S., Chu, K., Roeloffs, R., Zhong, C., Mikusa, J. P., Hernandez, G., Gauvin, D., Wade, C., Zhu, C., Pai, M., Scanio, M., Shi, L., Drizin, I., Gregg, R., Matulenko, M., Hakeem, A., Gross, M., Johnson, M., Marsh, K., Wagoner, P. K., Sullivan, J. P., Faltynek, C. R. and Krafte, D. S. (2007). **A-803467, a potent and selective Nav1.8 sodium channel blocker, attenuates neuropathic and inflammatory pain in the rat.** *Proc Natl Acad Sci U S A* 104(20), 8520-8525, doi: 10.1073/pnas.0611364104.
- Ji, G. and Neugebauer, V. (2011). **Pain-related deactivation of medial prefrontal cortical neurons involves mGluR1 and GABA(A) receptors.** *J Neurophysiol* 106(5), 2642-2652, doi: 10.1152/jn.00461.2011.
- Ji, G., Sun, H., Fu, Y., Li, Z., Pais-Vieira, M., Galhardo, V. and Neugebauer, V. (2010). **Cognitive impairment in pain through amygdala-driven prefrontal cortical deactivation.** *J Neurosci* 30(15), 5451-5464, doi: 10.1523/jneurosci.0225-10.2010.
- Ji, R. R., Chamesian, A. and Zhang, Y. Q. (2016). **Pain regulation by non-neuronal cells and inflammation.** *Science* 354(6312), 572-577, doi: 10.1126/science.aaf8924.
- Johnson, Z. V., Revis, A. A., Burdick, M. A. and Rhodes, J. S. (2010). **A similar pattern of neuronal Fos activation in 10 brain regions following exposure to reward- or aversion-associated contextual cues in mice.** *Physiol Behav* 99(3), 412-418, doi: 10.1016/j.physbeh.2009.12.013.
- Julius, D. and Carlson, J. R. (2015). **Editorial overview: molecular biology of sensation.** *Curr Opin Neurobiol* 34, v-vi, doi: 10.1016/j.conb.2015.07.001.
- Jurik, A., Auffenberg, E., Klein, S., Deussing, J. M., Schmid, R. M., Wotjak, C. T. and Thoeringer, C. K. (2015). **Roles of prefrontal cortex and paraventricular thalamus in affective and mechanical components of visceral nociception.** *Pain* 156(12), 2479-2491, doi: 10.1097/j.pain.0000000000000318.

REFERENCE

- Kahle, K. T., Staley, K. J., Nahed, B. V., Gamba, G., Hebert, S. C., Lifton, R. P. and Mount, D. B. (2008). **Roles of the cation-chloride cotransporters in neurological disease.** *Nat Clin Pract Neurol* 4(9), 490-503, doi: 10.1038/ncpneuro0883.
- Kanaka, C., Ohno, K., Okabe, A. and Sato, K. (2001). **The differential expression patterns of messenger RNAs encoding K-Cl cotransporters (KCC1,2) and Na-K-2Cl cotransporter (NKCC1) in the rat nervous system.** *Neuroscience* 104(4), 933-946, doi: 10.1016/S0306-4522(01)00149-x.
- Kim, J., Pignatelli, M., Xu, S., Itohara, S. and Tonegawa, S. (2016). **Antagonistic negative and positive neurons of the basolateral amygdala.** *Nat Neurosci* 19(12), 1636-1646, doi: 10.1038/nn.4414.
- Kiritoshi, T. and Neugebauer, V. (2018). **Pathway-Specific Alterations of Cortico-Amygdala Transmission in an Arthritis Pain Model.** *ACS Chem Neurosci* 9(9), 2252-2261, doi: 10.1021/acscchemneuro.8b00022.
- Kitamura, T., Ogawa, S. K., Roy, D. S., Okuyama, T., Morrissey, M. D., Smith, L. M., Redondo, R. L. and Tonegawa, S. (2017). **Engrams and circuits crucial for systems consolidation of a memory.** *Science* 356(6333), 73-78, doi: 10.1126/science.aam6808.
- Knapska, E. and Maren, S. (2009). **Reciprocal patterns of c-Fos expression in the medial prefrontal cortex and amygdala after extinction and renewal of conditioned fear.** *Learn Mem* 16(8), 486-493, doi: 10.1101/lm.1463909.
- Knowlton, W. M., Palkar, R., Lippoldt, E. K., McCoy, D. D., Baluch, F. and McKemy, D. D. (2013). **A sensory-labeled line for cold: TRPM8-expressing sensory neurons define the cellular basis for cold, cold pain, and cooling-mediated analgesia.** *J Neurosci* 33(7), 2837-2848, doi: 10.1523/JNEUROSCI.1943-12.2013.
- Koltzenburg, M., Lundberg, L. E. R. and Torebjörk, E. H. (1992). **Dynamic and static components of mechanical hyperalgesia in human hairy skin.** *Pain* 51(2), 207-219, doi: 10.1016/0304-3959(92)90262-a.
- Kummer, K. K., Mitrić, M., Kalpachidou, T. and Kress, M. (2020). **The Medial Prefrontal Cortex as a Central Hub for Mental Comorbidities Associated with Chronic Pain.** *Int J Mol Sci* 21(10), doi: 10.3390/ijms21103440.

REFERENCE

Kuner, R. (2010). **Central mechanisms of pathological pain.** *Nat Med* 16(11), 1258-1266, doi: 10.1038/nm.2231.

Kuner, R. and Flor, H. (2016). **Structural plasticity and reorganisation in chronic pain.** *Nat Rev Neurosci* 18(1), 20-30, doi: 10.1038/nrn.2016.162.

Kuner, R. and Kuner, T. (2021). **Cellular Circuits in the Brain and Their Modulation in Acute and Chronic Pain.** *Physiol Rev* 101(1), 213-258, doi: 10.1152/physrev.00040.2019.

Labrenz, F., Icenhour, A., Schlamann, M., Forsting, M., Bingel, U. and Elsenbruch, S. (2016). **From Pavlov to pain: How predictability affects the anticipation and processing of visceral pain in a fear conditioning paradigm.** *Neuroimage* 130, 104-114, doi: 10.1016/j.neuroimage.2016.01.064.

Laird, J. M., Souslova, V., Wood, J. N. and Cervero, F. (2002). **Deficits in visceral pain and referred hyperalgesia in Nav1.8 (SNS/PN3)-null mice.** *J Neurosci* 22(19), 8352-8356, doi: 10.1523/jneurosci.22-19-08352.2002.

Lammel, S., Lim, B. K., Ran, C., Huang, K. W., Betley, M. J., Tye, K. M., Deisseroth, K. and Malenka, R. C. (2012). **Input-specific control of reward and aversion in the ventral tegmental area.** *Nature* 491(7423), 212-217, doi: 10.1038/nature11527.

Laurent, V. and Westbrook, R. F. (2009). **Inactivation of the infralimbic but not the prelimbic cortex impairs consolidation and retrieval of fear extinction.** *Learn Mem* 16(9), 520-529, doi: 10.1101/lm.1474609.

LeDoux, J. E. (2000). **Emotion circuits in the brain.** *Annu Rev Neurosci* 23, 155-184, doi: 10.1146/annurev.neuro.23.1.155.

Lee, I. O., Whitehead, R. A., Ries, C. R., Schwarz, S. K., Puil, E. and MacLeod, B. A. (2013). **Evaluation of a novel mouse model of intracisternal strychnine-induced trigeminal allodynia.** *Can J Anaesth* 60(8), 780-786, doi: 10.1007/s12630-013-9975-x.

Lennertz, R. C., Kossyeva, E. A., Smith, A. K. and Stucky, C. L. (2012). **TRPA1 mediates mechanical sensitization in nociceptors during inflammation.** *PLoS One* 7(8), e43597, doi: 10.1371/journal.pone.0043597.

Lin, H. C., Huang, Y. H., Chao, T. H., Lin, W. Y., Sun, W. Z. and Yen, C. T. (2014). **Gabapentin reverses central hypersensitivity and suppresses**

REFERENCE

medial prefrontal cortical glucose metabolism in rats with neuropathic pain. *Mol Pain* 10, 63, doi: 10.1186/1744-8069-10-63.

Liu, X., Ramirez, S., Pang, P. T., Puryear, C. B., Govindarajan, A., Deisseroth, K. and Tonegawa, S. (2012). **Optogenetic stimulation of a hippocampal engram activates fear memory recall.** *Nature* 484(7394), 381-385, doi: 10.1038/nature11028.

Luo, L., Callaway, E. M. and Svoboda, K. (2018). **Genetic Dissection of Neural Circuits: A Decade of Progress.** *Neuron* 98(2), 256-281, doi: 10.1016/j.neuron.2018.03.040.

Ma, W., Saunders, P. A., Somogyi, R., Poulter, M. O. and Barker, J. L. (1993). **Ontogeny of GABAA receptor subunit mRNAs in rat spinal cord and dorsal root ganglia.** *J Comp Neurol* 338(3), 337-359, doi: 10.1002/cne.903380303.

Mai JK, P. G. (2011). **The human nervous system.** Academic Press.

Mandadi, S. and Roufogalis, B. D. (2008). **ThermoTRP channels in nociceptors: taking a lead from capsaicin receptor TRPV1.** *Curr Neuropharmacol* 6(1), 21-38, doi: 10.2174/157015908783769680.

Mao, S., Garzon-Muvdi, T., Di Fulvio, M., Chen, Y., Delpire, E., Alvarez, F. J. and Alvarez-Leefmans, F. J. (2012). **Molecular and functional expression of cation-chloride cotransporters in dorsal root ganglion neurons during postnatal maturation.** *J Neurophysiol* 108(3), 834-852, doi: 10.1152/jn.00970.2011.

Maren, S. (2001). **Neurobiology of Pavlovian fear conditioning.** *Annu Rev Neurosci* 24, 897-931, doi: 10.1146/annurev.neuro.24.1.897.

Matsuo, N., Reijmers, L. and Mayford, M. (2008). **Spine-type-specific recruitment of newly synthesized AMPA receptors with learning.** *Science* 319(5866), 1104-1107, doi: 10.1126/science.1149967.

Mattis, J., Tye, K. M., Ferenczi, E. A., Ramakrishnan, C., O'Shea, D. J., Prakash, R., Gunaydin, L. A., Hyun, M., Fenno, L. E., Gradinaru, V., Yizhar, O. and Deisseroth, K. (2011). **Principles for applying optogenetic tools derived from direct comparative analysis of microbial opsins.** *Nat Methods* 9(2), 159-172, doi: 10.1038/nmeth.1808.

McCoy, S. S., Crowson, C. S., Maradit-Kremers, H., Therneau, T. M., Roger, V. L., Matteson, E. L. and Gabriel, S. E. (2013). **Longterm outcomes and**

REFERENCE

treatment after myocardial infarction in patients with rheumatoid arthritis. *J Rheumatol* 40(5), 605-610, doi: 10.3899/jrheum.120941.

Melzack, R. and Wall, P. D. (1965). **Pain mechanisms: a new theory.** *Science* 150(3699), 971-979, doi: 10.1126/science.150.3699.971.

Meulders, A., Jans, A. and Vlaeyen, J. W. S. (2015). **Differences in pain-related fear acquisition and generalization: an experimental study comparing patients with fibromyalgia and healthy controls.** *Pain* 156(1), 108-122, doi: 10.1016/j.pain.000000000000016.

Meulders, A., Meulders, M., Stouten, I., De Bie, J. and Vlaeyen, J. W. (2017). **Extinction of Fear Generalization: A Comparison Between Fibromyalgia Patients and Healthy Control Participants.** *J Pain* 18(1), 79-95, doi: 10.1016/j.jpain.2016.10.004.

Meyer, R. A., Ringkamp, M., Campbell, J.N., and Raja, S.N. (2008). **Peripheral mechanisms of cutaneous nociception.** In Wall and Melzack's *Textbook of Pain*. S.B. McMahon and M. Koltzenburg, eds. (Philadelphia: Elsevier), 3-34.

Miraucourt, L. S., Moisset, X., Dallel, R. and Voisin, D. L. (2009). **Glycine inhibitory dysfunction induces a selectively dynamic, morphine-resistant, and neurokinin 1 receptor-independent mechanical allodynia.** *J Neurosci* 29(8), 2519-2527, doi: 10.1523/jneurosci.3923-08.2009.

Moehring, F., Halder, P., Seal, R. P. and Stucky, C. L. (2018). **Uncovering the Cells and Circuits of Touch in Normal and Pathological Settings.** *Neuron* 100(2), 349-360, doi: 10.1016/j.neuron.2018.10.019.

Mollenauer, S., Bryson, R., Robison, M. and Phillips, C. (1992). **Noise avoidance in the C57BL/6J mouse.** *Animal Learning & Behavior* 20(1), 25-32, doi: 10.3758/BF03199943.

Moratalla, R., Robertson, H. A. and Graybiel, A. M. (1992). **Dynamic regulation of NGFI-A (zif268, egr1) gene expression in the striatum.** *J Neurosci* 12(7), 2609-2622, doi: 10.1523/jneurosci.12-07-02609.1992.

Morawska, M. M. and Fendt, M. (2012). **The effects of muscimol and AMNo82 injections into the medial prefrontal cortex on the expression and extinction of conditioned fear in mice.** *J Exp Biol* 215(Pt 8), 1394-1398, doi: 10.1242/jeb.068213.

REFERENCE

Morgan, J. I., Cohen, D. R., Hempstead, J. L. and Curran, T. (1987). **Mapping patterns of c-fos expression in the central nervous system after seizure.** *Science* 237(4811), 192-197, doi: 10.1126/science.3037702.

Murthy, S. E., Loud, M. C., Daou, I., Marshall, K. L., Schwaller, F., Kühnemund, J., Francisco, A. G., Keenan, W. T., Dubin, A. E., Lewin, G. R. and Patapoutian, A. (2018). **The mechanosensitive ion channel Piezo2 mediates sensitivity to mechanical pain in mice.** *Sci Transl Med* 10(462), doi: 10.1126/scitranslmed.aat9897.

Namburi, P., Beyeler, A., Yorozu, S., Calhoun, G. G., Halbert, S. A., Wichmann, R., Holden, S. S., Mertens, K. L., Anahtar, M., Felix-Ortiz, A. C., Wickersham, I. R., Gray, J. M. and Tye, K. M. (2015). **A circuit mechanism for differentiating positive and negative associations.** *Nature* 520(7549), 675-678, doi: 10.1038/nature14366.

Neugebauer, V. (2015). **Amygdala pain mechanisms.** *Handb Exp Pharmacol* 227, 261-284, doi: 10.1007/978-3-662-46450-2_13.

Nguyen, Q. A. and Nicoll, R. A. (2018). **The GABA(A) Receptor β Subunit Is Required for Inhibitory Transmission.** *Neuron* 98(4), 718-725.e713, doi: 10.1016/j.neuron.2018.03.046.

Ochoa, J. L. and Yarnitsky, D. (1993). **Mechanical hyperalgesias in neuropathic pain patients: dynamic and static subtypes.** *Ann Neurol* 33(5), 465-472, doi: 10.1002/ana.410330509.

Olsen, R. W. and Sieghart, W. (2009). **GABA A receptors: subtypes provide diversity of function and pharmacology.** *Neuropharmacology* 56(1), 141-148, doi: 10.1016/j.neuropharm.2008.07.045.

Olson, W., Abdus-Saboor, I., Cui, L., Burdige, J., Raabe, T., Ma, M. and Luo, W. (2017). **Sparse genetic tracing reveals regionally specific functional organization of mammalian nociceptors.** *Elife* 6, doi: 10.7554/eLife.29507.

Ong, W. Y., Stohler, C. S. and Herr, D. R. (2019). **Role of the Prefrontal Cortex in Pain Processing.** *Mol Neurobiol* 56(2), 1137-1166, doi: 10.1007/s12035-018-1130-9.

Ongür, D. and Price, J. L. (2000). **The organization of networks within the orbital and medial prefrontal cortex of rats, monkeys and humans.** *Cereb Cortex* 10(3), 206-219, doi: 10.1093/cercor/10.3.206.

REFERENCE

Orefice, L. L., Zimmerman, A. L., Chirila, A. M., Sleboda, S. J., Head, J. P. and Ginty, D. D. (2016). **Peripheral Mechanosensory Neuron Dysfunction Underlies Tactile and Behavioral Deficits in Mouse Models of ASDs.** *Cell* 166(2), 299-313, doi: 10.1016/j.cell.2016.05.033.

Oshiro, Y., Quevedo, A. S., McHaffie, J. G., Kraft, R. A. and Coghill, R. C. (2009). **Brain mechanisms supporting discrimination of sensory features of pain: a new model.** *J Neurosci* 29(47), 14924-14931, doi: 10.1523/jneurosci.5538-08.2009.

Pagadala, N. S., Bjorndahl, T. C., Blinov, N., Kovalenko, A. and Wishart, D. S. (2013). **Molecular docking of thiamine reveals similarity in binding properties between the prion protein and other thiamine-binding proteins.** *J Mol Model* 19(12), 5225-5235, doi: 10.1007/s00894-013-1979-5.

Peirs, C., Dallel, R. and Todd, A. J. (2020). **Recent advances in our understanding of the organization of dorsal horn neuron populations and their contribution to cutaneous mechanical allodynia.** *J Neural Transm (Vienna)* 127(4), 505-525, doi: 10.1007/s00702-020-02159-1.

Peirs, C., Williams, S.-Paul G., Zhao, X., Walsh, Claire E., Gedeon, Jeremy Y., Cagle, Natalie E., Goldring, Adam C., Hioki, H., Liu, Z., Marell, Paulina S. and Seal, Rebecca P. (2015a). **Dorsal Horn Circuits for Persistent Mechanical Pain.** *Neuron* 87(4), 797-812.

Peirs, C., Williams, S. G., Zhao, X., Arokiaraj, C. M., Ferreira, D. W., Noh, M. C., Smith, K. M., Halder, P., Corrigan, K. A., Gedeon, J. Y., Lee, S. J., Gatto, G., Chi, D., Ross, S. E., Goulding, M. and Seal, R. P. (2021). **Mechanical Allodynia Circuitry in the Dorsal Horn Is Defined by the Nature of the Injury.** *Neuron* 109(1), 73-90.e77, doi: 10.1016/j.neuron.2020.10.027.

Peirs, C., Williams, S. P., Zhao, X., Walsh, C. E., Gedeon, J. Y., Cagle, N. E., Goldring, A. C., Hioki, H., Liu, Z., Marell, P. S. and Seal, R. P. (2015b). **Dorsal Horn Circuits for Persistent Mechanical Pain.** *Neuron* 87(4), 797-812, doi: 10.1016/j.neuron.2015.07.029.

Perrin-Terrin, A. S., Jeton, F., Pichon, A., Frugière, A., Richalet, J. P., Bodineau, L. and Voituren, N. (2016). **The c-FOS Protein Immunohistological Detection: A Useful Tool As a Marker of Central Pathways Involved in Specific Physiological Responses In Vivo and Ex Vivo.** *J Vis Exp(110)*, doi: 10.3791/53613.

REFERENCE

Persohn, E., Malherbe, P. and Richards, J. G. (1991). **In situ hybridization histochemistry reveals a diversity of GABAA receptor subunit mRNAs in neurons of the rat spinal cord and dorsal root ganglia.** *Neuroscience* 42(2), 497-507, doi: 10.1016/0306-4522(91)90392-2.

Petitjean, H., Bourojeni, F. B., Tsao, D., Davidova, A., Sotocinal, S. G., Mogil, J. S., Kania, A. and Sharif-Naeini, R. (2019). **Recruitment of Spinoparabrachial Neurons by Dorsal Horn Calretinin Neurons.** *Cell Rep* 28(6), 1429-1438.e1424, doi: 10.1016/j.celrep.2019.07.048.

Petitjean, H., Pawlowski, S. A., Fraine, S. L., Sharif, B., Hamad, D., Fatima, T., Berg, J., Brown, C. M., Jan, L. Y., Ribeiro-da-Silva, A., Braz, J. M., Basbaum, A. I. and Sharif-Naeini, R. (2015). **Dorsal Horn Parvalbumin Neurons Are Gate-Keepers of Touch-Evoked Pain after Nerve Injury.** *Cell Rep* 13(6), 1246-1257, doi: 10.1016/j.celrep.2015.09.080.

Phillips, C. J. (2009). **The Cost and Burden of Chronic Pain.** *Reviews in Pain* 3(1), 2-5, doi: 10.1177/2049463709000300102.

Plath, N., Ohana, O., Dammermann, B., Errington, M. L., Schmitz, D., Gross, C., Mao, X., Engelsberg, A., Mahlke, C., Welzl, H., Kobalz, U., Stawrakakis, A., Fernandez, E., Waltereit, R., Bick-Sander, A., Therstappen, E., Cooke, S. F., Blanquet, V., Wurst, W., Salmen, B., Bösl, M. R., Lipp, H. P., Grant, S. G., Bliss, T. V., Wolfer, D. P. and Kuhl, D. (2006). **Arc/Arg3.1 is essential for the consolidation of synaptic plasticity and memories.** *Neuron* 52(3), 437-444, doi: 10.1016/j.neuron.2006.08.024.

Polgár, E., Hughes, D. I., Riddell, J. S., Maxwell, D. J., Puskár, Z. and Todd, A. J. (2003). **Selective loss of spinal GABAergic or glycinergic neurons is not necessary for development of thermal hyperalgesia in the chronic constriction injury model of neuropathic pain.** *Pain* 104, 229-239, doi: 10.1016/s0304-3959(03)00011-3.

Prescott, T. J., Montes González, F. M., Gurney, K., Humphries, M. D. and Redgrave, P. (2006). **A robot model of the basal ganglia: behavior and intrinsic processing.** *Neural Netw* 19(1), 31-61, doi: 10.1016/j.neunet.2005.06.049.

Price, T. J., Cervero, F., Gold, M. S., Hammond, D. L. and Prescott, S. A. (2009). **Chloride regulation in the pain pathway.** *Brain Res Rev* 60(1), 149-170, doi: 10.1016/j.brainresrev.2008.12.015.

Price, T. J., Hargreaves, K. M. and Cervero, F. (2006). **Protein expression and mRNA cellular distribution of the NKCC1 cotransporter in the**

REFERENCE

dorsal root and trigeminal ganglia of the rat. *Brain Res* 1112(1), 146-158, doi: 10.1016/j.brainres.2006.07.012.

Raccuglia, D., McCurdy, L. Y., Demir, M., Gorur-Shandilya, S., Kunst, M., Emonet, T. and Nitabach, M. N. (2016). **Presynaptic GABA Receptors Mediate Temporal Contrast Enhancement in Drosophila Olfactory Sensory Neurons and Modulate Odor-Driven Behavioral Kinetics.** *eNeuro* 3(4), doi: 10.1523/eneuro.0080-16.2016.

Raja, S. N., Carr, D. B., Cohen, M., Finnerup, N. B., Flor, H., Gibson, S., Keefe, F. J., Mogil, J. S., Ringkamp, M., Sluka, K. A., Song, X. J., Stevens, B., Sullivan, M. D., Tutelman, P. R., Ushida, T. and Vader, K. (2020). **The revised International Association for the Study of Pain definition of pain: concepts, challenges, and compromises.** *Pain* 161(9), 1976-1982, doi: 10.1097/j.pain.0000000000001939.

Ramirez, S., Liu, X., Lin, P. A., Suh, J., Pignatelli, M., Redondo, R. L., Ryan, T. J. and Tonegawa, S. (2013). **Creating a false memory in the hippocampus.** *Science* 341(6144), 387-391.

Ramirez, S., Liu, X., MacDonald, C. J., Moffa, A., Zhou, J., Redondo, R. L. and Tonegawa, S. (2015). **Activating positive memory engrams suppresses depression-like behaviour.** *Nature* 522(7556), 335-339, doi: 10.1038/nature14514.

Rashid, M. I., Mujawar, L. H., Shahzad, T., Almeelbi, T., Ismail, I. M. and Oves, M. (2016). **Bacteria and fungi can contribute to nutrients bioavailability and aggregate formation in degraded soils.** *Microbiol Res* 183, 26-41, doi: 10.1016/j.micres.2015.11.007.

Redondo, R. L., Kim, J., Arons, A. L., Ramirez, S., Liu, X. and Tonegawa, S. (2014). **Bidirectional switch of the valence associated with a hippocampal contextual memory engram.** *Nature* 513(7518), 426-430, doi: 10.1038/nature13725.

Reichling, D. B. and Levine, J. D. (2009). **Critical role of nociceptor plasticity in chronic pain.** *Trends Neurosci* 32(12), 611-618, doi: 10.1016/j.tins.2009.07.007.

Reijmers, L. G., Perkins, B. L., Matsuo, N. and Mayford, M. (2007). **Localization of a stable neural correlate of associative memory.** *Science* 317(5842), 1230-1233, doi: 10.1126/science.1143839.

REFERENCE

Restivo, L., Vetere, G., Bontempi, B. and Ammassari-Teule, M. (2009). **The formation of recent and remote memory is associated with time-dependent formation of dendritic spines in the hippocampus and anterior cingulate cortex.** *J Neurosci* *29(25)*, 8206-8214, doi: 10.1523/jneurosci.0966-09.2009.

Rigotti, M., Barak, O., Warden, M. R., Wang, X. J., Daw, N. D., Miller, E. K. and Fusi, S. (2013). **The importance of mixed selectivity in complex cognitive tasks.** *Nature* *497(7451)*, 585-590, doi: 10.1038/nature12160.

Rivera, C., Voipio, J., Payne, J. A., Ruusuvuori, E., Lahtinen, H., Lamsa, K., Pirvola, U., Saarma, M. and Kaila, K. (1999). **The K⁺/Cl⁻ co-transporter KCC2 renders GABA hyperpolarizing during neuronal maturation.** *Nature* *397(6716)*, 251-255, doi: 10.1038/16697.

Rocha-González, H. I., Mao, S. and Alvarez-Leefmans, F. J. (2008). **Na⁺,K⁺,2Cl⁻ cotransport and intracellular chloride regulation in rat primary sensory neurons: thermodynamic and kinetic aspects.** *J Neurophysiol* *100(1)*, 169-184, doi: 10.1152/jn.01007.2007.

Roudaut, Y., Lonigro, A., Coste, B., Hao, J., Delmas, P. and Crest, M. (2012). **Touch sense: functional organization and molecular determinants of mechanosensitive receptors.** *Channels (Austin)* *6(4)*, 234-245, doi: 10.4161/chan.22213.

Rusu, A. C., Kreddig, N., Hallner, D., Hülsebusch, J. and Hasenbring, M. I. (2014). **Fear of movement/(Re)injury in low back pain: confirmatory validation of a German version of the Tampa Scale for Kinesiophobia.** *BMC Musculoskelet Disord* *15*, 280, doi: 10.1186/1471-2474-15-280.

Sakai, K. and Akiyama, T. (2020). **New insights into the mechanisms behind mechanical itch.** *Exp Dermatol* *29(8)*, 680-686, doi: 10.1111/exd.14143.

Sakurai, K., Zhao, S., Takatoh, J., Rodriguez, E., Lu, J., Leavitt, A. D., Fu, M., Han, B. X. and Wang, F. (2016). **Capturing and Manipulating Activated Neuronal Ensembles with CANE Delineates a Hypothalamic Social-Fear Circuit.** *Neuron* *92(4)*, 739-753, doi: 10.1016/j.neuron.2016.10.015.

Sangha, S., Robinson, P. D., Greba, Q., Davies, D. A. and Howland, J. G. (2014). **Alterations in reward, fear and safety cue discrimination**

REFERENCE

after inactivation of the rat prelimbic and infralimbic cortices. *Neuropsychopharmacology* 39(10), 2405-2413, doi: 10.1038/npp.2014.89.

Segev, I. (1990). **Computer study of presynaptic inhibition controlling the spread of action potentials into axonal terminals.** *J Neurophysiol* 63(5), 987-998, doi: 10.1152/jn.1990.63.5.987.

Sharif-Naeini, R. (2015). **Contribution of mechanosensitive ion channels to somatosensation.** *Prog Mol Biol Transl Sci* 131, 53-71, doi: 10.1016/bs.pmbts.2014.11.011.

Shi, Y., Chen, Y. and Wang, Y. (2019). **Kir2.1 Channel Regulation of Glycinergic Transmission Selectively Contributes to Dynamic Mechanical Allodynia in a Mouse Model of Spared Nerve Injury.** *Neurosci Bull* 35(2), 301-314, doi: 10.1007/s12264-018-0285-8.

Sierra-Mercado, D., Jr., Corcoran, K. A., Lebrón-Milad, K. and Quirk, G. J. (2006). **Inactivation of the ventromedial prefrontal cortex reduces expression of conditioned fear and impairs subsequent recall of extinction.** *Eur J Neurosci* 24(6), 1751-1758, doi: 10.1111/j.1460-9568.2006.05014.x.

Sierra-Mercado, D., Padilla-Coreano, N. and Quirk, G. J. (2011). **Dissociable roles of prelimbic and infralimbic cortices, ventral hippocampus, and basolateral amygdala in the expression and extinction of conditioned fear.** *Neuropsychopharmacology* 36(2), 529-538, doi: 10.1038/npp.2010.184.

Silva, J., Nichols, J., Theunissen, T. W., Guo, G., van Oosten, A. L., Barrandon, O., Wray, J., Yamanaka, S., Chambers, I. and Smith, A. (2009). **Nanog is the gateway to the pluripotent ground state.** *Cell* 138(4), 722-737, doi: 10.1016/j.cell.2009.07.039.

Singhmar, P., Huo, X., Eijkelkamp, N., Berciano, S. R., Baameur, F., Mei, F. C., Zhu, Y., Cheng, X., Hawke, D., Mayor, F., Jr., Murga, C., Heijnen, C. J. and Kavelaars, A. (2016). **Critical role for Epac1 in inflammatory pain controlled by GRK2-mediated phosphorylation of Epac1.** *Proc Natl Acad Sci U S A* 113(11), 3036-3041, doi: 10.1073/pnas.1516036113.

Smith, A. M., Floerke, V. A. and Thomas, A. K. (2016). **Retrieval practice protects memory against acute stress.** *Science* 354(6315), 1046-1048, doi: 10.1126/science.aah5067.

REFERENCE

Smith, K. M., Browne, T. J., Davis, O. C., Coyle, A., Boyle, K. A., Watanabe, M., Dickinson, S. A., Iredale, J. A., Gradwell, M. A., Jobling, P., Callister, R. J., Dayas, C. V., Hughes, D. I. and Graham, B. A. (2019). **Calretinin positive neurons form an excitatory amplifier network in the spinal cord dorsal horn.** *Elife* 8, doi: 10.7554/eLife.49190.

Smith, S. M., Nichols, T. E., Vidaurre, D., Winkler, A. M., Behrens, T. E., Glasser, M. F., Ugurbil, K., Barch, D. M., Van Essen, D. C. and Miller, K. L. (2015). **A positive-negative mode of population covariation links brain connectivity, demographics and behavior.** *Nat Neurosci* 18(11), 1565-1567, doi: 10.1038/nn.4125.

Solorzano, C., Villafuerte, D., Meda, K., Cevikbas, F., Bráz, J., Sharif-Naeini, R., Juarez-Salinas, D., Llewellyn-Smith, I. J., Guan, Z. and Basbaum, A. I. (2015). **Primary afferent and spinal cord expression of gastrin-releasing peptide: message, protein, and antibody concerns.** *J Neurosci* 35(2), 648-657, doi: 10.1523/jneurosci.2955-14.2015.

Tan, L. L., Pelzer, P., Heintl, C., Tang, W., Gangadharan, V., Flor, H., Sprengel, R., Kuner, T. and Kuner, R. (2017). **A pathway from midcingulate cortex to posterior insula gates nociceptive hypersensitivity.** *Nat Neurosci* 20(11), 1591-1601, doi: 10.1038/nn.4645.

Tappe-Theodor, A. and Kuner, R. (2014). **Studying ongoing and spontaneous pain in rodents--challenges and opportunities.** *Eur J Neurosci* 39(11), 1881-1890, doi: 10.1111/ejn.12643.

Todd, A. J. (2010a). **Neuronal circuitry for pain processing in the dorsal horn.** *Nat Rev Neurosci* 11(12), 823-836, doi: 10.1038/nrn2947.

Todd, A. J. (2010b). **Neuronal circuitry for pain processing in the dorsal horn.** *Nature reviews. Neuroscience* 11(12), 823-836, doi: 10.1038/nrn2947.

Todd, A. J. (2017). **Identifying functional populations among the interneurons in laminae I-III of the spinal dorsal horn.** *Mol Pain* 13, 1744806917693003, doi: 10.1177/1744806917693003.

Todd, K. H., Funk, K. G., Funk, J. P. and Bonacci, R. (1996). **Clinical significance of reported changes in pain severity.** *Ann Emerg Med* 27(4), 485-489, doi: 10.1016/s0196-0644(96)70238-x.

Torebjörk, H. E., Lundberg, L. E. and LaMotte, R. H. (1992). **Central changes in processing of mechanoreceptive input in**

REFERENCE

capsaicin-induced secondary hyperalgesia in humans. *J Physiol* 448, 765-780, doi: 10.1113/jphysiol.1992.sp019069.

Vlaeyen, J. W. S. and Linton, S. J. (2000). **Fear-avoidance and its consequences in chronic musculoskeletal pain: a state of the art.** *Pain* 85(3), 317-332, doi: 10.1016/s0304-3959(99)00242-0.

Wager, T. D., Atlas, L. Y., Lindquist, M. A., Roy, M., Woo, C. W. and Kross, E. (2013). **An fMRI-based neurologic signature of physical pain.** *N Engl J Med* 368(15), 1388-1397, doi: 10.1056/NEJMoa1204471.

Wiech, K. and Tracey, I. (2013). **Pain, decisions, and actions: a motivational perspective.** *Front Neurosci* 7, 46, doi: 10.3389/fnins.2013.00046.

Willis, W. D., Jr. (1999). **Dorsal root potentials and dorsal root reflexes: a double-edged sword.** *Exp Brain Res* 124(4), 395-421, doi: 10.1007/s002210050637.

Xiu, J., Zhang, Q., Zhou, T., Zhou, T. T., Chen, Y. and Hu, H. (2014). **Visualizing an emotional valence map in the limbic forebrain by TAI-FISH.** *Nat Neurosci* 17(11), 1552-1559, doi: 10.1038/nn.3813.

Ye, L., Allen, W. E., Thompson, K. R., Tian, Q., Hsueh, B., Ramakrishnan, C., Wang, A. C., Jennings, J. H., Adhikari, A., Halpern, C. H., Witten, I. B., Barth, A. L., Luo, L., McNab, J. A. and Deisseroth, K. (2016). **Wiring and Molecular Features of Prefrontal Ensembles Representing Distinct Experiences.** *Cell* 165(7), 1776-1788, doi: 10.1016/j.cell.2016.05.010.

Zangenehpour, S. and Chaudhuri, A. (2001). **Neural activity profiles of the neocortex and superior colliculus after bimodal sensory stimulation.** *Cereb Cortex* 11(10), 924-935, doi: 10.1093/cercor/11.10.924.

Zhang, Q., He, Q., Wang, J., Fu, C. and Hu, H. (2018). **Use of TAI-FISH to visualize neural ensembles activated by multiple stimuli.** *Nat Protoc* 13(1), 118-133, doi: 10.1038/nprot.2017.134.

Zhang, Z., Ferretti, V., Güntan, Í., Moro, A., Steinberg, E. A., Ye, Z., Zecharia, A. Y., Yu, X., Vyssotski, A. L., Brickley, S. G., Yustos, R., Pillidge, Z. E., Harding, E. C., Wisden, W. and Franks, N. P. (2015). **Neuronal ensembles sufficient for recovery sleep and the sedative actions of α 2 adrenergic agonists.** *Nat Neurosci* 18(4), 553-561, doi: 10.1038/nn.3957.

REFERENCE

Zimmerman, A. L., Kovatsis, E. M., Pozsgai, R. Y., Tasnim, A., Zhang, Q. and Ginty, D. D. (2019). **Distinct Modes of Presynaptic Inhibition of Cutaneous Afferents and Their Functions in Behavior**. *Neuron* *102*(2), 420-434.e428, doi: 10.1016/j.neuron.2019.02.002.

Zurborg, S., Piszczek, A., Martínez, C., Hublitz, P., Banchaabouchi, M. A., Moreira, P., Perlas, E. and Heppenstall, P. A. (2011). **Generation and Characterization of an Advillin-Cre Driver Mouse Line**. *Molecular Pain* *7*.

PUBLICATIONS

7 Publications

Veronica Bonalume, Lucia Caffino, Luca F. Castelnovo, Alessandro Faroni, Flavio Giavarini, **Sheng Liu**, Donatella Caruso, Martin Schmelz, Fabio Fumagalli, Richard W. Carr and Valerio Magnaghi. Schwann Cell Autocrine and Paracrine Regulatory Mechanisms, Mediated by Allopregnanolone and BDNF, Modulate PKC ϵ in Peripheral Sensory Neurons. *Cells* 2020, 9, 1874; doi:10.3390/cells9081874

Veronica Bonalume, Lucia Caffino, Luca F. Castelnovo, Alessandro Faroni, **Sheng Liu**, Jing Hu, Marco Milanese, Giambattista Bonanno, Kyra Sohns, Tal Hoffmann, Roberto De Col, Martin Schmelz, FabioFumagalli, Valerio Magnaghi and Richard Carr. Axonal GABAA stabilizes excitability in unmyelinated sensory axons secondary to NKCC1 activity. *J. Physiol.* 2021, 599.17; doi: 10.1113/JP279664

ACKNOWLEDGMENTS

Acknowledgments

Firstly, I would like to thank my supervisor Prof. Dr. Rohini Kuner for her kindless support and excellent mentoring, and for her valuable comments and selfless help during my academic difficulties. I also would like to thank Dr. Jing Hu, her patience and effort in discussion trained my scientific thinking and view. Her passion for science is always rousing my effort on my first project, this motivated me to be able to finish the first part of my thesis. Likewise, I would like to thank Dr. Richard Carr, Dr. Manfred Oswald and Prof. Dr. Stefan Lechner for their generous academic assistance, it is always a pleasure to discuss with them. I also love to thank my other supportive colleagues in Tuebingen and Heidelberg, Dr. Da Guo, Flavia Flattini, Dr. Nitin Agarwal, Dr. Anke Tappe-Theodor, Dr. Manuela Simonetti, Dr. Linette Tan, Dunja Baumgartl-Ahlert, Nadine Gehrig, Karin Meyer, Hans-Josef Wrede, Zheng Gan, Yong Xie, Han Li, Oscar Retana, Paul Naser, Tessa Frank, Danial Rangel Rojas and Alina Stegemann, your friendliness makes our lab such a pleasant place to work.

I would like to thank my family, the love of my life, Dr. Ting Ding. Your support and help giving me the confidence to finish my studies. Thank you for raising Nicole in Heidelberg with me and for giving birth to Yushu, it was a great life experience to be accompany with family in Germany. I would like to thank my parents and Ting Ding's parents for their support. I also thank all the friends I have made in Germany, your support has brought me to this state.

It is an end and will be a starting point. “Die Philosophen haben die Welt nur verschieden interpretiert, es kommt aber darauf an sie zu verändern.” Here, I wish to quote Karl Marx's aphorism in order to inspire myself, to pursue the light of truth.

CURRICULUM VITAE

Curriculum Vitae

Personal

Surname, Name: Liu, Sheng

Gender: Male

Date of birth: 12.05.1986

Place of birth: Gui Zhou

Nationality: China

Marital status: Married

Address: Hilzweg 15, 69121, Heidelberg, Baden-württemberg, Germany

Mobile Phone: +49 15221337578

Email: sheng.liu@pharma.uni-heidelberg.de; liushengsaint@gmail.com

Education

Bachelor of Engineering, Zunyi Medical University, China, 2004-2008

Field of Study: Bioengineering

Internship Training: Key Laboratory of Basic Pharmacology of China Education Ministry

Master of Science, Zunyi Medical University, China, 2010-2013

Field of Study: Biochemistry and molecular biology, Stem cell immunology

Training at: Key Laboratory of cell engineering of Guizhou Province

Supervisor: Prof. Daixiong Chen

PhD Training, Tübingen University, Germany, 2016-2017

Field of Study: Neuroscience

Training at: Centre for Integrative Neuroscience (CIN)

Supervisor: Dr. Jing Hu

PhD Training (Dr.sc.hum), Heidelberg University, Germany 2017-2021

Field of Study: Neuroscience, Pain neuroscience

Training at: Pharmacology insititute

Supervisor: Prof. Dr. Rohini Kuner

Employment

Pathology technician, Lecturer of Pathology, 2008-

Work at: Department of Pathology, Affiliated Hospital of Zunyi Medical University

EIDESSTATTLICHE VERSICHERUNG

EIDESSTATTLICHE VERSICHERUNG

1. Bei der eingereichten Dissertation zu dem Thema

.....
handelt es sich um meine eigenständig erbrachte Leistung.

2. Ich habe nur die angegebenen Quellen und Hilfsmittel benutzt und mich keiner unzulässigen Hilfe Dritter bedient. Insbesondere habe ich wörtlich oder sinngemäß aus anderen Werken übernommene Inhalte als solche kenntlich gemacht.

3. Die Arbeit oder Teile davon habe ich bislang nicht an einer Hochschule des In- oder Auslands als Bestandteil einer Prüfungs- oder Qualifikationsleistung vorgelegt.*

4. Die Richtigkeit der vorstehenden Erklärungen bestätige ich.

5. Die Bedeutung der eidesstattlichen Versicherung und die strafrechtlichen Folgen einer unrichtigen oder unvollständigen eidesstattlichen Versicherung sind mir bekannt.

Ich versichere an Eides statt, dass ich nach bestem Wissen die reine Wahrheit erkläre und nichts verschwiegen habe.

Ort und Datum

Unterschrift

* Wenn dies nicht zutrifft, machen Sie folgende Angaben:

3. Die Arbeit oder Teile davon habe ich wie folgt an einer Hochschule des In- oder Auslands als Bestandteil einer Prüfungs- oder Qualifikationsleistung vorgelegt:

Titel der Arbeit:

Hochschule und Jahr:

Art der Prüfungs- oder Qualifikationsleistung: